Cell Reports

Resource

Unraveling the phenotypic states of human innate-like T cells: Comparative insights with conventional T cells and mouse models

Graphical abstract

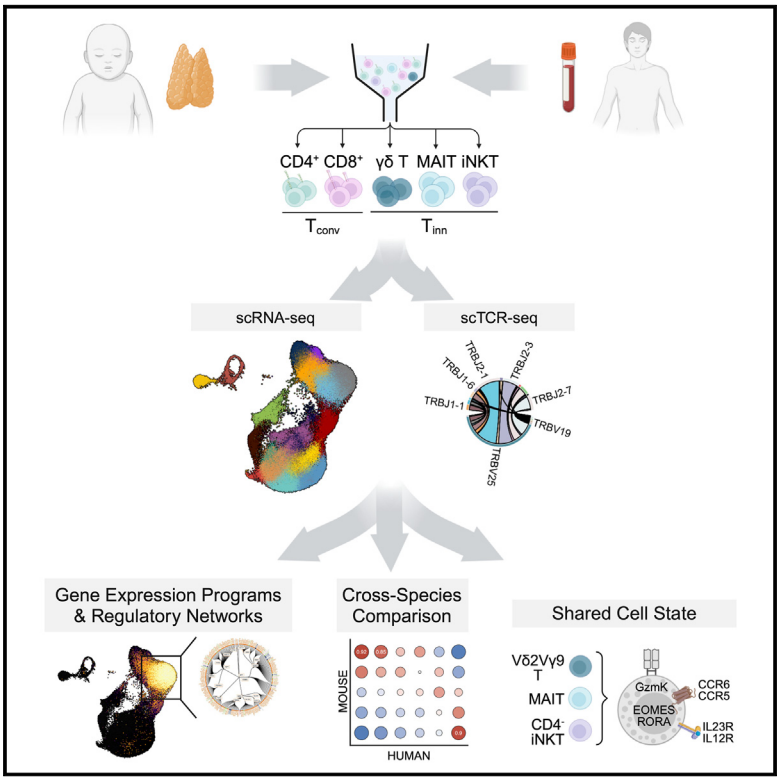

Authors

Liyen Loh, Salomé Carcy, Harsha S. Krovi, ..., Tonya Brunetti, Hannah V. Meyer, Laurent Gapin

Correspondence

hmeyer@cshl.edu (H.V.M.), laurent.gapin@cuanschutz.edu (L.G.)

In brief

Our study presents a comprehensive atlas of human innate T (T_{inn}) cells in the thymus and blood, highlighting their blended type 1 and type 17 transcriptional profiles. Loh et al. use single-cell RNA sequencing and flow cytometry to reveal species-specific distinctions and potential divergent developmental pathways of T_{inn} compared to conventional T cells.

Highlights

- Comprehensive atlas of human T_{inn} cells in thymus and blood
- Most postnatal thymic T_{inn} cells resemble naive T_{conv} cells
- Adult blood T_{inn} cells display a mixed type 1/type 17 effector program
- Human T_{inn} cells do not form distinct subsets like mouse T_{inn} cells

Loh et al., 2024, Cell Reports *43*, 114705
September 24, 2024
https://doi.org/10.1016/j.celrep.2024.114705

CellPress

Cell Reports

CellPress
OPEN ACCESS

Resource

Unraveling the phenotypic states of human innate-like T cells: Comparative insights with conventional T cells and mouse models

Liyen Loh,[1,6] Salomé Carcy,[2,3,6] Harsha S. Krovi,[4] Joanne Domenico,[1] Andrea Spengler,[1] Yong Lin,[3] Joshua Torres,[3] Rishvanth K. Prabakar,[3] William Palmer,[1] Paul J. Norman,[1] Matthew Stone,[5] Tonya Brunetti,[1] Hannah V. Meyer,[3,6,7,*] and Laurent Gapin[1,6,7,8,*]

[1]University of Colorado Anschutz Medical Campus, Aurora, CO, USA
[2]School of Biological Sciences, Cold Spring Harbor Laboratory, Cold Spring Harbor, NY, USA
[3]Simons Center for Quantitative Biology, Cold Spring Harbor Laboratory, Cold Spring Harbor, NY, USA
[4]Brigham and Women's Hospital, Boston, MA, USA
[5]Children's Hospital Colorado, Aurora, CO, USA
[6]These authors contributed equally
[7]Senior author
[8]Lead contact
*Correspondence: hmeyer@cshl.edu (H.V.M.), laurent.gapin@cuanschutz.edu (L.G.)
https://doi.org/10.1016/j.celrep.2024.114705

SUMMARY

The "innate-like" T cell compartment, known as T_{inn}, represents a diverse group of T cells that straddle the boundary between innate and adaptive immunity. We explore the transcriptional landscape of T_{inn} compared to conventional T cells (T_{conv}) in the human thymus and blood using single-cell RNA sequencing (scRNA-seq) and flow cytometry. In human blood, the majority of T_{inn} cells share an effector program driven by specific transcription factors, distinct from those governing T_{conv} cells. Conversely, only a fraction of thymic T_{inn} cells displays an effector phenotype, while others share transcriptional features with developing T_{conv} cells, indicating potential divergent developmental pathways. Unlike the mouse, human T_{inn} cells do not differentiate into multiple effector subsets but develop a mixed type 1/type 17 effector potential. Cross-species analysis uncovers species-specific distinctions, including the absence of type 2 T_{inn} cells in humans, which implies distinct immune regulatory mechanisms across species.

INTRODUCTION

Conventional $CD4^+$ and $CD8^+$ T cells (T_{conv}) are essential for adaptive immunity, recognizing peptide antigens presented by HLA class I or II proteins via their T cell antigen receptors (TCRs). Upon antigenic stimulation, these T cells undergo transcriptional and epigenetic changes, secreting pro-inflammatory cytokines, acquiring cytotoxic abilities to clear pathogens, or forming memory T cells for rapid response upon reencounter. Thus, T_{conv} cells within the circulation are heterogeneous and are commonly classified into naive (T_n), central memory (T_{cm}), effector memory (T_{em}), and terminally differentiated effector memory (T_{emra}) subsets.[1–3]

Innate-like T cells (T_{inn}), such as invariant natural killer T (iNKT) cells, mucosal-associated invariant T (MAIT) cells, and certain γδ T cells, maintain consistent TCRs among individuals and function without prior pathogen exposure. They account for 10%–20% of human T cells.[4,5] T_{inn} cells, originating from thymic progenitors, do not recognize peptides presented by HLA class I or II. Instead, iNKT cells use semi-invariant TCRs to recognize lipid antigens presented by CD1D.[6] MAIT cells, also characterized by semi-invariant TCRs,[7] recognize riboflavin precursor-derived metabolites presented by MR1.[8,9] Some γδ T cells recognize self- and foreign phosphoantigens in conjunction with the transmembrane butyrophilin-family receptors BTN2A1-BTN3A1-BTN3A2 complex.[10–12] The antigens recognized by other human γδ T cell populations remain unclear.[13] Thus, T_{inn} cells enhance immune detection of diverse threats.[14–16] Furthermore, the secretion of cytokines at steady state by mouse iNKT cells influences surrounding cells and T_{conv} development,[17–19] suggesting that they may also function as gatekeepers, ensuring proper T cell development and maturation.

The conservation of T_{inn} cells throughout mammalian evolution indicates their crucial and non-redundant role in the immune system, which may be attributed to their rapid activation kinetics and their ability for TCR-independent activation.[20–22] In mice, the rapid effector capacity of T_{inn} cells stems from unique transcriptional programs formed during their development in the thymus.[23,24] Analogous to CD4 T_{conv} cells, which can be polarized by cytokines into T helper (Th) phenotypes such as Th1, Th2, and Th17 that secrete interferon-γ (IFN-γ), interleukin-4

(IL-4), and IL-17, respectively, mouse T_{inn} cells diverge into distinct, terminally differentiated subsets that can be readily identified based on the expression of specific transcription factors (TFs) such as PLZF, GATA3, T-bet, and RORγt.[17]

In this study, using single-cell genomics and flow cytometry, we assessed the range of phenotypic states T_{conv} and T_{inn} cells can adopt *in vivo* in the human thymus and blood. We uncovered that unlike adult blood T_{inn} cells most postnatal thymic T_{inn} cells resemble naive T_{conv} cells, with few displaying an "effector" state. A distinct transcriptional program is shared among human T_{inn} cells, and major TFs driving this program are also expressed in mice. However, unlike the mouse, human T_{inn} cells do not form distinct subsets but develop a mixed type 1/type 17 effector program. We further highlight differences in CD1D and SLAMF6 expression in the thymus between the two species, which could potentially impact the maturation process of iNKT cells in humans. This comprehensive transcriptomic dataset of human T_{inn} cells provides a valuable resource to explore their fundamental properties and may serve as a guide for their strategic application in immunotherapeutic approaches.

RESULTS

Single-cell RNA-sequencing analysis of T cell maturation and post-maturation stages in humans

We explored the transcriptional profiles of T_{inn} and T_{conv} cells through single-cell RNA sequencing (scRNA-seq) of antibody DNA-barcoded ("hashtags") tetramer-sorted iNKT (PBS57-CD1d tetramer$^+$, TRAV10$^+$), MAIT (5-OP-RU-MR1 tetramer$^+$, TRAV1–2$^+$), and total γδ T cells, along with single-positive (SP) CD4 and CD8 T_{conv} cells from pediatric thymus and adult blood samples (Figure S1). A subset of samples was also subjected to VDJ sequencing (Figure 1A and Table S1). We analyzed 78,355 cells (37,369 pediatric thymus and 40,986 adult blood) after quality control, integrating them into a reference dataset (Figures 1B, 1C, S2A, and S2B). Using unsupervised clustering, we identified 18 distinct and stable clusters (c), primarily separating into thymus (c0–c9) or blood-associated regions (c12–c17, Figures 1C and S2C), with transitioning clusters (c10 and c11) showing cells from both tissues (Figures 1D and 1E), representing naive T cells prepared to leave the thymus or just entering the blood, in agreement with their over-representation of an "egress" gene signature[25] (Figure 1F and Table S3).

Cluster identities and transcriptional states were determined using reference genes (Figures S3A and S3B; Table S2), with cell types validated by neighbor voting[26] with the human thymus atlas[27] (Figure S4). Early T cell development included immature single positive (ISP) cells (c0 and c1), double-positive (DP) thymocytes (c2), and early SP stages characterized by *CCR9* expression (c3 for CD4 SP and c9 for CD8 SP). Later stages expressed *CCR7* (c11 for CD4 SP, c10 for CD8 SP; Figure S5A). Differentially expressed gene (DEG) analysis comparing CD4 SP cells (c3 and c11) to CD8 SP cells (c9 and c10) further confirms these annotations (Figure S5B). Specialized lineages were also detected, including CD8αα cells (*GNG4* and *NUCB2*), thymic γδ T cells (*TRDC*, *TRGC2*), and regulatory T cells (T_{regs}) with high expression of *FOXP3* (c5, c6, and c7, respectively). Other signaling states included "agonist" cells with high levels of TF transcripts associated with TCR signaling (c4; *NR4A1*, *EGR1*, *EGR3*, and *NFKBID*), cells with high expression of type I IFN signaling genes (*IFI6*, *MX1*, and *IFI44L* in c8), and AP-1 TFs (*JUN*, *FOS*, *JUNB* in c12). We also found cells (c13 through c17) expressing effector-encoding genes (*GZMK*, *GZMH*, *GZMB*, *PRF1*, and *CCL5*), suggesting involvement in effector functions of these cells (Figures S3A, S3B, and S5A). Altogether, we observed cells with distinct transcriptional profiles, representing unique cell types (CD8αα, T_{regs}) and stages of T cell development and maturation.

Identification of the gene-expression programs that characterize T cell populations in thymus and blood

Deciphering scRNA-seq data can be challenging due to the complexity of gene-expression patterns reflecting cell identity and activity. We used consensus non-negative matrix factorization (cNMF)[28] to reduce dimensionality, identifying 12 gene-expression programs (GEPs; Figure 1K and Table S4). Each cell type's contribution to these GEPs was assessed, revealing some GEPs shared across cell types, with others unique to specific clusters (Figures 1G and 1K). GEPs 7–11 were linked to thymic γδ T cells, T_{regs}, thymic CD8αα T cells, quiescent ISP, and proliferating ISP, respectively (Figure 1K). GEP 12 was excluded due to batch effects (Figure S6). GEPs 1 and 2, marked by *CCR9* and *CCR7*, were active in early and late thymic T cells, respectively. GEP3 was expressed by naive T cells. GEPs 4, 5, and 6, associated with "effectorness," were active in clusters 12, 13–14, and 15–17, respectively (Figures 1G–1K). Leveraging insights from these GEPs, we conducted an in-depth analysis of thymic and blood T cell populations, providing an integrated understanding of T cell differentiation and function.

Gene-expression similarities between αβ thymocyte lineages

We separated each sample by cell type and tissue, using the identifying tag (Figure 1G). CD4$^+$ thymic cells were found in clusters 0–4, 7, 8, and 11, while CD8$^+$ thymic cells were in clusters 2 and 5–10. Cell proportions in each cluster were consistent across samples, with about 1% (1.1% ± 0.4%) of the cells showing an effector signature (Figures 1G–1I and Table S3). Thymic iNKT cells were distributed similarly to conventional CD4$^+$ SP, and thymic MAIT cells shared clusters with CD8$^+$ SP (Figure 1G). Thymic γδ T cells were distinct, mainly in cluster 6 and GEP7 (Figures 1G and 1K).

Global gene-expression analysis between thymocyte lineages revealed three distinct patterns. First, effector stages of iNKT, MAIT, and γδ thymocytes (clusters 12–17) exhibited high gene-expression similarity. Second, non-effector γδ thymocytes showed no expression similarity to other lineages. Third, non-effector iNKT and MAIT thymocytes (clusters 0–11) resembled CD4$^+$ and CD8$^+$ thymocytes, respectively (Figure 2A). This suggests that specific subpopulations of iNKT thymocytes engage transcriptional programs akin to those of conventional CD4$^+$ thymocytes, with a parallel observation between MAIT and CD8$^+$ thymocytes. Pseudo-bulk DEG analysis between non-effector iNKT/CD4$^+$ and non-effector MAIT/CD8$^+$ further demonstrated that non-effector iNKT and CD4$^+$ thymocytes share 43

CellPress
OPEN ACCESS

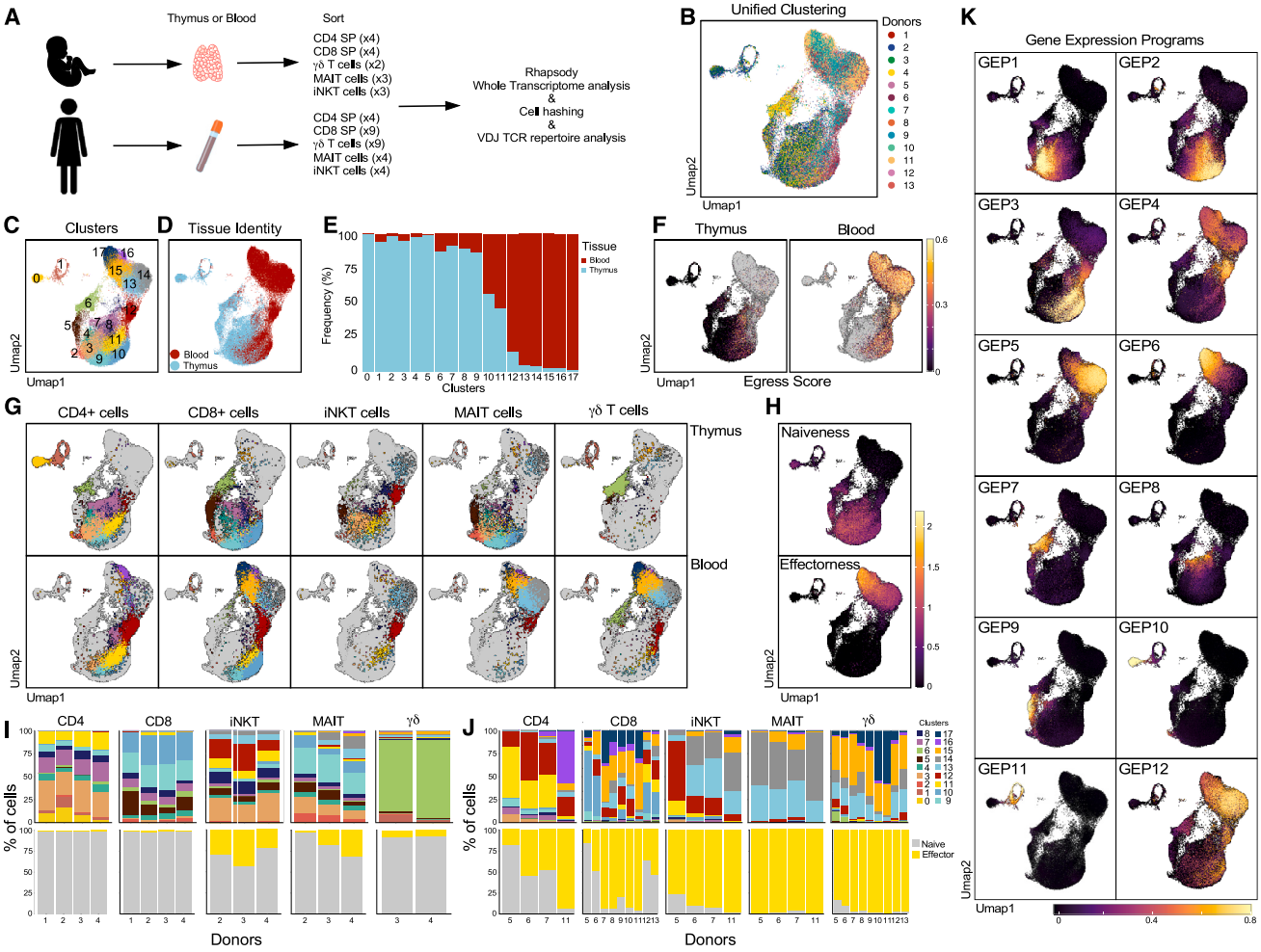

Figure 1. Integrative view on T_{inn} and T_{conv} development and peripheral function

(A) Experimental setup specifying donor type (postnatal/adult), tissue, and sorted cell types.

(B) Harmony batch-corrected and integrated dataset across donors, tissues, and cell types.

(C–E) (C) Stable Louvain-derived cell clusters distributed across (D) both blood and thymus-derived cells and (E) their respective frequencies in these clusters.

(F) "Egress" score on thymus- and blood-derived cells.

(G) Cells color coded by cluster (as in C) visualized by their hashtag-sorted cell type (columns) and the tissue they originated from (rows).

(H–J) (H) Projection of naive and effector scores and the proportion of (I) thymic and (J) blood cell types per donor, classified on the basis of these scores (bottom row); top row shows analogous proportions by cell cluster (as in C).

(K) Gene-expression programs (GEPs) in thymus and blood identified using cNMF, with color scale representing GEP usage. Sample numbers for all panels as depicted in (A). Score defining genes as described in text.

commonly upregulated and 38 commonly downregulated genes (Figure 2B). Key genes such as *GATA3*, *ZBTB7B*, and *CD40LG* were upregulated in non-effector iNKT thymocytes, indicating CD4 lineage differentiation, while *CD8A*, *CD8B*, and *RUNX3* were elevated in non-effector MAIT thymocytes. Using DEG analysis between $CD4^+$/MAIT and $CD8^+$/iNKT cells as a negative control revealed only *EPHB6*, *ZFAS1*, and *EEF1A1* as differentially expressed (Figure 2B). Comparing conventional $CD4^+$/$CD8^+$ thymocytes with non-effector iNKT/MAIT cells highlighted 11 DEGs (Figure 2C), including *ZBTB16* and SLAM family receptors *SLAMF5* (CD84) and *SLAMF6*, underscoring specific pathways crucial for effector differentiation, similar to observations in mice.[23]

Unbiased transcriptomic analysis of human T_{inn} differentiation

To further explore the transcriptional heterogeneity of human T_{inn} thymocytes, we re-analyzed iNKT and MAIT cell populations individually (Figures 2D–2E and S7). We identified seven clusters for both cell types (Figure 2D), with some variability in their proportion across donors (Figures S7B and S7F). Five major cell signatures were shared across T_{conv}, iNKT, and MAIT cells (Figures S3C and S3D). First, we observed a distinctive gene signature associated with CD8αα T cells (captured by GEP9; Figure S8; Tables S5 and S6). This signature was characterized by the heightened expression of *NUCB2*, *MINDY2*, and *HIVEP3* (Figures S3C and S3D), and intriguingly, it was observed in both iNKT and

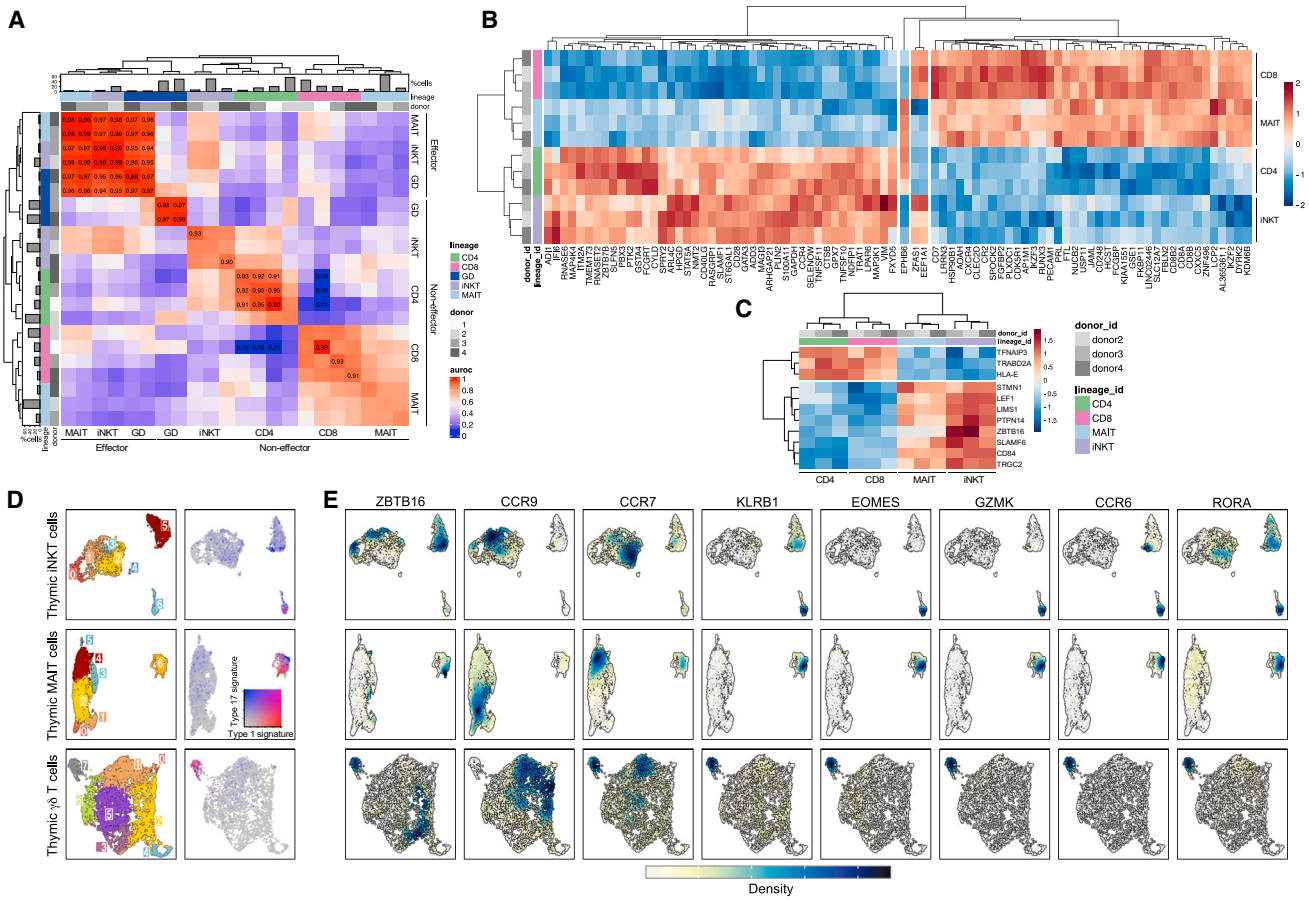

Figure 2. Gene-expression patterns in thymocyte lineages

(A) Heatmap showing MetaNeighbor's AUROC scores between thymocytes split by donor, lineage, and non-effector (c0–11) versus effector (c12–17) clusters. Barplots indicate thymocyte proportions per lineage.

(B) Pseudo-bulk differential expression analysis between CD4$^+$/iNKT and CD8$^+$/MAIT thymocytes in naive clusters (3, 9, 10, 11). As a negative control, the only three genes that were differentially expressed between CD4$^+$/MAIT and CD8$^+$/iNKT thymocytes are displayed in the center of the heatmap.

(C) Pseudo-bulk differential expression analysis between CD4$^+$/CD8$^+$ and iNKT/MAIT thymocytes in naive clusters (3, 9, 10, 11). For both (B) and (C), heatmap displays the expression level of genes (represented with color scale as a *Z* score of the average normalized expression) that are significantly differentially expressed ($p_{adj} < 0.01$).

(D) Clustering of hashtag-separated thymic iNKT cells (top), MAIT cells (middle), and γδ T cells (bottom). Right panel shows the score of type I and type III effector gene signature for the corresponding thymic lineage.

(E) Kernel density estimates of the normalized expression level of genes of interest. The expression level distribution varies between genes and lineage. The range of kernel density estimate values also varies between each panel (from 0 to 0.04 for the smallest range and 0 to 0.4 for the largest range). A unique color scale was represented to indicate the direction of the values.

MAIT cells (termed NKT_c0 and MAIT_c1; Figures S7C and S7G). This subset of thymic *CD8A*-expressing iNKT cells, which also exhibited some *PLZF* expression while lacking *KLRB1* (coding for CD161), *EOMES*, and *GZMK* expression (Figure 2E), could be readily identified using flow cytometry (Figure S9). Second, we identified a shared pattern of expression for the *CCR9* and *CCR7* chemokine receptors across T_{conv} cells, iNKT cells, and MAIT cells (Figure 2E). Initially, iNKT and MAIT cells exhibited an upregulation of *CCR9* in conjunction with *TOX* and *SATB1* (Figures S3C and S3D), resembling the developmental program of early developing CD4 SP and CD8 SP cells, respectively. Subsequently, the elevated expression of *CCR7* marked cells at a seemingly more advanced developmental stage (termed NKT_c2 and MAIT_c4). These sequential waves of chemokine receptor expression align with gene modules GEP1 and GEP2 (Figure S8 and Table S4), suggesting their sequential induction during the development of CD4, CD8, iNKT, and MAIT cells. These findings establish that the human thymus harbors iNKT and MAIT cells with a transcriptome resembling that of developing naive T_{conv} cells. The existence of such naive-like populations (CD161$^-$ EOMES$^-$GZMK$^-$) of iNKT and MAIT cells in the human thymus was confirmed by flow cytometry (Figure S9).

Third, we discovered iNKT and MAIT cells characterized by upregulation of genes associated with type I IFN signaling such as *MX1* and *IFI6*, similar to CD4 and CD8 SP cells (NKT_c3 and MAIT_c5; Figures S3C and S3D). Fourth, TCR signaling/AP-1

CellPress
OPEN ACCESS

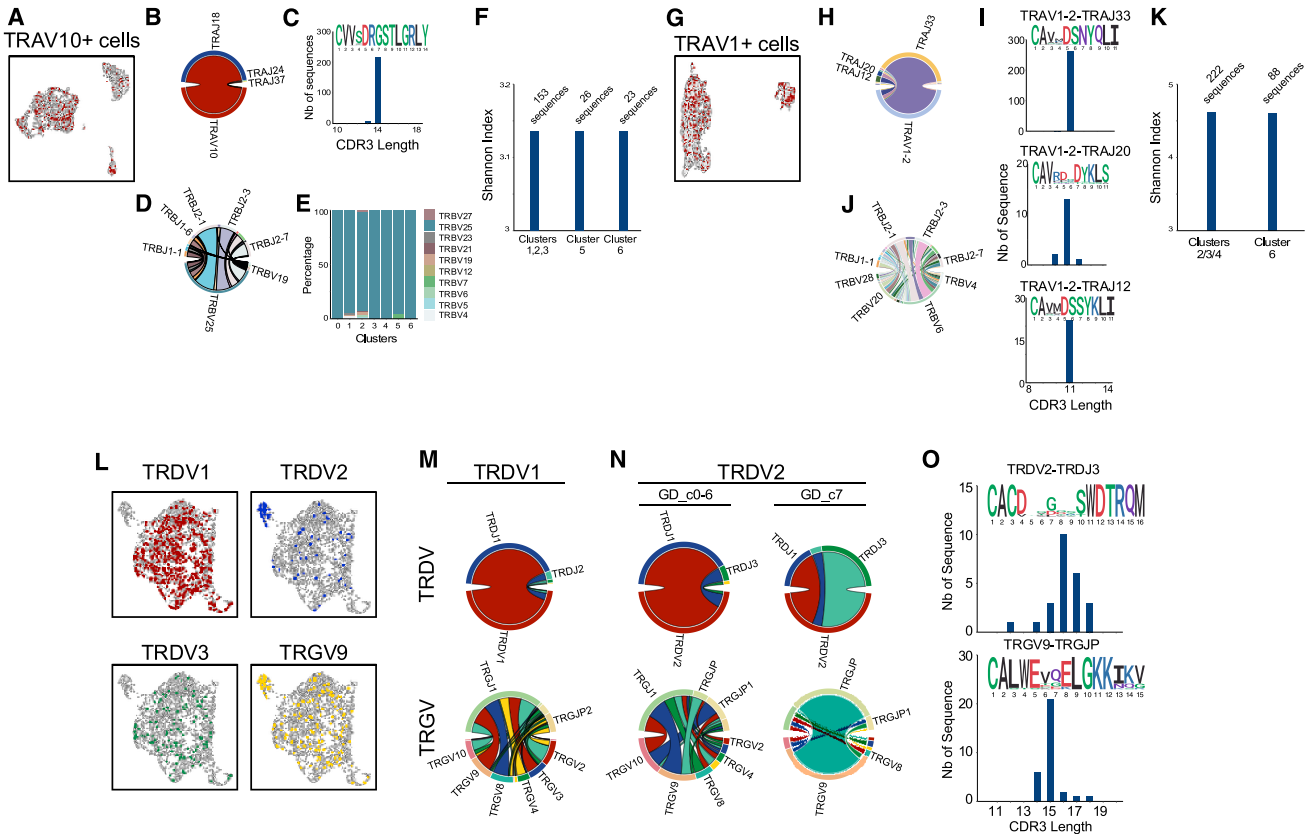

Figure 3. Innate T cell TCR diversity during development

Cells with VDJ sequencing and their cell-type-specific characteristic chain arrangement for thymic iNKT cells (A), MAIT cells (G), and γδ T cells (L). For each cell type, the respective proportions of gene segment usage in each chain (B and D; H and J; M and N) are shown together with their CDR3 length and sequence logo (C, I, O) and their cluster-specific usage (E, with clusters as in Figure 2A). Shannon index as an estimation of TCR diversity in the naive-like and effector-like iNKT (F) and MAIT (K) cells, based on clusters in Figure 2D. *n* = 1 human thymus sample for all panels.

signatures were found in iNKT cells, with AP-1 TFs *FOS* and *JUN* upregulated alongside *ZBTB16* and *KLRB1*. These cells also expressed *CD4* transcripts but not *CD8A* (NKT_c5; Figures 2E and S3C). The TCR signature was more pronounced in MAIT cells, where a small subset showed clear upregulation of genes involved in TCR signaling (*NR4A1*, *NFKBID*, *REL*; MAIT_c3; Figure S3D). Unlike T_{conv}, a proportion of both thymic iNKT and MAIT cells displayed an "effector" signature. iNKT cells in cluster 6 (NKT_c6) express classically iNKT-associated genes along with upregulation of effector genes usually associated with type 1 or type 17 immunity (*EOMES*/*GZMK* and *RORA*/*CCR6*, respectively; Figures 2E and S3C). Some of these cells expressed *CD8A* transcripts, suggesting that $CD4^+$ and $CD8^+$ iNKT cells might develop into transcriptionally distinct subsets, with $CD8^+$ iNKT cells having a more effector-associated signature. We found the same type 1 (*EOMES*/*GZMK*) and type 17 (*RORA*/*CCR6*) immunity effector co-expression signatures in MAIT cells (MAIT_c6; Figures 2D and S3D), with upregulation of genes encoding for granzymes (*GZMA* and *GZMK*) and chemokines (*CCL5*), as well as genes previously associated with MAIT cells[29,30] (*KLRB1*, *SLC4A10*, *IL23R*; Figure 2E).

Analysis of the thymic γδ T cells identified eight distinct clusters (Figures 2D, S3E, and S7I–S7L; Table S7), confirming previous findings on pediatric γδ thymocytes[25] with immature populations (GD_c0, 1, 2), TCR activation profiles (GD_c3), type I IFN response (GD_c6), and effector γδ T cells with egress and mixed type 1/type 17 effector potential (GD_c7). We also observed cells with a cycling gene signature (GD_c4), which was notably absent in iNKT and MAIT cells. Overall, we found a shared utilization of a mixed type 1/type 17 effector programs by iNKT, MAIT, and γδ T cells, with 28.7% ± 22.3% of thymic T_{inn} cells displaying this effector signature (Figures 1G and 1I, in clusters 12–17).

Lastly, because effector T_{inn} cells in the thymus might represent cells that initially acquired an effector signature in the blood and subsequently recirculated back to the thymus, we compared expression profiles between thymic and blood effector iNKT and MAIT cells. We found distinctive tissue-specific gene-expression profiles for both cell types (Figure S5C), indicating that thymic effector T_{inn} cells are unlikely to be derived from recirculating blood cells.

Effect of clonal selection on iNKT, MAIT, and γδ T cells' effector states

To investigate whether T_{inn} cells with an effector transcriptome had distinct TCR repertoires compared to naive T_{inn} cells, we conducted paired VDJ sequencing (Figure 3).

For iNKT cells, most VDJ sequenced cells used the *TRAV10* gene segment (encoding for the Vα24 chain) rearranged with *TRAJ18* (Figures 3A and 3B), resulting in a canonical CDR3α sequence of 14 amino acids (Figure 3C), crucial for antigen recognition.[31] This invariant TCRα chain paired with diverse TCRβ rearrangements, mainly involving the *TBV25* chain (Figure 3D), and was used evenly across all clusters (Figure 3E). The Shannon index, a measure of TCR diversity, revealed that no clonal selection had occurred or was associated with effector transcriptome development (Figure 3F), and no shared TCR clonotypes were identified between naive- and effector-like cells.

Thymic MAIT cells primarily used the *TRAV1–2* gene segment (encoding for the Vα7.2 chain) with *TRAJ33*, *TRAJ20*, and *TRAJ12* (Figures 3G and 3H), maintaining a conserved Y95 residue in the CDR3α loop (Figure 3I) essential for MAIT cell activation.[32,33] These TCRα chains paired with diverse TCRβ chains (Figure 3J) dominated by *TRBV6*, *TRBV20*, and *TRBV4* gene segments.[34,35] Like iNKT cells, MAIT cells showed no shared TCR clonotypes and no clonal selection in effector transcriptome cells (MAIT_c6) compared to naive-like cells (MAIT_c2-4), based on the Shannon index (Figure 3K).

Effector γδ T cells (GD_c7) were enriched for cells expressing *TRDV2* and *TRGV9* gene segments, while *TRDV1* and *TRDV3* segments were excluded from this cluster (Figure 3L). Some *TRDV2*$^+$ or *TRGV9*$^+$ cells were also found in non-effector clusters, suggesting a potential role for these gene segments in the development of effector γδ T cells in the postnatal human thymus. Supporting this hypothesis, we observed that the rearrangements of both the Vδ2 chains and associated Vγ9 chains differed largely between cells in the effector versus non-effector clusters (Figure 3N). Specifically, the Vγ9 chains of effector cells were found to be preferentially rearranged with the TRGJP gene segment and enriched for the public CDR3 sequence typically found among Vδ2Vγ9 γδ T cells in adult blood[36] (Figure 3O), whereas Vδ2$^+$ cells in the non-effector clusters showed more diverse Vγ gene usage and rearrangements (Figure 3N). In summary, the acquisition of effector programs in iNKT and MAIT cells is not associated with changes in TCR diversity, whereas Vδ2 and Vγ9 chain rearrangements in γδ T cells suggest a predisposition toward the effector program.

Gene-expression programs that characterize T cell effector functions

To further characterize the functionality of T_{inn} and T_{conv} cells in the blood, we examined the distribution of these cell types across transcriptional clusters. Conventional CD4$^+$ T cells were primarily located in cluster 11 (naive CD4 T cells) and cluster 7 (T_{regs}). CD4$^+$ T cells also appeared in effector clusters, particularly clusters 12 and 16, with proportions varying among donors (18.4%–93.7%; Figures 1G and 1J). Blood CD8$^+$ T cells were predominantly in cluster 10 (naive CD8 T cells), with varying proportions in effector clusters, reflecting differences in donor immunological history (16.5%–94%; Figure 1J). In contrast, the majority of blood T_{inn} cells (∼94.3% ± 6.7%) were distributed across effector clusters 12–17, regardless of donor (Figure 1J).

We next investigated transcriptional states in blood T cell populations using cell hashtags to reanalyze blood iNKT cells, MAIT cells, γδ T cells, and T_{conv} CD4$^+$ and CD8$^+$ T cells individually (Figures 4A and 4B). Each cell type was found within previously identified GEPs (GEP3–6; Figure 1K; Tables S8, S9, S10, S11, and S12), albeit with varying proportions for each cell type (Figures 4C and 4D). To contextualize these GEPs, we computed overlap scores and statistically assessed their enrichment with literature-derived signatures.[37–40] Subsequently, we scored the joint signature-GEP interactions in our dataset (Figure S10). GEP3 was found to be closely associated with signatures of naive T cell characteristics. In contrast, GEP4 displayed similarities with T_{cm}, T_{em}, or literature-derived signatures classified as a mix thereof (T_{cm}/T_{em}), while GEP6 exhibited characteristics akin to T_{emra}. GEP5, on the other hand, shared elements with T_{em} cells and previously identified CD8 MAIT signatures (Figure S10A).

Blood iNKT cells predominantly expressed GEP3 or GEP5, with some expressing GEP4 or GEP6 (Figure 4D). GEP4-expressing iNKT cells had *CD4* transcripts, while GEP5 and GEP6 cells lost *CD4* expression (Figures S11A and S11B). To validate this observation, we examined the cellular phenotype of blood iNKT cells. Blood CD4$^+$ iNKT cells were mostly PLZF$^-$CD161$^-$EOMES$^-$GZMK$^-$ but CCR7$^+$, indicating a naive GEP3 program (Figure S11C). In contrast, CD8$^+$ and double-negative iNKT cells were mostly PLZF$^+$CD161$^+$ and displayed an effector phenotype (EOMES$^+$GZMK$^+$CCR7$^-$CD62L$^-$; Figure S11). Interestingly, the distribution of these programs varied significantly among different donors (Figure 4B). These findings are in line with previous data indicating that CD4-negative iNKT cells become more prevalent in the blood with age, eventually becoming the dominant population in the adult blood iNKT cell compartment.[41,42] This suggests that CD4-negative iNKT cells may originate from CD4$^+$ iNKT cells that undergo a loss of CD4 expression as they transition toward a more effector-like state. Conversely, when examining MAIT cells in the blood, we observed that the majority of them exhibited the GEP5 program, with only a minor fraction utilizing the GEP6 program (Figure 4D). This GEP phenotype was further confirmed by flow cytometry, revealing that most MAIT cells were CD8$^+$ and, interestingly, that all MAIT cells displayed a uniform effector state (characterized by PLZF$^+$CD161$^+$EOMES$^+$GZMK$^+$CCR7$^-$CD62L$^-$), regardless of CD8 expression (Figure S12). These findings indicate that MAIT cells in the bloodstream primarily exist in an exclusive transcriptional state.

Blood γδ T cells were stratified into five clusters: naive (c0, GEP3), cycling (c4, GEP11), and clusters c1–c3 categorized into GEP5 or GEP6 programs (Figures 4C and 4D). This division in GEP utilization closely mirrored the specific TCR usage among these cells. TRDV2/TRGV9-expressing cells were predominantly GEP5, while TRDV1$^+$ or TRDV3$^+$ cells were enriched in GEP6 (Figures S13A–S13C). Flow cytometry confirmed Vγ9$^+$Vδ2$^+$ T cells primarily expressed PLZF and GZMK, while Vδ2$^-$ T cells were increased in GZMB$^+$ cells (Figures S13D and S13E). Thus, GEP5 is an effector gene module unique to T_{inn} cells, indicating common transcriptional states in human T_{inn} cells.

The distribution of CD4 and CD8 T_{conv} cells in the blood revealed two primary patterns. T_{conv} cells were found either within clusters containing naive cells (clusters 0 and 1) characterized by high expression of GEP3 or dispersed across clusters of cells displaying a gradient of the GEP6 program, with intermediary

CellPress
OPEN ACCESS

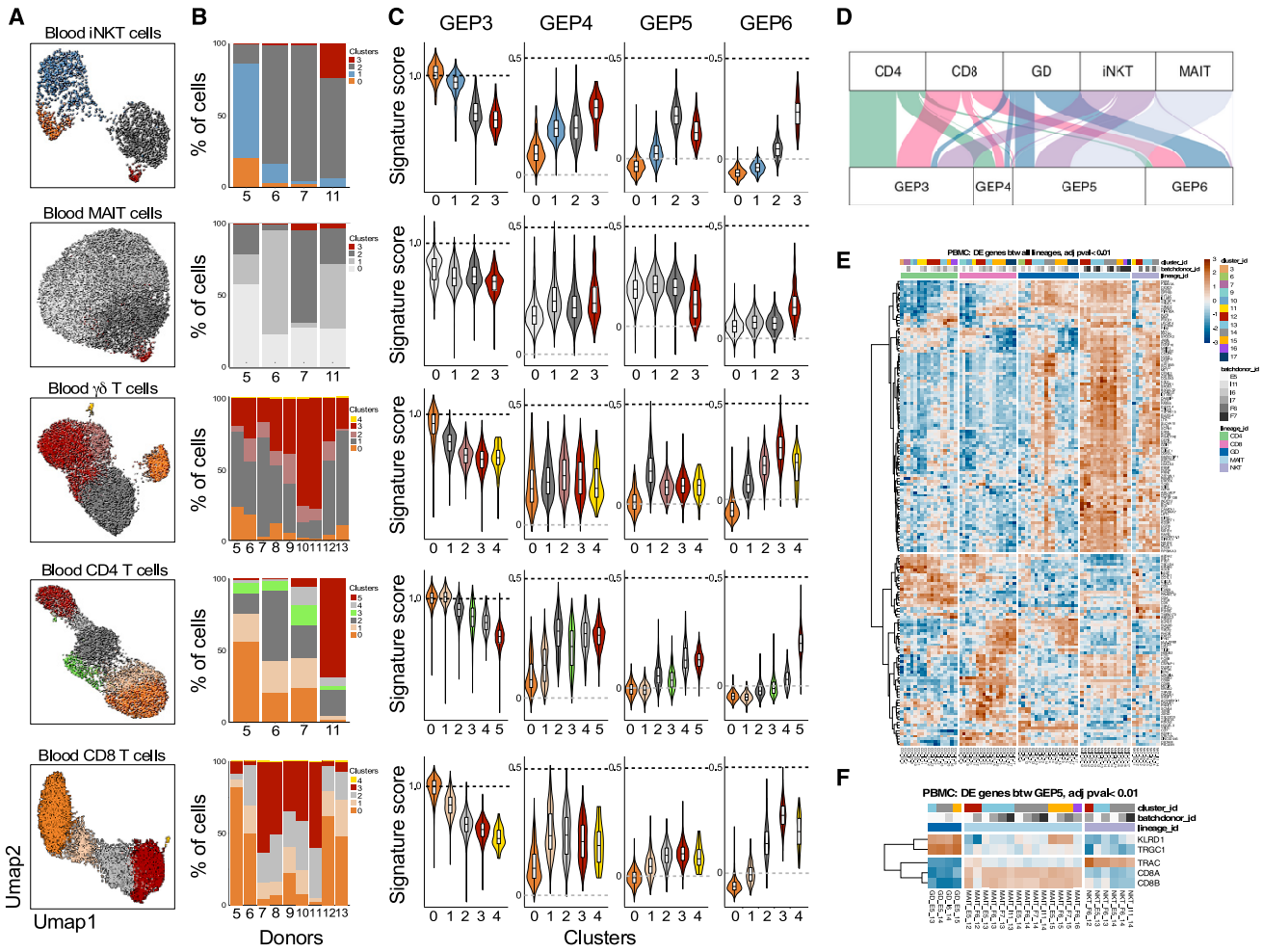

Figure 4. Gene-expression programs in circulating T_{inn} and T_{conv}

(A–C) (A) Clustering of hashtag-separated blood iNKT, MAIT, γδ T, CD4, and CD8 T cells, (B) the respective proportion of cells per cluster and donor, and (C) the effector GEP signature scores (as in Figure 1K) per cell type and cluster.

(D) Top GEP usage for each cell type, based on cNMF-derived usage matrix.

(E) Pseudo-bulk, pairwise differential gene expression between cell types.

(F) Cell-type-specific genes among T_{inn} cells using GEP5. For both (E) and (F), heatmaps depict the expression level of genes (represented with color scale as a *Z* score of the average normalized expression) that are significantly differentially expressed ($p_{adj} < 0.01$). $n = 4, 4, 9, 4$, and 9 for iNKT, MAIT, γδ, CD4, and CD8 cells, respectively.

cells expressing GEP4 (Figure S14). The proportions of cells in these clusters exhibited variations among donors (Figure 4B). Together, these findings underscore the distinct associations between different T cell types and effector programs. In the blood, $CD4^-$ iNKT, MAIT, and $V\gamma9^+V\delta2^+$ γδ T cells predominantly employ the GEP5 program, a program also shared by effector T_{inn} cells in the thymus (Figure S8). Conversely, conventional $CD4^+$ and $CD8^+$ T cells transition into effector cells along a gradient defined by the GEP6 program. Notably, this GEP6 program is also shared by $V\delta3^+$ and $V\delta1^+$ γδ T cells.

Next, we used pairwise DEG analyses between T cell lineages in human blood to identify lineage-specific genes. We uncovered a total of 167 genes that exhibited significant differential expression ($p_{adj} < 0.01$) in at least two of the comparisons we conducted (Figure 4E). These distinct patterns of DEGs provided insights into changes linked to the transition from a "naive" state to an "effector" state across cell types. Furthermore, we identified genes that were commonly expressed by two distinct cell types when compared to the others. Nevertheless, we did not readily discern any gene-expression patterns specific to a particular cell type. However, intriguingly, among these, a group of 104 genes distinguished γδ, MAIT, and iNKT cells from T_{conv} CD4 and CD8 T cells, with 63% overlapping with GEP5. Given that only $V\gamma9^+/V\delta2^+$ T cells share the GEP5 program with iNKT and MAIT cells, while $V\delta2^-$ T cells exhibit greater similarity to T_{conv} cells as they share the GEP6 program (Figure S13C), we explored whether we could identify cell-type-specific gene signatures specifically among GEP5-expressing cells using the same analytical approach. Surprisingly, the results demonstrated that the only significant DEGs between iNKT, MAIT,

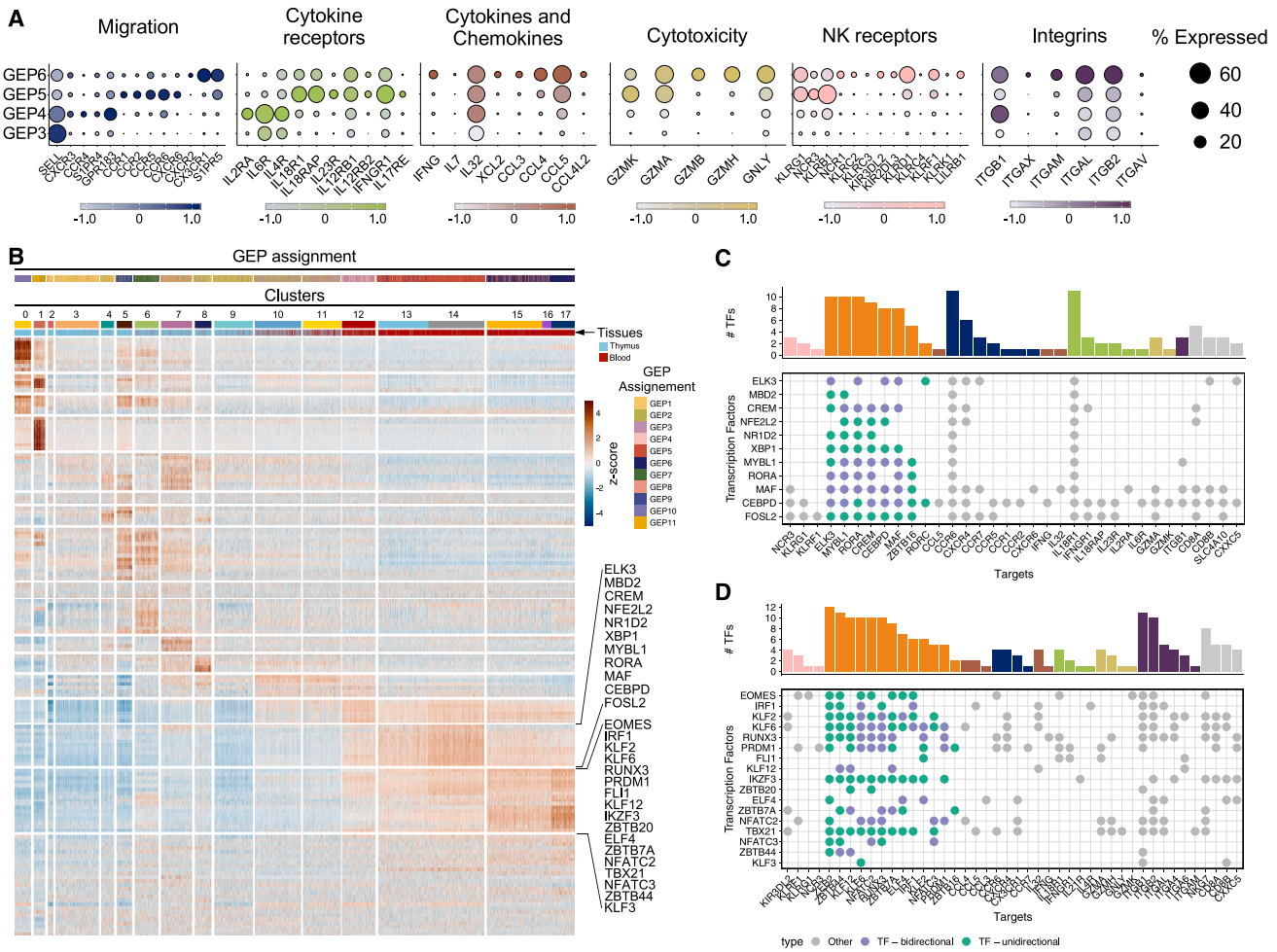

Figure 5. Effector gene-expression programs in T_{inn} and T_{conv}

(A) Key genes categorized by function and depicted by their expression level (*Z*-score color scale) and percentage of expression in cells belonging to the indicated GEPs.

(B–D) (B) Single-cell regulatory network inference and clustering of TFs and enrichment score per cell (as row-scaled *Z* scores), ordered by cluster (as in Figure 1C), with tissue of origin and GEP assignment (based on cNMF usage) indicated by color bar. Two row clusters are marked, which are preferentially enriched in T_{inn} (upper bracket) and T_{conv} (lower bracket). (C and D) TFs with pronounced activity in (C) T_{inn} and (D) T_{conv} (corresponding to brackets in B) and their targets. Green dots indicate TFs (y axis) that have other TFs as their target (x axis), where purple labels TFs that can interact in either direction. The marginal bar chart shows the number of TFs per target, color coded by their functional categorization (as in A).

and γδ T cells employing the GEP5 program (Figure 4F) were genes encoding the constant regions of the TCR genes (*TRGC1*, *TRAC*), the CD8 coreceptor (*CD8A*, *CD8B*), and the CD94 receptor (encoded by *KLRD1*). Thus, human blood T_{inn} cells, which encompass iNKT, MAIT, and $V\gamma9^{+}/V\delta2^{+}$ cells, distinguish themselves from T_{conv} cells by employing a specific gene program, but there is minimal transcriptional difference among T_{inn} cells themselves.

The effector GEPs exhibit distinct migration, cytokine, chemokine, and integrin characteristics established by distinct gene-regulatory networks

The differentiation states of T cells are intricately linked to their phenotypic, functional, and migratory attributes, making their characterization clinically relevant. Each GEP aligns with distinct sets of chemokine and cytokine receptors as well as molecules related to cytotoxicity, NK receptors, and integrins (Figure 5A). For example, the GEP4 program, shared by T_{cm}/T_{em} (Figure S10) and some iNKT cells depending on the donor (Figures 4B–4D), shows high expression of chemokine receptors *CXCR3* and *CCR4*, sphingosine-1-phosphate receptor 4, and oxysterol receptor *GPR183*, with the latter offering survival and migratory signals to thymocytes and CD4 T follicular helper cells.[43] GEP4 also features high levels of *IL2RA*, *IL6R*, *IL4R*, and *ITGB1*, while conspicuously lacking cytotoxic molecules (Figure 5A). In contrast, the GEP5 program, predominant in T_{inn} cells across most donors (Figures 4B–4D), shows elevated expression of *CCR1*, *CCR2*, *CCR5*, and *CCR6*, as well as *CXCR6* and cytokine receptors such as *IL18R1*, *IL18RAP*, *IL12RB1*, *IL12RB2*, *IL23R*, and *IFNGR1* (Figure 5A). This pattern includes *GZMA* and

GZMK but lacks *GZMB* and *GZMH* (Figures 5A and S5A) and features the NK receptor *KLRB1*. On the other hand, the GEP6 program, mainly associated with T_{em}/T_{emra} cells (Figure S10) and $V\delta1^+$ and $V\delta3^+$ γδ T cells across the majority of donors (Figures 4B, 4C, and S13), shows increased *CX3CR1* expression (Figure S14), correlating with effector state differentiation in CD4 and CD8 T cells.[44] GEP6 includes *IFNG*, *CCL4*, *CCL5*, and *KLRD1*, several integrins (*ITGAL*, *ITGB2*, *ITGAM*), and cytotoxicity genes such as *GZMB*, *GZMH*, and granulysin (*GNLY*), with reduced *GZMK* compared to GEP5 (Figure 5A). These findings align with studies indicating that $GZMK^+$ and $GZMB^+$ cells delineate T_{cm} and T_{em}/T_{emra} cell populations.[45,46]

We then used a network inference approach to identify the activity of regulons—TFs and their targets—in single cells.[47] We identified 149 of such regulons, with 11 regulons more active in T_{inn} compared to T_{conv} cells (Figure 5B). These regulons were governed by TFs such as *ELK3*, *MBD2*, *CREM*, *NFE2L2*, *NR1D2*, *XBP1*, *MYBL1*, *RORA*, *MAF*, *CEBPD*, and *FOSL2*. Curated analysis of their predicted target genes indicates that these TFs may play a central role in shaping the unique transcriptional profile observed in T_{inn} cells during steady-state conditions. This role encompasses the regulation of chemokine and cytokine receptors as well as other genes associated with T_{inn} cells, including *ZBTB16* (encoding PLZF), the master regulator of the T_{inn} cell lineage (Figure 5C). A second group of regulons exhibited enriched activity within effector T_{conv} cells, although some shared activity with T_{inn} cells (including *EOMES*, *RUNX3*, *PRDM1*, and *FLI1*; Figure 5B). As T_{conv} cells differentiate into $T_{em/emra}$ cells, there is an increased activity of regulons driven by *TBX21*, *KLF*, and *NFAT* family TFs (Figures 5B and 5D), in agreement with their functions in regulating the cytolytic activity of CD8 T cells.[48–50] Taken together, we discovered novel candidate regulators of T_{inn} and T_{conv} effector programs, along with their predicted target genes, which warrant further experimental validation.

Cross-species analysis of thymic T_{inn} cell development

Only a minority of human T_{inn} thymocytes display an effector phenotype, contrasting with the predominant effector association of mouse T_{inn} thymocytes, which develop into distinct effector subsets.[23,51,52] To explore transcriptional similarities between mouse and human T_{inn} cells in the thymus, we constructed a reference mouse T_{inn} dataset from nine studies.[51–59] This dataset revealed 13 transcriptionally distinct clusters, with iNKT, MAIT, and γδ T cells coexisting in variable proportions (Figures 6A and S15; Table S13). Lineage-specific clusters included those unique to γδ T cells (c1 and c2, immature $Cd24a^+Gzma^+$ cells[51,58]), signaling cells (c3 and c4), cycling cells (c5), type 1 cells (c8 and c9), type 2 cells (c6 and c7), and type 17 cells (c10 and c11). Cluster 0, expressing markers such as *Sell* (encoding for Cd62l), *Klf2*, *Ccr7*, *Foxo1*, and *S1pr1*, likely represents T_{inn} cells positively selected on thymic epithelial cells (TECs), bypassing the "innate" pathway.[23,60] We performed a cross-species comparison of cell identities by assessing the pairwise correspondence between murine T_{inn} signatures and human iNKT, MAIT, and γδ T cell clusters (Figure 6B). Human iNKT cells in cluster 0 (NKT_c0), exhibiting a CD8αα T cell gene signature, showed the strongest resemblance to signaling cells (Figure 6B), likely due to shared TCR activation genes. Conversely, cells with an effector profile (NKT_c5 and NKT_c6) showed the closest relationship to mouse type 1 and to a lower extent type 17 cells (Figure 6B). Importantly, we did not find human clusters corresponding uniquely to specific mouse subsets, confirming that human iNKT cells do not differentiate into distinct subsets but rather acquire a mixed type 1/type 17 transcriptome. We also did not detect any human iNKT cell clusters that matched with the mouse type 2 subset with a high degree of confidence (area under the receiver operator characteristic curve [AUROC] > 0.65; Figure 6B), suggesting that type 2 iNKT cells are likely absent in the human thymus. Corroborating this finding, we did not detect any expression of IL-4- or IL-13-encoding transcripts in human thymic iNKT cells, which are typically associated with mouse type 2 thymic iNKT cells. Similar patterns were observed for MAIT and γδ T cells in the human thymus, with effector cells resembling more closely mouse type 1 and type 17 effector cells (Figure 6B). This indicates that human T_{inn} cells follow a distinctive path with mixed effector potential, unlike the mouse model with multiple effector subsets.

We next assessed whether the TFs driving human T_{inn} cell regulons (Figure 5A) were also expressed in mouse T_{inn} cells (Figure 6C). Most TFs were indeed expressed in mouse T_{inn} cells, although their expression varied across clusters. However, exceptions included *CEBPD*, *EOMES*, and *MYBL1*, which were highly expressed in human T_{inn} cells (Figure S5A) but barely detectable in mouse T_{inn} cells (Figure 6C). Conversely, mouse type 1 T_{inn} cells exhibited high T-bet levels (encoded by *Tbx21*, Figure 6C), while human T_{inn} cells had low T-bet expression (Figures S5A, S11B, and S12B). These findings highlight some species-specific differences in TF expression that could play a role in modulating T_{inn} cell development and functions.

CD1D, SLAMF6, and SLAMF1 expression in the mouse and human thymus

The existence of T_{inn} cells in the human thymus with a transcriptome similar to developing T_{conv} cells raises questions about their origin. In mice, a subset of MAIT cells is positively selected by radiation-resistant TECs, which do not lead to a memory or effector phenotype acquisition.[52,59] This is because TECs lack SLAM receptors, crucial for T_{inn} commitment.[61] Although this is more common among MAIT cells, some thymic mouse iNKT cells also exhibit a similar transcriptome.[23]

We hypothesized that naive T_{inn} cells in humans might result from a similar TEC-mediated selection process. Given the challenge of detecting surface MR1 expression at steady state, we investigated CD1D protein expression in the thymus instead. Mouse TECs have been reported to express CD1d on their surface.[62] scRNA-seq of the mouse thymus[27] confirmed *Cd1d1* expression across various cell types, including thymocytes and cortical and medullary TECs (Figures 7A and 7B). Flow-cytometry analyses corroborated these findings (Figures 7C and 7D).

In contrast, human thymus scRNA-seq data[27] showed a more limited pattern of *CD1D* and *SLAMF6* expression (Figures 7E and 7F). Human DP thymocytes express *CD1D* transcripts and surface CD1D molecules, but this expression is lost in mature SP thymocytes. Flow cytometry confirmed that, as in mice,[61] SLAMF1 is expressed by human DP and SP thymocytes, but

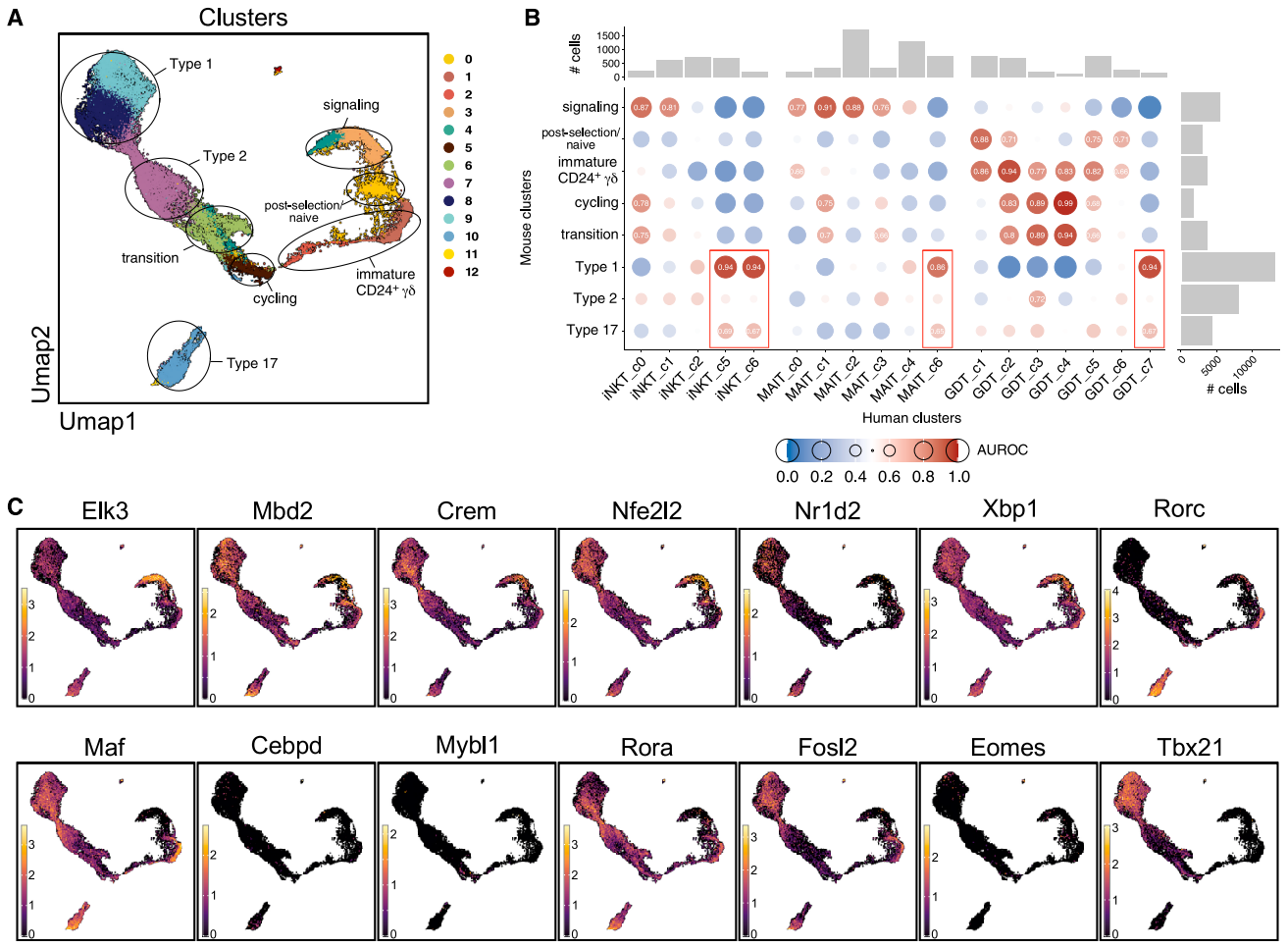

Figure 6. Cross-species comparison of mouse and human T_{inn} development

(A) Mouse T_{inn} reference atlas with seven characteristic cell states highlighted, which are found across lineages (as in Figure S15).

(B) MetaNeighbor analyses showing pairwise correspondence (AUROC scores) between murine T_{inn} (as in A) and human iNKT, MAIT, and γδ T cell clusters (as in Figure 2D). Marginal bar charts indicate number of cells in the corresponding clusters.

(C) Expression of human regulon-driving TFs (as in Figure 5) together with murine TFs of importance in T_{inn} development (*Rorc*, *Tbx21*) projected on mouse T_{inn} reference atlas (as in A).

SLAMF6 is not detectable on the surface of human thymocytes (Figure 7H). Additionally, human cortical TECs (cTECs) express CD1D transcripts and have surface CD1D protein, whereas medullary TECs (mTECs) do not (Figures 7G and 7H). This interspecies difference in CD1D and SLAM family members' expression might affect iNKT cell development, given the crucial role of mTECs in murine iNKT cell development.[19,63]

DISCUSSION

In this study, we employed multi-modal single-cell transcriptomics to explore the diverse phenotypic states of T_{inn} cells within the human thymus and blood. By comparing these states to those of T_{conv} cells, we provided insights into human T cell biology and a comprehensive resource for further studies of health and disease. Our work emphasizes T_{inn} cells as promising candidates for immunotherapies.[64–66]

Our study demonstrated that the majority of T_{inn} cells in adult human blood exhibit a distinct transcriptional program shared by most iNKT, MAIT, and Vδ2Vγ9$^+$ T cells under steady-state conditions. This program implies a blended type 1/type 17 transcriptional pattern, driven by specific TFs that enable the expression of distinct chemokine and cytokine receptors, NK receptors, and cytotoxic molecules. This equips T_{inn} cells to swiftly respond to cytokines such as IL-12, IL-18, and IL-23 independently of TCR signaling.[22,67] Notably, human T_{inn} cells constitutively express GZMK but lack GZMB while also expressing cathepsins necessary for activating granzymes.[68] This suggests that T_{inn} cells are prepared to release active GZMK upon stimulation,[69] which can induce pro-inflammatory cytokines[45,70] and activate complement,[71] implying a role in immune regulation and inflammatory responses. In contrast, mouse T_{inn} cells do not express *GZMK* transcripts but possess pre-formed cytokine-encoding transcripts, allowing for immediate responses.[72,73] Hence,

CellPress
OPEN ACCESS

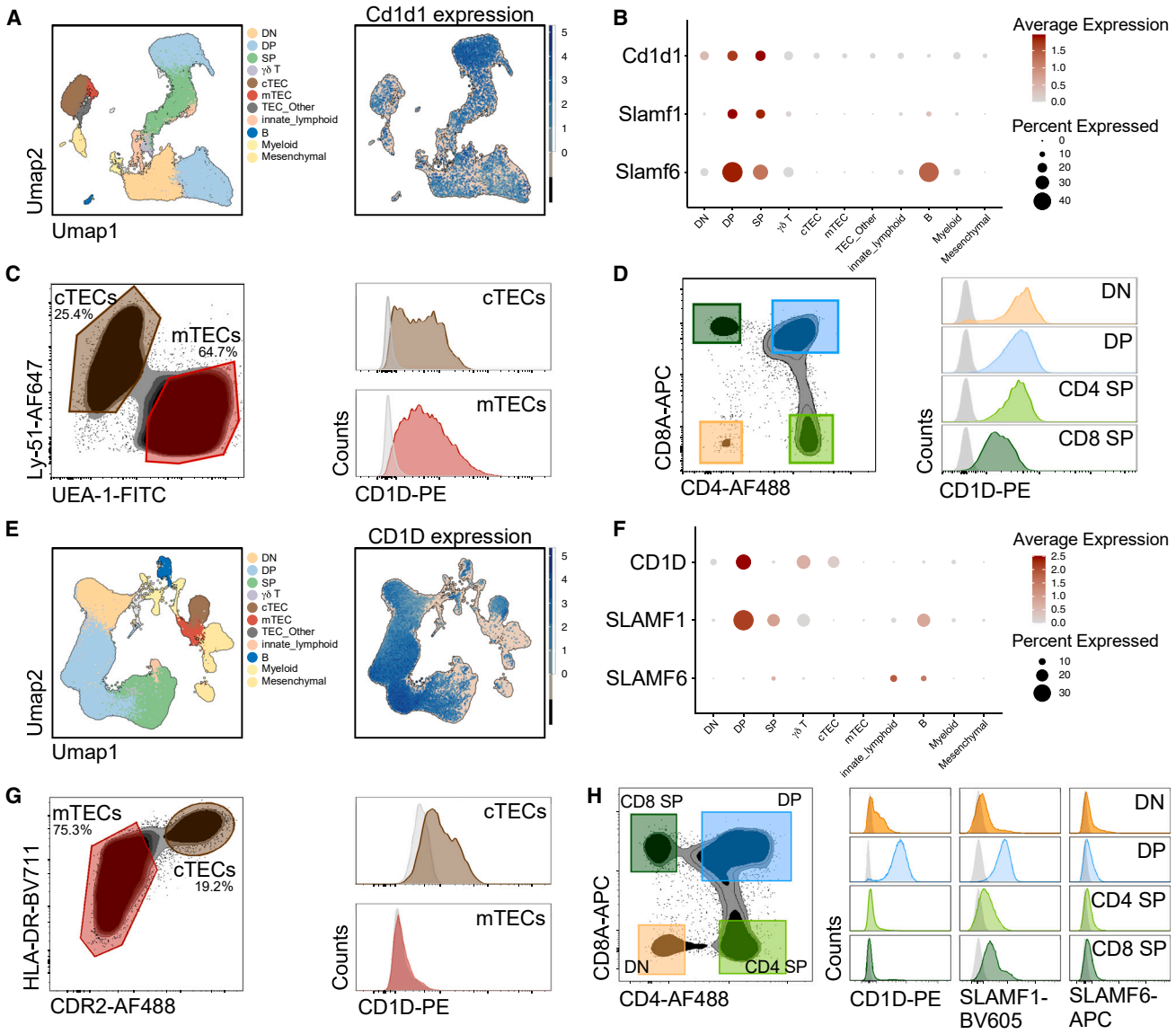

Figure 7. CD1D, SLAMF1, and SLAMF6 gene and protein expression in mouse and human thymus

(A) Clustering of thymic cell populations and (E) their expression of *Cd1d1* (mouse)/*CD1D* (human) derived from the mouse and human thymus cell atlas, respectively.[27] (B and F) Normalized expression of *Cd1d1*/*CD1D* and *Slam*/*SLAM* transcripts across thymic cell populations. Flow cytometry of (C and G) mouse and human TECs and (D and H) thymocyte subsets.

despite their evolutionary conservation, T_{inn} cells may have evolved species-specific mechanisms to provide early signaling and amplification of the adaptive immune response.

We identified TFs and their predicted target genes with increased transcriptional activity in human T_{inn} cells compared to naive and effector T_{conv} cells. Many of these TFs are associated with IFN-γ, cytotoxicity,[48–50,74] and IL-17 production,[75–77] consistent with the type 1/type 17 transcriptional program observed in T_{inn} cells. In mice, the Th1/Th17 paradigm identifies IL-12 and IL-23 as cytokines that induce IFN-γ and IL-17 production, respectively. By contrast, activating human MAIT cells through their TCR or with IL-12 and IL-18, and stimulating T_{inn} cells with IL-23, results in IFN-γ production.[67,78] Yet, only a subset of these cells produces IL-17 in the same conditions, a phenomenon thought to be influenced by epigenetic modifications at the IL-17 gene loci.[78] Underlining the importance of understanding the regulation of IL-17 production in T_{inn} cells, IL-17 production in human MAIT cells is increased in diseases such as severe asthma, community-acquired pneumonia in children,[79,80] and colorectal cancer patients.[81] Interestingly, NR1D family TFs, associated with Th17 cell regulation,[77,82] drive regulons in human T_{inn} cells. These factors are regulated by the circadian clock, suggesting that circadian rhythms might affect IL-17 production in T_{inn} cells, a hypothesis that warrants further investigation.

While many TFs essential for the human T_{inn} program are also expressed in mouse T_{inn} cells, there are notable exceptions such as *CEBPD*, *EOMES*, and *MYBL1*, which are highly expressed in human T_{inn} cells but barely detectable in mouse T_{inn}. CEBPD regulates CCR6 in human MAIT cells[83] and may play a crucial role in the human T_{inn} program. MYBL1 is expressed in human T_{inn} cells,[84] but its function remains to be defined. EOMES, essential for mouse iNKT cell development, shows low expression under steady-state conditions in mice[85,86] but is highly expressed in human T_{inn} cells. By contrast, T-bet is highly expressed in type 1 mouse T_{inn} cells and is essential for their development and functions.[86,87] However, human effector T_{inn} cells, which are most similar to mouse type 1 T_{inn} cells, express relatively low levels of T-bet. Instead, T-bet's expression and activity were correlated with the acquisition of the GEP6 program by T_{conv} cells in humans. These findings suggest the possibility of species-specific transcriptional regulation of T_{inn} cells, which could be relevant for their future therapeutic applications. Curiously, high-confidence regulons such as PLZF and Rorγt were not identified in the gene-regulatory network of human T_{inn} cells, possibly due to the relatively low gene detection in this context.

In the postnatal thymus, iNKT and MAIT cells display a transcriptional profile similar to that of developing conventional $CD4^+$ and $CD8^+$ T cells. Unlike conventional thymocytes selected by cTECs, murine iNKT and MAIT cells undergo selection by DP thymocytes via SLAM family receptors, leading to PLZF expression and effector differentiation.[61,88,89] A minor fraction of murine MAIT cells with a naive-like phenotype is TEC selected.[52] The corresponding expression patterns of CD1d on cTECs and DP thymocytes in both murine and human thymus suggests a similar selection of human iNKT thymocytes by cTECs or DP thymocytes. The expression of PLZF in non-effector iNKT cells, as observed through both scRNA-seq and flow cytometry, supports the hypothesis of DP selection. However, the initial selection process may not provide all necessary signals for complete maturation, as cells just experiencing positive selection are more akin to $CD4^+$ and $CD8^+$ T_{conv} cells. Additional signals may be required for human iNKT and MAIT cells to acquire effector functionalities. This hypothesis aligns with the prevalence of naive iNKT and MAIT cells in human cord blood and the gradual increase in effector T_{inn} cells with age.[41,42,90] Unlike murine T_{inn} cells, which use SLAMF6 and SLAMF1 to induce PLZF expression and effector maturation,[61] human thymocytes do not express SLAMF6, possibly affecting T_{inn} cell maturation. Additionally, human mTECs lack CD1D expression, which could also contribute to the variations in iNKT cell maturation observed in cross-species analyses.[19,63]

Our study highlights a distinct path taken by T_{inn} cells with an effector program in the human postnatal thymus, characterized by a mixed type 1/type 17 effector potential, contrasting with mice where T_{inn} cells split into multiple effector subsets. We did not observe specific clusters of proliferative human iNKT and MAIT thymocytes. In mice, proliferative thymic iNKT and MAIT cell clusters are identifiable[52,54,55] and reflect the proliferative burst following positive selection,[91] crucial for establishing a substantial T_{inn} cell pool. While T_{inn} cells constitute 1%–2% of thymocytes in mice, their proportion is much lower in pediatric humans. Moreover, our analysis did not reveal any type 2 T_{inn} cells in humans, unlike in mice, where thymus-resident iNKT2 cells significantly impact the thymic environment through IL-4 production.[17,18,63,92,93] The scarcity of type 2 T_{inn} cells in the human thymus suggests that these phenomena may be species specific or regulated by different cell types in humans.

Taken together, our findings hold significance in elucidating the diverse functional attributes of human T_{inn} cells and their potential applications in immunotherapeutic contexts.

Limitations of the study

Our study presents a comprehensive atlas of human T_{inn} cells in the thymus and blood, revealing a blended type 1 and type 17 transcriptional profile. However, there are several limitations to consider. We noted variations in effector cell percentages among donors, which may be influenced by factors such as age, sex, or immunological history. Additionally, our analysis focused on steady-state transcriptional profiles, leaving unclear how these profiles might change in various disease states. Comparing pediatric thymic T cells with adult blood samples introduces age-related differences that could impact transcriptional profiles. Ideally, matched samples would offer a more accurate comparison, but the limited availability of iNKT and MAIT cells in neonates presents challenges in obtaining sufficient cell quantities. Future research should explore thymus-derived fetal T_{inn} cells to investigate whether they exhibit specific type 1 and type 17 profiles akin to those described in mice. Recent studies on fetal $\gamma\delta$ T cells suggest that fetal T_{inn} cells might also develop unique transcriptional subsets.[25] Given that iNKT and MAIT cells appear from gestational weeks 18–23[94,95] and fetal hematopoietic stem and progenitor cells are predisposed to innate-like lymphocytes,[96] examining these cells could yield insights into their development and function. Furthermore, the potential for distinct waves of T_{inn} cells arising from fetal versus adult hematopoietic stem cells in mice[97] highlights the need for further investigation into their transcriptional differences.

RESOURCE AVAILABILITY

Lead contact

Further information and requests for resources and reagents should be directed to and will be fulfilled by the lead contact, Laurent Gapin (laurent.gapin@cuanschutz.edu).

Materials availability

This study did not generate new unique reagents.

Data and code availability

- Data that support the findings of this study, including the raw data and Seurat object, were deposited in NCBI GEO with the accession code GEO: GSE249684. The data from this study is also displayed as a ShinyCell application at https://xspeciestcells.cshl.edu/.
- The code used for all analyses presented in this study is publicly available on GitHub: https://github.com/meyer-lab-cshl/xspeciestcells. The code for the browser application can be found at https://github.com/meyer-lab-cshl/xspeciestcells-shiny.
- Any additional information required to reanalyze the data reported in this paper is available from the lead contact upon request.

ACKNOWLEDGMENTS

We thank members of our laboratories for thoughtful discussions and critical comments on the manuscript; Drs. Jennifer Matsuda, James Scott-Browne,

Ross Kedl, Jesse Gillis, Douglas Fearon, and Leslie Berg for critical comments and support; the Flow Core and the University of Colorado flow cytometry shared resource facility for assistance with cell sorting; Dr. Roberta Pelanda for the development of the Human Immune Tissue Network Biobank, the Clinical Research Support Team (CReST), and the Clinical and Translational Research Center (supported by NIH/NCATS Colorado CTSA grant UL1 TR002535) at the University of Colorado Anschutz Medical Campus; the Genomics Core at the University of Colorado Anschutz Medical Campus for sequencing and the National Institutes of Health core facility for CD1d and MR1-tetramers; Sarah Chapin for help in setting up the Shiny app; Eun Seo Park and Jong Kyoung Kim for sharing their mouse γδ T cells Seurat object; Daniel P. Caron and Donna L. Farber for sharing their across-tissues T cell AnnData object; and Ania Lorenc and Gosia Trynka for sharing their Seurat object of human peripheral blood T cells. This work was supported by National Institutes of Health grants R21AI163454 and R01AI130198 (to L.G.), R01AI158410 (to P.J.N.), and R01AI167862-01 (to H.M.). S.C. is supported through the Florence Gould and Annette Kade Fellowships with the Cold Spring Harbor Laboratory of Biological Sciences. This research was further supported by the Simons Center for Quantitative Biology at Cold Spring Harbor Laboratory, the Cold Spring Harbor Laboratory and Northwell Health Affiliation, and the Pershing Square Foundation. It was performed with assistance from the Cancer Center Pilot Awards Program and the CSHL Shared Resources, including the CSHL Flow Cytometry Shared Resource, which are supported by the Cancer Center support grant 5P30CA045508 as well as assistance from the NIH grant S10OD028632-01 at Cold Spring Harbor Laboratory. Computational infrastructure was supported by the Alpine HPC system, which is jointly funded by the University of Colorado Boulder, the University of Colorado Anschutz Medical Campus, Colorado State University, and the National Science Foundation (award 2201538). Additionally, this study was partly supported by the NIH P30CA046934 Bioinformatics and Biostatistics Shared Resource core at the University of Colorado Anschutz Medical Campus.

AUTHOR CONTRIBUTIONS

Conceptualization of this study was done by L.L., H.S.K., S.C., H.V.M., and L.G. Analysis of cells and tissues was done by L.L., S.C., J.D., A.S., Y.L., and J.T. Bioinformatics analysis and tool development were carried out by L.G., S.C., H.V.M., and T.B. Funding was acquired by H.V.M. and L.G. Key resources included human tissues from M.S., while some blood CD8 and γδ T cell scRNA-seq data were from W.P. and P.J.N. Supervision of the study was done by H.V.M. and L.G. Writing of the original drafts was done by S.C., H.V.M., and L.G., with review and editing by L.L., S.C., H.S.K., T.B., H.V.M., and L.G.

DECLARATION OF INTERESTS

The authors declare no competing interests.

DECLARATION OF GENERATIVE AI AND AI-ASSISTED TECHNOLOGIES IN THE WRITING PROCESS

During the preparation of this work the authors used ChatGPT in order to improve language and readability. After using this tool/service, the authors reviewed and edited the content as needed and take full responsibility for the content of the publication.

STAR★METHODS

Detailed methods are provided in the online version of this paper and include the following:

- KEY RESOURCES TABLE
- EXPERIMENTAL MODEL AND STUDY PARTICIPANT DETAILS
  - Mice
  - Human
- METHOD DETAILS
  - Murine thymus samples
  - Human thymus samples – Thymocytes
  - Human thymus samples – thymic epithelial cells
  - Human peripheral blood samples
  - Magnetic-bead enrichment of iNKT and MAIT cells
  - Fluorescence-activated cell sorting
  - Flow cytometry — Thymic and peripheral blood T cells
  - Flow cytometry -— CD1d, SLAMF1, SLAMF6
  - Single-cell RNA sequencing
  - Single-cell RNA-seq data analysis
  - LISI metric and analysis of cluster stability
  - TCR analysis
  - Identification of differentially expressed genes between clusters
  - Characterizing the replicability of cell types defined by scRNAseq between studies and between species
  - Identification of gene expression programs
  - Scoring of gene signatures
  - Gene regulatory network inference
  - Comparison of gene expression programs with gene signatures from the literature
  - Pseudo-bulk differential expression analysis
  - Creation of a reference scRNAseq mouse T_{inn} dataset
- QUANTIFICATION AND STATISTICAL ANALYSIS
  - Pseudo-bulk differential expression analysis in thymic samples
  - Pseudo-bulk differential expression analysis in PBMC samples
  - Comparison of GEPs with gene signatures from the literature

SUPPLEMENTAL INFORMATION

Supplemental information can be found online at https://doi.org/10.1016/j.celrep.2024.114705.

Received: May 13, 2024
Revised: July 23, 2024
Accepted: August 16, 2024
Published: September 10, 2024

REFERENCES

1. Sallusto, F., Lenig, D., Förster, R., Lipp, M., and Lanzavecchia, A. (1999). Two subsets of memory T lymphocytes with distinct homing potentials and effector functions. Nature *401*, 708–712. https://doi.org/10.1038/44385.
2. Kaech, S.M., and Cui, W. (2012). Transcriptional control of effector and memory CD8+ T cell differentiation. Nat. Rev. Immunol. *12*, 749–761. https://doi.org/10.1038/nri3307.
3. Jameson, S.C., and Masopust, D. (2018). Understanding Subset Diversity in T Cell Memory. Immunity *48*, 214–226. https://doi.org/10.1016/j.immuni.2018.02.010.
4. Godfrey, D.I., Uldrich, A.P., McCluskey, J., Rossjohn, J., and Moody, D.B. (2015). The burgeoning family of unconventional T cells. Nat. Immunol. *16*, 1114–1123. https://doi.org/10.1038/ni.3298.
5. Mayassi, T., Barreiro, L.B., Rossjohn, J., and Jabri, B. (2021). A multilayered immune system through the lens of unconventional T cells. Nature *595*, 501–510. https://doi.org/10.1038/s41586-021-03578-0.
6. Matsuda, J.L., Mallevaey, T., Scott-Browne, J., and Gapin, L. (2008). CD1d-restricted iNKT cells, the 'Swiss-Army knife' of the immune system. Curr. Opin. Immunol. *20*, 358–368. https://doi.org/10.1016/j.coi.2008.03.018.
7. Legoux, F., Salou, M., and Lantz, O. (2017). Unconventional or Preset alphabeta T Cells: Evolutionarily Conserved Tissue-Resident T Cells Recognizing Nonpeptidic Ligands. Annu. Rev. Cell Dev. Biol. *33*, 511–535. https://doi.org/10.1146/annurev-cellbio-100616-060725.
8. Kjer-Nielsen, L., Patel, O., Corbett, A.J., Le Nours, J., Meehan, B., Liu, L., Bhati, M., Chen, Z., Kostenko, L., Reantragoon, R., et al. (2012). MR1

presents microbial vitamin B metabolites to MAIT cells. Nature *491*, 717–723. https://doi.org/10.1038/nature11605.

9. Corbett, A.J., Eckle, S.B.G., Birkinshaw, R.W., Liu, L., Patel, O., Mahony, J., Chen, Z., Reantragoon, R., Meehan, B., Cao, H., et al. (2014). T-cell activation by transitory neo-antigens derived from distinct microbial pathways. Nature *509*, 361–365. https://doi.org/10.1038/nature13160.
10. Harly, C., Guillaume, Y., Nedellec, S., Peigné, C.M., Mönkkönen, H., Mönkkönen, J., Li, J., Kuball, J., Adams, E.J., Netzer, S., et al. (2012). Key implication of CD277/butyrophilin-3 (BTN3A) in cellular stress sensing by a major human gammadelta T-cell subset. Blood *120*, 2269–2279. https://doi.org/10.1182/blood-2012-05-430470.
11. Rigau, M., Ostrouska, S., Fulford, T.S., Johnson, D.N., Woods, K., Ruan, Z., McWilliam, H.E.G., Hudson, C., Tutuka, C., Wheatley, A.K., et al. (2020). Butyrophilin 2A1 is essential for phosphoantigen reactivity by gammadelta T cells. Science *367*, eaay5516. https://doi.org/10.1126/science.aay5516.
12. Karunakaran, M.M., Willcox, C.R., Salim, M., Paletta, D., Fichtner, A.S., Noll, A., Starick, L., Nohren, A., Begley, C.R., Berwick, K.A., et al. (2020). Butyrophilin-2A1 Directly Binds Germline-Encoded Regions of the Vgamma9Vdelta2 TCR and Is Essential for Phosphoantigen Sensing. Immunity *52*, 487–498.e486. https://doi.org/10.1016/j.immuni.2020.02.014.
13. Deseke, M., and Prinz, I. (2020). Ligand recognition by the gammadelta TCR and discrimination between homeostasis and stress conditions. Cell. Mol. Immunol. *17*, 914–924. https://doi.org/10.1038/s41423-020-0503-y.
14. Godfrey, D.I., Koay, H.F., McCluskey, J., and Gherardin, N.A. (2019). The biology and functional importance of MAIT cells. Nat. Immunol. *20*, 1110–1128. https://doi.org/10.1038/s41590-019-0444-8.
15. Hayday, A.C. (2019). gammadelta T Cell Update: Adaptate Orchestrators of Immune Surveillance. J. Immunol. *203*, 311–320. https://doi.org/10.4049/jimmunol.1800934.
16. Chandra, S., and Kronenberg, M. (2015). Activation and Function of iNKT and MAIT Cells. Adv. Immunol. *127*, 145–201. https://doi.org/10.1016/bs.ai.2015.03.003.
17. Lee, Y.J., Holzapfel, K.L., Zhu, J., Jameson, S.C., and Hogquist, K.A. (2013). Steady-state production of IL-4 modulates immunity in mouse strains and is determined by lineage diversity of iNKT cells. Nat. Immunol. *14*, 1146–1154. https://doi.org/10.1038/ni.2731.
18. Breed, E.R., Voboril, M., Ashby, K.M., Martinez, R.J., Qian, L., Wang, H., Salgado, O.C., O'Connor, C.H., and Hogquist, K.A. (2022). Type 2 cytokines in the thymus activate Sirpalpha(+) dendritic cells to promote clonal deletion. Nat. Immunol. *23*, 1042–1051. https://doi.org/10.1038/s41590-022-01218-x.
19. Cui, G., Shimba, A., Jin, J., Ogawa, T., Muramoto, Y., Miyachi, H., Abe, S., Asahi, T., Tani-Ichi, S., Dijkstra, J.M., et al. (2022). A circulating subset of iNKT cells mediates antitumor and antiviral immunity. Sci. Immunol. *7*, eabj8760. https://doi.org/10.1126/sciimmunol.abj8760.
20. Harly, C., Robert, J., Legoux, F., and Lantz, O. (2022). gammadelta T, NKT, and MAIT Cells During Evolution: Redundancy or Specialized Functions? J. Immunol. *209*, 217–225. https://doi.org/10.4049/jimmunol.2200105.
21. Leite-De-Moraes, M.C., Hameg, A., Arnould, A., Machavoine, F., Koezuka, Y., Schneider, E., Herbelin, A., and Dy, M. (1999). A distinct IL-18-induced pathway to fully activate NK T lymphocytes independently from TCR engagement. J. Immunol. *163*, 5871–5876.
22. Ussher, J.E., Bilton, M., Attwod, E., Shadwell, J., Richardson, R., de Lara, C., Mettke, E., Kurioka, A., Hansen, T.H., Klenerman, P., and Willberg, C.B. (2014). CD161++ CD8+ T cells, including the MAIT cell subset, are specifically activated by IL-12+IL-18 in a TCR-independent manner. Eur. J. Immunol. *44*, 195–203. https://doi.org/10.1002/eji.201343509.
23. Krovi, S.H., Loh, L., Spengler, A., Brunetti, T., and Gapin, L. (2022). Current insights in mouse iNKT and MAIT cell development using single cell transcriptomics data. Semin. Immunol. *60*, 101658. https://doi.org/10.1016/j.smim.2022.101658.
24. Baranek, T., de Amat Herbozo, C., Mallevaey, T., and Paget, C. (2022). Deconstructing iNKT cell development at single-cell resolution. Trends Immunol. *43*, 503–512. https://doi.org/10.1016/j.it.2022.04.012.
25. Sanchez Sanchez, G., Papadopoulou, M., Azouz, A., Tafesse, Y., Mishra, A., Chan, J.K.Y., Fan, Y., Verdebout, I., Porco, S., Libert, F., et al. (2022). Identification of distinct functional thymic programming of fetal and pediatric human gammadelta thymocytes via single-cell analysis. Nat. Commun. *13*, 5842. https://doi.org/10.1038/s41467-022-33488-2.
26. Crow, M., Paul, A., Ballouz, S., Huang, Z.J., and Gillis, J. (2018). Characterizing the replicability of cell types defined by single cell RNA-sequencing data using MetaNeighbor. Nat. Commun. *9*, 884. https://doi.org/10.1038/s41467-018-03282-0.
27. Park, J.E., Botting, R.A., Dominguez Conde, C., Popescu, D.M., Lavaert, M., Kunz, D.J., Goh, I., Stephenson, E., Ragazzini, R., Tuck, E., et al. (2020). A cell atlas of human thymic development defines T cell repertoire formation. Science *367*, eaay3224. https://doi.org/10.1126/science.aay3224.
28. Kotliar, D., Veres, A., Nagy, M.A., Tabrizi, S., Hodis, E., Melton, D.A., and Sabeti, P.C. (2019). Identifying gene expression programs of cell-type identity and cellular activity with single-cell RNA-Seq. Elife *8*, e43803. https://doi.org/10.7554/eLife.43803.
29. Dusseaux, M., Martin, E., Serriari, N., Péguillet, I., Premel, V., Louis, D., Milder, M., Le Bourhis, L., Soudais, C., Treiner, E., and Lantz, O. (2011). Human MAIT cells are xenobiotic-resistant, tissue-targeted, CD161hi IL-17-secreting T cells. Blood *117*, 1250–1259. https://doi.org/10.1182/blood-2010-08-303339.
30. Park, D., Kim, H.G., Kim, M., Park, T., Ha, H.H., Lee, D.H., Park, K.S., Park, S.J., Lim, H.J., and Lee, C.H. (2019). Differences in the molecular signatures of mucosal-associated invariant T cells and conventional T cells. Sci. Rep. *9*, 7094. https://doi.org/10.1038/s41598-019-43578-9.
31. Scott-Browne, J.P., Matsuda, J.L., Mallevaey, T., White, J., Borg, N.A., McCluskey, J., Rossjohn, J., Kappler, J., Marrack, P., and Gapin, L. (2007). Germline-encoded recognition of diverse glycolipids by natural killer T cells. Nat. Immunol. *8*, 1105–1113. https://doi.org/10.1038/ni1510.
32. Reantragoon, R., Kjer-Nielsen, L., Patel, O., Chen, Z., Illing, P.T., Bhati, M., Kostenko, L., Bharadwaj, M., Meehan, B., Hansen, T.H., et al. (2012). Structural insight into MR1-mediated recognition of the mucosal associated invariant T cell receptor. J. Exp. Med. *209*, 761–774. https://doi.org/10.1084/jem.20112095.
33. Young, M.H., U'Ren, L., Huang, S., Mallevaey, T., Scott-Browne, J., Crawford, F., Lantz, O., Hansen, T.H., Kappler, J., Marrack, P., and Gapin, L. (2013). MAIT cell recognition of MR1 on bacterially infected and uninfected cells. PLoS One *8*, e53789. https://doi.org/10.1371/journal.pone.0053789.
34. Reantragoon, R., Corbett, A.J., Sakala, I.G., Gherardin, N.A., Furness, J.B., Chen, Z., Eckle, S.B.G., Uldrich, A.P., Birkinshaw, R.W., Patel, O., et al. (2013). Antigen-loaded MR1 tetramers define T cell receptor heterogeneity in mucosal-associated invariant T cells. J. Exp. Med. *210*, 2305–2320. https://doi.org/10.1084/jem.20130958.
35. Tilloy, F., Treiner, E., Park, S.H., Garcia, C., Lemonnier, F., de la Salle, H., Bendelac, A., Bonneville, M., and Lantz, O. (1999). An invariant T cell receptor alpha chain defines a novel TAP-independent major histocompatibility complex class Ib-restricted alpha/beta T cell subpopulation in mammals. J. Exp. Med. *189*, 1907–1921. https://doi.org/10.1084/jem.189.12.1907.
36. Davey, M.S., Willcox, C.R., Hunter, S., Kasatskaya, S.A., Remmerswaal, E.B.M., Salim, M., Mohammed, F., Bemelman, F.J., Chudakov, D.M., Oo, Y.H., and Willcox, B.E. (2018). The human Vdelta2(+) T-cell compartment comprises distinct innate-like Vgamma9(+) and adaptive Vgamma9(-) subsets. Nat. Commun. *9*, 1760. https://doi.org/10.1038/s41467-018-04076-0.

37. Cano-Gamez, E., Soskic, B., Roumeliotis, T.I., So, E., Smyth, D.J., Baldrighi, M., Willé, D., Nakic, N., Esparza-Gordillo, J., Larminie, C.G.C., et al. (2020). Single-cell transcriptomics identifies an effectorness gradient shaping the response of CD4(+) T cells to cytokines. Nat. Commun. *11*, 1801. https://doi.org/10.1038/s41467-020-15543-y.

38. Rose, J.R., Akdogan-Ozdilek, B., Rahmberg, A.R., Powell, M.D., Hicks, S.L., Scharer, C.D., and Boss, J.M. (2023). Distinct transcriptomic and epigenomic modalities underpin human memory T cell subsets and their activation potential. Commun. Biol. *6*, 363. https://doi.org/10.1038/s42003-023-04747-9.

39. Poon, M.M.L., Caron, D.P., Wang, Z., Wells, S.B., Chen, D., Meng, W., Szabo, P.A., Lam, N., Kubota, M., Matsumoto, R., et al. (2023). Tissue adaptation and clonal segregation of human memory T cells in barrier sites. Nat. Immunol. *24*, 309–319. https://doi.org/10.1038/s41590-022-01395-9.

40. Terekhova, M., Swain, A., Bohacova, P., Aladyeva, E., Arthur, L., Laha, A., Mogilenko, D.A., Burdess, S., Sukhov, V., Kleverov, D., et al. (2023). Single-cell atlas of healthy human blood unveils age-related loss of NKG2C(+)GZMB(-)CD8(+) memory T cells and accumulation of type 2 memory T cells. Immunity *56*, 2836–2854.e9. https://doi.org/10.1016/j.immuni.2023.10.013.

41. Berzins, S.P., Cochrane, A.D., Pellicci, D.G., Smyth, M.J., and Godfrey, D.I. (2005). Limited correlation between human thymus and blood NKT cell content revealed by an ontogeny study of paired tissue samples. Eur. J. Immunol. *35*, 1399–1407. https://doi.org/10.1002/eji.200425958.

42. Sandberg, J.K., Stoddart, C.A., Brilot, F., Jordan, K.A., and Nixon, D.F. (2004). Development of innate CD4+ alpha-chain variable gene segment 24 (Valpha24) natural killer T cells in the early human fetal thymus is regulated by IL-7. Proc. Natl. Acad. Sci. USA *101*, 7058–7063. https://doi.org/10.1073/pnas.0305986101.

43. Li, J., Lu, E., Yi, T., and Cyster, J.G. (2016). EBI2 augments Tfh cell fate by promoting interaction with IL-2-quenching dendritic cells. Nature *533*, 110–114. https://doi.org/10.1038/nature17947.

44. Zwijnenburg, A.J., Pokharel, J., Varnaite, R., Zheng, W., Hoffer, E., Shryki, I., Comet, N.R., Ehrstrom, M., Gredmark-Russ, S., Eidsmo, L., and Gerlach, C. (2023). Graded expression of the chemokine receptor CX3CR1 marks differentiation states of human and murine T cells and enables cross-species interpretation. Immunity *56*, 1955–1974.e1910. https://doi.org/10.1016/j.immuni.2023.06.025.

45. Jonsson, A.H., Zhang, F., Dunlap, G., Gomez-Rivas, E., Watts, G.F.M., Faust, H.J., Rupani, K.V., Mears, J.R., Meednu, N., Wang, R., et al. (2022). Granzyme K(+) CD8 T cells form a core population in inflamed human tissue. Sci. Transl. Med. *14*, eabo0686. https://doi.org/10.1126/scitranslmed.abo0686.

46. Duquette, D., Harmon, C., Zaborowski, A., Michelet, X., O'Farrelly, C., Winter, D., Koay, H.F., and Lynch, L. (2023). Human Granzyme K Is a Feature of Innate T Cells in Blood, Tissues, and Tumors, Responding to Cytokines Rather than TCR Stimulation. J. Immunol. *211*, 633–647. https://doi.org/10.4049/jimmunol.2300083.

47. Aibar, S., González-Blas, C.B., Moerman, T., Huynh-Thu, V.A., Imrichova, H., Hulselmans, G., Rambow, F., Marine, J.C., Geurts, P., Aerts, J., et al. (2017). SCENIC: single-cell regulatory network inference and clustering. Nat. Methods *14*, 1083–1086. https://doi.org/10.1038/nmeth.4463.

48. Intlekofer, A.M., Takemoto, N., Wherry, E.J., Longworth, S.A., Northrup, J.T., Palanivel, V.R., Mullen, A.C., Gasink, C.R., Kaech, S.M., Miller, J.D., et al. (2005). Effector and memory CD8+ T cell fate coupled by T-bet and eomesodermin. Nat. Immunol. *6*, 1236–1244. https://doi.org/10.1038/ni1268.

49. Klein-Hessling, S., Muhammad, K., Klein, M., Pusch, T., Rudolf, R., Flöter, J., Qureischi, M., Beilhack, A., Vaeth, M., Kummerow, C., et al. (2017). NFATc1 controls the cytotoxicity of CD8(+) T cells. Nat. Commun. *8*, 511. https://doi.org/10.1038/s41467-017-00612-6.

50. Nah, J., and Seong, R.H. (2022). Kruppel-like factor 4 regulates the cytolytic effector function of exhausted CD8 T cells. Sci. Adv. *8*, eadc9346. https://doi.org/10.1126/sciadv.adc9346.

51. Lee, M., Lee, E., Han, S.K., Choi, Y.H., Kwon, D.I., Choi, H., Lee, K., Park, E.S., Rha, M.S., Joo, D.J., et al. (2020). Single-cell RNA sequencing identifies shared differentiation paths of mouse thymic innate T cells. Nat. Commun. *11*, 4367. https://doi.org/10.1038/s41467-020-18155-8.

52. Legoux, F., Gilet, J., Procopio, E., Echasserieau, K., Bernardeau, K., and Lantz, O. (2019). Molecular mechanisms of lineage decisions in metabolite-specific T cells. Nat. Immunol. *20*, 1244–1255. https://doi.org/10.1038/s41590-019-0465-3.

53. Koay, H.F., Su, S., Amann-Zalcenstein, D., Daley, S.R., Comerford, I., Miosge, L., Whyte, C.E., Konstantinov, I.E., d'Udekem, Y., Baldwin, T., et al. (2019). A divergent transcriptional landscape underpins the development and functional branching of MAIT cells. Sci. Immunol. *4*, eaay6039. https://doi.org/10.1126/sciimmunol.aay6039.

54. Baranek, T., Lebrigand, K., de Amat Herbozo, C., Gonzalez, L., Bogard, G., Dietrich, C., Magnone, V., Boisseau, C., Jouan, Y., Trottein, F., et al. (2020). High Dimensional Single-Cell Analysis Reveals iNKT Cell Developmental Trajectories and Effector Fate Decision. Cell Rep. *32*, 108116. https://doi.org/10.1016/j.celrep.2020.108116.

55. Harsha Krovi, S., Zhang, J., Michaels-Foster, M.J., Brunetti, T., Loh, L., Scott-Browne, J., and Gapin, L. (2020). Thymic iNKT single cell analyses unmask the common developmental program of mouse innate T cells. Nat. Commun. *11*, 6238. https://doi.org/10.1038/s41467-020-20073-8.

56. Maas-Bauer, K., Lohmeyer, J.K., Hirai, T., Ramos, T.L., Fazal, F.M., Litzenburger, U.M., Yost, K.E., Ribado, J.V., Kambham, N., Wenokur, A.S., et al. (2021). Invariant natural killer T-cell subsets have diverse graft-versus-host-disease-preventing and antitumor effects. Blood *138*, 858–870. https://doi.org/10.1182/blood.2021010887.

57. Wang, J., Adrianto, I., Subedi, K., Liu, T., Wu, X., Yi, Q., Loveless, I., Yin, C., Datta, I., Sant'Angelo, D.B., et al. (2023). Integrative scATAC-seq and scRNA-seq analyses map thymic iNKT cell development and identify Cbfbeta for its commitment. Cell Discov. *9*, 61. https://doi.org/10.1038/s41421-023-00547-x.

58. Li, Z., Yang, Q., Tang, X., Chen, Y., Wang, S., Qi, X., Zhang, Y., Liu, Z., Luo, J., Liu, H., et al. (2022). Single-cell RNA-seq and chromatin accessibility profiling decipher the heterogeneity of mouse gammadelta T cells. Sci. Bull. *67*, 408–426. https://doi.org/10.1016/j.scib.2021.11.013.

59. Chandra, S., Ascui, G., Riffelmacher, T., Chawla, A., Ramírez-Suástegui, C., Castelan, V.C., Seumois, G., Simon, H., Murray, M.P., Seo, G.Y., et al. (2023). Transcriptomes and metabolism define mouse and human MAIT cell populations. Sci. Immunol. *8*, eabn8531. https://doi.org/10.1126/sciimmunol.abn8531.

60. Salou, M., Legoux, F., and Lantz, O. (2021). MAIT cell development in mice and humans. Mol. Immunol. *130*, 31–36. https://doi.org/10.1016/j.molimm.2020.12.003.

61. Griewank, K., Borowski, C., Rietdijk, S., Wang, N., Julien, A., Wei, D.G., Mamchak, A.A., Terhorst, C., and Bendelac, A. (2007). Homotypic interactions mediated by Slamf1 and Slamf6 receptors control NKT cell lineage development. Immunity *27*, 751–762. https://doi.org/10.1016/j.immuni.2007.08.020.

62. Forestier, C., Park, S.H., Wei, D., Benlagha, K., Teyton, L., and Bendelac, A. (2003). T cell development in mice expressing CD1d directed by a classical MHC class II promoter. J. Immunol. *171*, 4096–4104. https://doi.org/10.4049/jimmunol.171.8.4096.

63. White, A.J., Jenkinson, W.E., Cowan, J.E., Parnell, S.M., Bacon, A., Jones, N.D., Jenkinson, E.J., and Anderson, G. (2014). An essential role for medullary thymic epithelial cells during the intrathymic development of invariant NKT cells. J. Immunol. *192*, 2659–2666. https://doi.org/10.4049/jimmunol.1303057.

64. Delfanti, G., Cortesi, F., Perini, A., Antonini, G., Azzimonti, L., de Lalla, C., Garavaglia, C., Squadrito, M.L., Fedeli, M., Consonni, M., et al. (2022). TCR-engineered iNKT cells induce robust antitumor response by dual

targeting cancer and suppressive myeloid cells. Sci. Immunol. *7*, eabn6563. https://doi.org/10.1126/sciimmunol.abn6563.

65. Dogan, M., Karhan, E., Kozhaya, L., Placek, L., Chen, X., Yigit, M., and Unutmaz, D. (2022). Engineering Human MAIT Cells with Chimeric Antigen Receptors for Cancer Immunotherapy. J. Immunol. *209*, 1523–1531. https://doi.org/10.4049/jimmunol.2100856.

66. Lee, D., Dunn, Z.S., Guo, W., Rosenthal, C.J., Penn, N.E., Yu, Y., Zhou, K., Li, Z., Ma, F., Li, M., et al. (2023). Unlocking the potential of allogeneic Vdelta2 T cells for ovarian cancer therapy through CD16 biomarker selection and CAR/IL-15 engineering. Nat. Commun. *14*, 6942. https://doi.org/10.1038/s41467-023-42619-2.

67. Philippot, Q., Ogishi, M., Bohlen, J., Puchan, J., Arias, A.A., Nguyen, T., Martin-Fernandez, M., Conil, C., Rinchai, D., Momenilandi, M., et al. (2023). Human IL-23 is essential for IFN-gamma-dependent immunity to mycobacteria. Sci. Immunol. *8*, eabq5204. https://doi.org/10.1126/sciimmunol.abq5204.

68. D'Angelo, M.E., Bird, P.I., Peters, C., Reinheckel, T., Trapani, J.A., and Sutton, V.R. (2010). Cathepsin H is an additional convertase of pro-granzyme B. J. Biol. Chem. *285*, 20514–20519. https://doi.org/10.1074/jbc.M109.094573.

69. Kurioka, A., Ussher, J.E., Cosgrove, C., Clough, C., Fergusson, J.R., Smith, K., Kang, Y.H., Walker, L.J., Hansen, T.H., Willberg, C.B., and Klenerman, P. (2015). MAIT cells are licensed through granzyme exchange to kill bacterially sensitized targets. Mucosal Immunol. *8*, 429–440. https://doi.org/10.1038/mi.2014.81.

70. Kaiserman, D., Zhao, P., Rowe, C.L., Leong, A., Barlow, N., Joeckel, L.T., Hitchen, C., Stewart, S.E., Hollenberg, M.D., Bunnett, N., et al. (2022). Granzyme K initiates IL-6 and IL-8 release from epithelial cells by activating protease-activated receptor 2. PLoS One *17*, e0270584. https://doi.org/10.1371/journal.pone.0270584.

71. Jonsson, A., Donado, C., Theisen, E., Jones, D., Nathan, A., Zhang, F., Raychaudhuri, S., and Brenner, M. (2023). Accelerating Medicines Partnership (AMP) RA/SLE. Granzyme K Elicits a New Pathway for Complement Activation in RA Synovium [abstract]. Arthritis Rheumatol. *75*, (*Suppl 9*).

72. Matsuda, J.L., Gapin, L., Baron, J.L., Sidobre, S., Stetson, D.B., Mohrs, M., Locksley, R.M., and Kronenberg, M. (2003). Mouse V alpha 14i natural killer T cells are resistant to cytokine polarization in vivo. Proc. Natl. Acad. Sci. USA *100*, 8395–8400. https://doi.org/10.1073/pnas.1332805100.

73. Govindarajan, S., Gaublomme, D., Van der Cruyssen, R., Verheugen, E., Van Gassen, S., Saeys, Y., Tavernier, S., Iwawaki, T., Bloch, Y., Savvides, S.N., et al. (2018). Stabilization of cytokine mRNAs in iNKT cells requires the serine-threonine kinase IRE1alpha. Nat. Commun. *9*, 5340. https://doi.org/10.1038/s41467-018-07758-x.

74. Istaces, N., Splittgerber, M., Lima Silva, V., Nguyen, M., Thomas, S., Le, A., Achouri, Y., Calonne, E., Defrance, M., Fuks, F., et al. (2019). EOMES interacts with RUNX3 and BRG1 to promote innate memory cell formation through epigenetic reprogramming. Nat. Commun. *10*, 3306. https://doi.org/10.1038/s41467-019-11233-6.

75. Yu, J.S., Hamada, M., Ohtsuka, S., Yoh, K., Takahashi, S., and Miaw, S.C. (2017). Differentiation of IL-17-Producing Invariant Natural Killer T Cells Requires Expression of the Transcription Factor c-Maf. Front. Immunol. *8*, 1399. https://doi.org/10.3389/fimmu.2017.01399.

76. Ciofani, M., Madar, A., Galan, C., Sellars, M., Mace, K., Pauli, F., Agarwal, A., Huang, W., Parkhurst, C.N., Muratet, M., et al. (2012). A validated regulatory network for Th17 cell specification. Cell *151*, 289–303. https://doi.org/10.1016/j.cell.2012.09.016.

77. Chang, C., Loo, C.S., Zhao, X., Solt, L.A., Liang, Y., Bapat, S.P., Cho, H., Kamenecka, T.M., Leblanc, M., Atkins, A.R., et al. (2019). The nuclear receptor REV-ERBalpha modulates Th17 cell-mediated autoimmune disease. Proc. Natl. Acad. Sci. USA *116*, 18528–18536. https://doi.org/10.1073/pnas.1907563116.

78. Garner, L.C., Amini, A., FitzPatrick, M.E.B., Lett, M.J., Hess, G.F., Filipowicz Sinnreich, M., Provine, N.M., and Klenerman, P. (2023). Single-cell analysis of human MAIT cell transcriptional, functional and clonal diversity. Nat. Immunol. *24*, 1565–1578. https://doi.org/10.1038/s41590-023-01575-1.

79. Lezmi, G., Abou-Taam, R., Garcelon, N., Dietrich, C., Machavoine, F., Delacourt, C., Adel-Patient, K., and Leite-de-Moraes, M. (2019). Evidence for a MAIT-17-high phenotype in children with severe asthma. J. Allergy Clin. Immunol. *144*, 1714–1716.e6. https://doi.org/10.1016/j.jaci.2019.08.003.

80. Lu, B., Liu, M., Wang, J., Fan, H., Yang, D., Zhang, L., Gu, X., Nie, J., Chen, Z., Corbett, A.J., et al. (2020). IL-17 production by tissue-resident MAIT cells is locally induced in children with pneumonia. Mucosal Immunol. *13*, 824–835. https://doi.org/10.1038/s41385-020-0273-y.

81. Borras, D.M., Verbandt, S., Ausserhofer, M., Sturm, G., Lim, J., Verge, G.A., Vanmeerbeek, I., Laureano, R.S., Govaerts, J., Sprooten, J., et al. (2023). Single cell dynamics of tumor specificity vs bystander activity in CD8(+) T cells define the diverse immune landscapes in colorectal cancer. Cell Discov *9*, 114. https://doi.org/10.1038/s41421-023-00605-4.

82. Yu, X., Rollins, D., Ruhn, K.A., Stubblefield, J.J., Green, C.B., Kashiwada, M., Rothman, P.B., Takahashi, J.S., and Hooper, L.V. (2013). TH17 cell differentiation is regulated by the circadian clock. Science *342*, 727–730. https://doi.org/10.1126/science.1243884.

83. Lee, C.H., Zhang, H.H., Singh, S.P., Koo, L., Kabat, J., Tsang, H., Singh, T.P., and Farber, J.M. (2018). C/EBPdelta drives interactions between human MAIT cells and endothelial cells that are important for extravasation. Elife *7*, e32532. https://doi.org/10.7554/eLife.32532.

84. Gutierrez-Arcelus, M., Teslovich, N., Mola, A.R., Polidoro, R.B., Nathan, A., Kim, H., Hannes, S., Slowikowski, K., Watts, G.F.M., Korsunsky, I., et al. (2019). Lymphocyte innateness defined by transcriptional states reflects a balance between proliferation and effector functions. Nat. Commun. *10*, 687. https://doi.org/10.1038/s41467-019-08604-4.

85. Shimizu, K., Sato, Y., Kawamura, M., Nakazato, H., Watanabe, T., Ohara, O., and Fujii, S.I. (2019). Eomes transcription factor is required for the development and differentiation of invariant NKT cells. Commun. Biol. *2*, 150. https://doi.org/10.1038/s42003-019-0389-3.

86. Townsend, M.J., Weinmann, A.S., Matsuda, J.L., Salomon, R., Farnham, P.J., Biron, C.A., Gapin, L., and Glimcher, L.H. (2004). T-bet Regulates the Terminal Maturation and Homeostasis of NK and Vα14i NKT Cells. Immunity *20*, 477–494. https://doi.org/10.1016/s1074-7613(04)00076-7.

87. Matsuda, J.L., Zhang, Q., Ndonye, R., Richardson, S.K., Howell, A.R., and Gapin, L. (2006). T-bet concomitantly controls migration, survival, and effector functions during the development of Valpha14i NKT cells. Blood *107*, 2797–2805. https://doi.org/10.1182/blood-2005-08-3103.

88. Bendelac, A. (1995). Positive selection of mouse NK1+ T cells by CD1-expressing cortical thymocytes. J. Exp. Med. *182*, 2091–2096. https://doi.org/10.1084/jem.182.6.2091.

89. Coles, M.C., and Raulet, D.H. (2000). NK1.1+ T cells in the liver arise in the thymus and are selected by interactions with class I molecules on CD4+CD8+ cells. J. Immunol. *164*, 2412–2418. https://doi.org/10.4049/jimmunol.164.5.2412.

90. Ben Youssef, G., Tourret, M., Salou, M., Ghazarian, L., Houdouin, V., Mondot, S., Mburu, Y., Lambert, M., Azarnoush, S., Diana, J.S., et al. (2018). Ontogeny of human mucosal-associated invariant T cells and related T cell subsets. J. Exp. Med. *215*, 459–479. https://doi.org/10.1084/jem.20171739.

91. Benlagha, K., Kyin, T., Beavis, A., Teyton, L., and Bendelac, A. (2002). A thymic precursor to the NK T cell lineage. Science *296*, 553–555. https://doi.org/10.1126/science.1069017.

92. White, A.J., Baik, S., Parnell, S.M., Holland, A.M., Brombacher, F., Jenkinson, W.E., and Anderson, G. (2017). A type 2 cytokine axis for thymus emigration. J. Exp. Med. *214*, 2205–2216. https://doi.org/10.1084/jem.20170271.

93. Weinreich, M.A., Odumade, O.A., Jameson, S.C., and Hogquist, K.A. (2010). T cells expressing the transcription factor PLZF regulate the development of memory-like CD8+ T cells. Nat. Immunol. *11*, 709–716. https://doi.org/10.1038/ni.1898.

94. Loh, L., Ivarsson, M.A., Michaëlsson, J., Sandberg, J.K., and Nixon, D.F. (2014). Invariant natural killer T cells developing in the human fetus accumulate and mature in the small intestine. Mucosal Immunol. *7*, 1233–1243. https://doi.org/10.1038/mi.2014.13.

95. Leeansyah, E., Loh, L., Nixon, D.F., and Sandberg, J.K. (2014). Acquisition of innate-like microbial reactivity in mucosal tissues during human fetal MAIT-cell development. Nat. Commun. *5*, 3143. https://doi.org/10.1038/ncomms4143.

96. Yuan, J., Nguyen, C.K., Liu, X., Kanellopoulou, C., and Muljo, S.A. (2012). Lin28b reprograms adult bone marrow hematopoietic progenitors to mediate fetal-like lymphopoiesis. Science *335*, 1195–1200. https://doi.org/10.1126/science.1216557.

97. Rudd, B.D. (2020). Neonatal T Cells: A Reinterpretation. Annu. Rev. Immunol. *38*, 229–247. https://doi.org/10.1146/annurev-immunol-091319-083608.

98. Rouse, R.V., Bolin, L.M., Bender, J.R., and Kyewski, B.A. (1988). Monoclonal antibodies reactive with subsets of mouse and human thymic epithelial cells. J. Histochem. Cytochem. *36*, 1511–1517. https://doi.org/10.1177/36.12.2461413.

99. Chen, Y.H., Chiu, N.M., Mandal, M., Wang, N., and Wang, C.R. (1997). Impaired NK1+ T cell development and early IL-4 production in CD1-deficient mice. Immunity *6*, 459–467. https://doi.org/10.1016/s1074-7613(00)80289-7.

100. McCarthy, D.J., Campbell, K.R., Lun, A.T.L., and Wills, Q.F. (2017). Scater: pre-processing, quality control, normalization and visualization of single-cell RNA-seq data in R. Bioinformatics *33*, 1179–1186. https://doi.org/10.1093/bioinformatics/btw777.

101. Korsunsky, I., Millard, N., Fan, J., Slowikowski, K., Zhang, F., Wei, K., Baglaenko, Y., Brenner, M., Loh, P.R., and Raychaudhuri, S. (2019). Fast, sensitive and accurate integration of single-cell data with Harmony. Nat. Methods *16*, 1289–1296. https://doi.org/10.1038/s41592-019-0619-0.

102. Blanco-Carmona, E. (2022). Generating publication ready visualizations for Single Cell transcriptomics using SCpubr. bioRxiv. https://doi.org/10.1101/2022.02.28.482303.

103. Gu, Z., Gu, L., Eils, R., Schlesner, M., and Brors, B. (2014). circlize Implements and enhances circular visualization in R. Bioinformatics *30*, 2811–2812. https://doi.org/10.1093/bioinformatics/btu393.

104. Wagih, O. (2017). ggseqlogo: a versatile R package for drawing sequence logos. Bioinformatics *33*, 3645–3647. https://doi.org/10.1093/bioinformatics/btx469.

105. Durinck, S., Spellman, P.T., Birney, E., and Huber, W. (2009). Mapping identifiers for the integration of genomic datasets with the R/Bioconductor package biomaRt. Nat. Protoc. *4*, 1184–1191. https://doi.org/10.1038/nprot.2009.97.

106. Durinck, S., Moreau, Y., Kasprzyk, A., Davis, S., De Moor, B., Brazma, A., and Huber, W. (2005). BioMart and Bioconductor: a powerful link between biological databases and microarray data analysis. Bioinformatics *21*, 3439–3440. https://doi.org/10.1093/bioinformatics/bti525.

107. Brunson, J.C. (2020). ggalluvial: Layered Grammar for Alluvial Plots. J. Open Source Softw. *5*, 2017. https://doi.org/10.21105/joss.02017.

108. Moerman, T., Aibar Santos, S., Bravo González-Blas, C., Simm, J., Moreau, Y., Aerts, J., and Aerts, S. (2019). GRNBoost2 and Arboreto: efficient and scalable inference of gene regulatory networks. Bioinformatics *35*, 2159–2161. https://doi.org/10.1093/bioinformatics/bty916.

109. Love, M.I., Huber, W., and Anders, S. (2014). Moderated estimation of fold change and dispersion for RNA-seq data with DESeq2. Genome Biol. *15*, 550. https://doi.org/10.1186/s13059-014-0550-8.

110. Ritchie, M.E., Phipson, B., Wu, D., Hu, Y., Law, C.W., Shi, W., and Smyth, G.K. (2015). limma powers differential expression analyses for RNA-sequencing and microarray studies. Nucleic Acids Res. *43*, e47. https://doi.org/10.1093/nar/gkv007.

111. Haghverdi, L., Lun, A.T.L., Morgan, M.D., and Marioni, J.C. (2018). Batch effects in single-cell RNA-sequencing data are corrected by matching mutual nearest neighbors. Nat. Biotechnol. *36*, 421–427. https://doi.org/10.1038/nbt.4091.

112. Germain, P.L., Lun, A., Garcia Meixide, C., Macnair, W., and Robinson, M.D. (2021). Doublet identification in single-cell sequencing data using scDblFinder. F1000Res. *10*, 979. https://doi.org/10.12688/f1000research.73600.2.

STAR★METHODS

KEY RESOURCES TABLE

REAGENT or RESOURCE	SOURCE	IDENTIFIER
Antibodies		
Human PBS57 CD1d tetramer PE	NIH tetramer core facility	N/A
Human 5-OP-RU MR1 tetramer PE	NIH tetramer core facility	N/A
Anti-human CCR7 – APC-Fire810 (clone G043H7)	Biolegend	Cat#353263; RRID: AB_2894483
Anti-human CD1d – PE (clone 51.1)	Biolegend	Cat#350305; RRID: AB_10642028
Anti-human CD3 purified (clone UCHT1)	Biolegend	Cat#300402; RRID: AB_314056
Anti-human CD3 – AF488 (clone OKT3)	Biolegend	Cat#317310; RRID: AB_571877
Anti-human CD3 – BUV496 (clone UCHT1)	BD Biosciences	Cat#612941; RRID: AB_2916883
Anti-human CD4 purified (clone RPA-T4)	Biolegend	Cat#300570; RRID: AB_2810427
Anti-human CD4 – AF488 (clone OKT4)	Thermo Fisher Scientific	Cat#53-0048-42; RRID: AB_10735503
Anti-human CD4 – redFluor710 (clone OKT4)	Tonbo biosciences	Cat#80–0048; RRID: AB_2621976
Anti-human CD4 – BV570 (clone RPA-T4)	Biolegend	Cat# 300533; RRID: AB_10896788
Anti-human CD8α purified (clone RPA-T8)	Biolegend	Cat#301002; RRID: AB_314120
Anti-human CD8α – APC (clone RPA-T8)	Thermo Fisher Scientific	Cat#17-0088-42; RRID: AB_10669564
Anti-human CD8α – BUV395 (clone RPA-T8)	BD Biosciences	Cat#563795; RRID: AB_2722501
Anti-human CD8α – PE-Cy7 (clone SK1)	Tonbo biosciences	Cat#60–0087; RRID: AB_3106994
Anti-human CD14 – eFluor450 (clone 61D3)	Thermo Fisher Scientific	Cat#48-0149-42; RRID: AB_1272050
Anti-human CD14 – PE-Cy5 (clone 61D3)	Thermo Fisher Scientific	Cat#15-0149-42; RRID: AB_2573058
Anti-human CD19 – eFluor450 (clone H1B19)	Thermo Fisher Scientific	Cat#48-0199-42; RRID: AB_1272053
Anti-human CD19 – PE-Cy5 (clone H1B19)	Thermo Fisher Scientific	Cat#15-0199-42; RRID: AB_10853658
Anti-human CD45 purified (clone HI30)	Biolegend	Cat#304002; RRID: AB_314390
Anti-human CD45 – AF647 (clone QA17A19)	Biolegend	Cat#393406; RRID: AB_2750083
Anti-human CD45 – BV421 (clone HI30)	Biolegend	Cat#304032; RRID: AB_2561357
Anti-human CD62L – BV650 (clone DREG-56)	Biolegend	Cat#304832; RRID: AB_2563821
Anti-human CD161 – BUV805 (clone HP-3G10)	BD Biosciences	Cat#749221; RRID: AB_2873599
Anti-human CD235a (clone HI264)	Biolegend	Cat#349102; RRID: AB_10612565
Anti-human Eomes – BUV737 (clone X4-83)	BD Horizon	Cat# 567170; RRID: AB_2916487
Anti-human EPCAM – BV421 (clone 9C4)	Biolegend	Cat#324220; RRID: AB_2563847
Anti-human GZMB – AF700 (clone GB11)	BD Biosciences	Cat#560213; RRID: AB_1645453
Anti-human GZMK – eFluor660 (clone G3H69)	Thermo Fisher Scientific	Cat#50-8897-42; RRID: AB_2574299
Anti-human HLADR – BV711 (clone L243)	Biolegend	Cat#307643; RRID: AB_11218794
Anti-human PLZF – PE-CF594 (clone R17-809)	BD Horizon	Cat#565738; RRID: AB_2739339
Anti-human T-bet – BV605 (clone 4B10)	Biolegend	Cat#644817; RRID: AB_11219388
Anti-human TCR γδ – BV650 (clone 11F2)	BD Biosciences	Cat#569510; RRID: AB_3106997
Anti-human Vα7.2 – BV785 (clone 3C10)	Biolegend	Cat#351721; RRID: AB_2566041
Anti-human Vα24 – PerCP-Cy5.5 (clone C15)	Biolegend	Cat#360004; RRID: AB_2562495
Anti-human Vδ1 – PerCP-Vio700 (clone REA173)	Miltenyi Biotec	Cat#130-120-441; RRID: AB_2784469
Anti-human Vδ2 – FITC (clone 123R3)	Miltenyi Biotec	Cat#130-125-095; RRID: AB_2819745
Anti-human Vγ9 – PE (clone B3)	BD Biosciences	Cat#555733; RRID: AB_396076
CDR2 purified[98]	Dr. Sheena Pinto	N/A
Anti-mouse CD1d – PE (clone 1B1)	Biolegend	Cat#123509; RRID: AB_1236547
Anti-mouse CD4 – AF488 (clone GK1.5)	Biolegend	Cat#100423; RRID: AB_389302
Anti-mouse CD8α – APC (clone 53–6.7)	Biolegend	Cat#100711; RRID: AB_312750
Anti-mouse CD45 (clone 30-F11)	Thermo Fisher Scientific	Cat#14-0451-85; RRID: AB_467252

(*Continued on next page*)

Continued

REAGENT or RESOURCE	SOURCE	IDENTIFIER
Anti-mouse CD45 – BV605 (clone 30-F11)	Biolegend	Cat#103139; RRID: AB_2562341
Anti-mouse CD90.2 purified (clone 53–2.1)	Biolegend	Cat#140302; RRID: AB_10641692
Anti-mouse EpCAM – BV421 (clone G8.8)	Biolegend	Cat#118225; RRID: AB_2563983
Goat anti-mouse IgG	Vector Laboratories	Cat#AI-9200-1.5; RRID: AB_3107016
Anti-mouse Ly51 – AF647 (clone 6C3)	Biolegend	Cat#108312; RRID: AB_2099613
Goat anti-rat IgG	Vector Laboratories	Cat#BA-9400-1.5; RRID: AB_3107017
Human Fc receptor blocking FcγR block	Miltenyi Biotec	Cat# 130-059-901; RRID: AB_2892112
Human Fc receptor blocking TruStain FcX	Biolegend	Cat#422302; RRID: AB_2818986
Mouse Fc receptor blocking anti-CD16/32 (clone 93)	Thermo Fisher Scientific	Cat#14-0161-85; RRID: AB_467134
UEA1 – FITC	Vector Laboratories	Cat#FL-1061; RRID: AB_2336767
Human Single Cell Sample Multiplexing Kit	BD Biosciences	Cat# 633781; RRID: AB_2870299
Biological samples		
Healthy human whole blood (Human Immune Tissue Network Biobank); COMIRB protocol #17-2159	Colorado Anschutz Medical Campus Clinical and Translational Sciences Institute, Aurora (USA)	N/A
Healthy human blood (from plateletpheresis leukoreduction filter chambers); Vitalant	Vitalant Blood Donation Center, Denver (USA)	N/A
Human pediatric thymic tissue; IRB protocol #20-0150	Children's Hospital Colorado, Aurora (USA)	N/A
Human pediatric thymic tissue; IRB protocol #IRB-23-4	Mount Sinai, New York City (USA)	N/A
Human pediatric thymic tissue; protocol #NHBR2101	Northwell Health Biospecimen Repository, Lake Success (USA)	N/A
Chemicals, peptides, and recombinant proteins		
Bovine Serum Albumin (BSA)	ThermoFisher Scientific	Cat#J10857-22
Collagenase type IV	StemCell Technologies	Cat#07427
Dispase I	Sigma-Aldrich	Cat#04942086001
DMSO	Sigma-Aldrich	Cat#D8418-100ML
DNase I	Sigma-Aldrich	Cat#11284932001
Fixable Viability Dye efluor780	ThermoFisher Scientific	Cat#65-0865-14
Fetal Bovine Serum (FBS)	Corning	Cat#35-010-CV
GlutaMAX	Gibco	Cat#35050-061
Liberase TH	Sigma-Aldrich	Cat#5401135001
2-Mercaptoethanol	Sigma-Aldrich	Cat#21985-023
2-Mercaptoethanol	Gibco	Cat#21985023
Penicillin/streptomycin	Gibco	Cat#15140-122
Non-essential amino acids	Sigma-Aldrich	Cat#11140-050
Sodium pyruvate	Sigma-Aldrich	Cat#11360-070
Ficoll-paque Premium	Cytiva	Cat#17544203
Critical commercial assays		
AF488 antibody labeling kit	ThermoFisher Scientific	Cat#A20181
Anti-PE microbeads	Miltenyi	Cat#130-048-801
BD Transcription Factor Buffer Set	BD Biosciences	Cat#562574
Live/dead Fixable Near-IR dead cell stain kit	ThermoFisher Scientific	Cat#L10119
BD Rhapsody Cartridge Kit	BD Biosciences	Cat#633773
BD Rhapsody Enhanced Cartridge Kit	BD Biosciences	Cat#664887
BD Rhapsody Cartridge Reagent Kit	BD Biosciences	Cat#633773
BD Rhapsody cDNA Kit	BD Biosciences	Cat#633773
BD Rhapsody TCR/BCR Amplification Kit	BD Biosciences	Cat#665345
BD Rhapsody WTA Amplification Kit	BD Biosciences	Cat#633801

(*Continued on next page*)

Continued

REAGENT or RESOURCE	SOURCE	IDENTIFIER
Deposited data		
Raw data (fastq files) Preprocessed Seurat object	This study	GEO: GSE249684
Web browser exploration tool (ShinyCell) of human and murine integrated datasets	This study	https://xspeciestcells.cshl.edu/
Code	This study	https://doi.org/10.5281/zenodo.13737916. https://doi.org/10.5281/zenodo.13251142
Experimental models: organisms/strains		
C57BL/6J	Jackson Laboratories	Strain #000664; RRID:IMSR_JAX:000664
C57BL/6J *CD1d1d2*$^{-/-}$	Bred in house	Chen et al.[99]
Software and algorithms		
Flow cytometry software FlowJo (v10.7.1)	BD Biosciences	RRID: SCR_008520
Flow cytometry software SpectroFlo (v3.0)	Cytek Biosciences	RRID: SCR_019826
FastQC (v0.11.9)	https://github.com/s-andrews/FastQC	RRID: SCR_014583
MultiQC (v1.12)	https://github.com/MultiQC/MultiQC	RRID: SCR_014982
cNMF (v1.5)	https://github.com/dylkot/cNMF	RRID: SCR_025495
Python (version $\geq$3.8)	https://www.python.org/	RRID: SCR_008394
R (version $\geq$4.0.3)	https://www.r-project.org/	RRID: SCR_001905
Other		
Public dataset – peripheral blood CD4$^+$ T cell gene signatures (Cano-Gamez et al.)	Cano-Gamez et al.[37]	Supplementary Data 6
Public dataset – peripheral blood T cell gene signatures (Rose et al.)	Rose et al.[38]	Supplementary Data 2, Supplementary Data 3
Public dataset – peripheral blood T cell gene signatures (Terekhova et al.)	Terekhova et al.[40]	Table S5
Public dataset – T cell gene signatures across human tissues (Poon et al.)	Poon et al.[39]	Table S6
Public dataset – scRNAseq of human thymus (Park et al.)	Park et al.[27]	https://datasets.cellxgene.cziscience.com/de8665a2-0476-4865-b4af-c7b8d3b1b87f.h5ad
Public dataset – scRNAseq of murine iNKT thymocytes (Baranek et al.)	Baranek et al.[54]	https://datasets.cellxgene.cziscience.com/de8665a2-0476-4865-b4af-c7b8d3b1b87f.h5ad
Public dataset – scRNAseq of murine iNKT thymocytes (Krovi et al.)	Krovi et al.[55]	GEO: GSE152786
Public dataset – scRNAseq of murine iNKT thymocytes (Maas-Bauer et al.)	Maas-Bauer et al.[56]	GEO: GSE172169
Public dataset – scRNAseq of murine iNKT thymocytes (Wang et al.)	Wang et al.[57]	GEO: GSE130184
Public dataset – scRNAseq of murine iNKT, MAIT, $\gamma\delta$ thymocytes (Lee et al.)	Lee et al.[51]	SRA: PRJNA549112
Public dataset – scRNAseq of murine MAIT thymocytes (Chandra et al.)	Chandra et al.[59]	GEO: GSE189484
Public dataset – scRNAseq of murine MAIT thymocytes (Koay et al.)	Koay et al.[53]	GEO: GSE137350
Public dataset – scRNAseq of murine MAIT thymocytes (Legoux et al.)	Legoux et al.[52]	EMBL-EBI: E-MTAB-7704
Public dataset – scRNAseq of murine $\gamma\delta$ thymocytes (Li et al.)	Li et al.[58]	GEO: GSE179422
HBSS	Gibco	Cat#14175079
HEPES (1M)	Gibco	Cat#15630080
RPMI 1640	Corning	Cat#10-040-CV

(*Continued on next page*)

Continued

REAGENT or RESOURCE	SOURCE	IDENTIFIER
RPMI 1640 with 25mM HEPES	Gibco	Cat#22400071
RPMI 1640 without phenol red	Gibco	Cat#11835030
TrypLE Express Enzyme	Gibco	Cat#12604013

EXPERIMENTAL MODEL AND STUDY PARTICIPANT DETAILS

Mice

C57BL/6 mice were purchased from Jackson Laboratories. The *Cd1d1d2*$^{-/-}$ mice backcrossed to the C57BL/6 background were previously described.[99] All mice used were between 6 and 15 weeks and age-matched for each experiment. Mice were raised in a specific pathogen-free environment at the Office of Laboratory Animal Research at the University of Colorado Anschutz Medical Campus or the Animal Core Facility at Cold Spring Harbor Laboratory. Animal procedures were approved by the UCD (00065) Institutional Animal Care and Use Committees and the Cold Spring Harbor Laboratory IACUC (23–1); all procedures were carried out in accordance with the approved guidelines.

Human

Thymus tissues were obtained from anonymous human donors who were undergoing medically necessary surgery where removal of a portion of the thymus was required to facilitate exposure of the operative field. No tissues were obtained specifically for the purposes of this study. This use of discarded tissue was approved by the Institutional Review Board (IRB) of the University of Colorado Anschutz Medical Campus (IRB-17-2159). Additional samples were collected under the Mount Sinai Biorepository with a Waiver of Consent and under the Northwell Health Biospecimen Repository (IRB 20–0150) with patient consent; the use of these human tissues was reviewed by Cold Spring Harbor Institutional Review Board. Pediatric thymus samples for scRNAseq came from individuals between 10 and 20 weeks old (Table S1), and samples used for flow cytometry experiments came from individuals between 4 days and 5 months old. Plateletpheresis leukoreduction filters (LRS chambers) were purchased from Vitalant Blood Center (Denver, CO, USA). Additional PBMCs were collected under COMIRB #17–2159 at the University of Colorado Clinical and Translation Research Centers (CTRC) which is a part of the Colorado Clinical and Translation Sciences Institute (CCTSI), with all donors having provided written informed consent. Overview of sample metadata is provided in Table S1.

METHOD DETAILS

Murine thymus samples

To isolate thymocytes, thymus tissue was immersed in RPMI 1640 media (Corning, #10-040-CV) and gently pressed through a 40μm cell strainer using the plunger of a 1 mL syringe. For TEC isolation, the thymus tissue was cut into small fragments and submerged in RPMI 1640 media without phenol red (Gibco, #11835030), supplemented with 20mM HEPES, 1.3 U/mL Liberase TH, and 100 U/mL DNase I. These tissue fragments were incubated for 5 min on ice followed by an additional 20 min at 37°C. After digestion, the solution was repeatedly mixed with a micropipette to ensure complete tissue disintegration. To stop the digestion process, cells were suspended in HBSS, 4% heat-inactivated FBS (HI-FBS, FBS preheated for 20 min at 56°C), 20mM HEPES, and 10U/mL DNase I. To remove immune cells, the cell suspension was incubated with rat anti-mouse CD90.2 (clone 53–2.1), anti-mouse CD45 (clone 30-F11), and anti-mouse CD45-BV605 (clone 30-F11) antibodies for 30 min at 4°C. Subsequently, the cell suspension was placed on panning plates coated with goat anti-rat IgG for 20 min at room temperature. Unattached cells were then transferred to new panning plates for a second depletion round. The remaining cell suspension, following this depletion process, was prepared for flow cytometry analysis.

Human thymus samples – Thymocytes

To extract thymocytes for both scRNAseq and flow cytometry, the thymus tissue was placed in complete RPMI 1640 media (Gibco, #22400–071), with 10% HI-FBS, 1% non-essential amino acids, 1% sodium pyruvate, 1X GlutaMAX, 1% Penicillin/Streptomycin, and 1X 2-Mercaptoethanol (Sigma-Aldrich #21985–023). The tissue was cut into small pieces, and gently pressed with the back of a 10 mL syringe to release thymocytes. The resulting suspension was passed through a 70 μm filter. Thymocytes were isolated using a Ficoll-Paque density gradient provided by Cytiva. Tetramer staining for MAIT and iNKT cells, and surface staining for CD4^{+}, CD8^{+} and γδ T cells was performed on freshly isolated thymocytes.

Human thymus samples – thymic epithelial cells

To enrich TECs for flow cytometry, thymus tissue was cut into small pieces and placed in RPMI 1640 media without phenol red (Gibco, #11835030), 5% HI-FBS, 1% Penicillin/Streptomycin, 10mM HEPES, and 0.55mM 2-Mercaptoethanol (Gibco,

#21985023). The thymus tissue in this media was stirred on a magnetic plate for 40 min. The supernatant was removed and replaced with fresh media every 10 min to remove released thymocytes. The remaining tissue chunks were placed in a digestion buffer consisting of RPMI 1640 media without phenol red (Gibco, #11835030), 2% HI-FBS, 20mM HEPES, 80 U/mL DNase I, 1.6 U/mL Dispase I, and 0.3 mg/mL Collagenase IV, for digestion at 37°C with gentle shaking. This digestion process was conducted in two sessions of 25 min each, in between which the supernatant was extracted and replaced with fresh digestion buffer. At the end of the digestion, the tissue chunks had nearly entirely disintegrated, and the digestion was halted by resuspending cells in the same buffer used for thymocyte release (RPMI 1640 media without phenol red, 5% HI-FBS, 1% Penicillin/Streptomycin, 10mM HEPES, 0.55mM 2-Mercaptoethanol). The combined supernatants were further incubated in TrypLE Express Enzyme, 1mM $MgCl_2$, 2mM $CaCl_2$, 100U/mL DNase I for 5 min at 37°C to obtain a single-cell suspension. The digestion was stopped by resuspending cells in the previously described thymocyte release buffer. To remove immune cells and erythrocytes, cells were incubated with mouse anti-human CD3 (clone UCHT1), anti-human CD4 (clone RPA-T4), anti-human CD8α (clone RPA-T8), anti-human CD45 (clone HI30) and anti-human CD235a (clone HI264) antibodies in HBSS, 4%HI-FBS and 20U/mL DNase I, for 30 min at 4°C. Cells were then placed on panning plates coated with goat anti-mouse IgG for 20 min at room temperature, and the unadhered cells were transferred to new panning plates for a second round of depletion. The remaining cells following depletion were then stained for flow cytometry.

Human peripheral blood samples

De-identified peripheral blood samples from the Human Immune Tissue Network Biobank (COMIRB # 17–2159) were collected using sodium heparin tubes. De-identified peripheral blood samples from the Vitalant Blood Center were acquired from plateletpheresis leukoreduction filter chambers (LRS). Peripheral blood mononuclear cells (PBMCs) were isolated from these samples using a Ficoll-Paque density gradient provided by Cytiva. PBMCs were cryopreserved in FBS with 10% DMSO and stored in liquid nitrogen.

Magnetic-bead enrichment of iNKT and MAIT cells

To enrich for thymic MAIT and thymic/blood iNKT cells, up to 2×10^9 cells were incubated with MR1-5-OP-RU-PE or CD1d-PBS57-PE tetramers respectively in MACS buffer (1X PBS, 0.5% BSA, 2mM EDTA), for 25 min at room temperature. Cells were washed twice and incubated with anti-PE microbeads, followed by separation using an autoMACS Pro Separator (Miltenyi) according to manufacturer's instructions. PE-microbead-labelled cells in the enriched fraction were stained with the specified panel of antibodies listed below.

Fluorescence-activated cell sorting

To sort $CD4^+$ T, $CD8^+$ T, γδ T, or peripheral blood MAIT cells, 2×10^6 cells unenriched cell suspensions were used. To sort iNKT cells (thymocytes or PBMCs) or thymic MAIT cells, the staining and sorting was performed on magnetic bead-enriched cell suspensions from 0.5 to 10×10^8 cells (above). All single cell suspensions were stained with efluor780 viability dye for 10 min at room temperature and washed once prior to cell surface staining. The cell suspensions were then stained in MACS buffer (1X PBS, 0.5% BSA, 2mM EDTA) at room temperature for 20 min, both with cell surface markers and a unique oligonucleotide-tagged antibody sample tag (Human Single Cell Sample Multiplexing Kit, BD Biosciences) to allow separation in downstream scRNAseq analyses. The following cell surface markers were included in the staining: CD3-AF488 (clone OKT3), CD14-eFluor450 (clone 61D3), CD19-eFluor450 (clone H1B19), Vα7.2-BV785 (clone 3C10), Vα24-PerCP-Cy5.5 (clone C15), CD4-redFluor710 (clone OKT4), CD8α-PE-Cy7 (clone SK1), TCRγδ-BV650 (clone 11F2), FcγR block. Following cell surface staining, cells were washed twice and resuspended in MACS buffer prior to cell sorting on the Aria 3 (BD Biosciences). Purified cell populations were sorted into MACS buffer. Validation of the cell sorting panel was performed on the Cytek Aurora flow cytometry system using SpectroFlo software (v3.0). Overall, from infant thymus and PBMC donors up to 5 populations were sorted after doublet, viability, B cell ($CD19^+CD3^-$) and monocyte ($CD14^+CD3^-$) discrimination: 1. MAIT cells (MR1-5-OP-RU-Tet^+Vα7.2$^+CD3^+$), 2. iNKT cells (CD1d-PBS57-Tet^+Vα24$^+CD3^+$), 3. γδ T cells ($CD3^+$TCRγδ$^+$), 4. $CD4^+$ T cells ($CD4^+CD8\alpha^-CD3^+$) and $CD8^+$ T cells ($CD8\alpha^+CD4^-CD3^+$). Cell subsets sorted for the different donors are listed in Table S1 and the gating strategy is shown in Figure S16.

Flow cytometry — Thymic and peripheral blood T cells

To confirm gene expression from scRNAseq analysis, MAIT and iNKT cells were enriched from the human thymus as described above, as were iNKT cells from human blood. Peripheral blood MAIT and γδ T cells were stained directly without enrichment. Single cell suspensions were stained as above with efluor780 viability dye prior to incubation at 37°C for 10 min with CCR7-APC-Fire810 (clone G043H7) and FcγR block. A combination of the following cell surface markers were subsequently added and cells were stained at room temperature for 15 min: CD3-BUV496 (clone UCHT1), CD14-PE-Cy5 (clone 61D3), CD19-PE Cy5 (clone H1B19), Vα7.2-BV785 (clone 3C10), Vα24-PerCP-Cy5.5 (clone C15), CD4-BV570 (clone RPA-T4), CD8α-BUV395 (clone RPA-T8), TCRγδ-BV650 (clone 11F2), Vδ1-PerCP-Vio700 (clone REA173), Vδ2-FITC (clone 123R3), Vγ9-PE (clone B3), CD161-BUV805 (clone HP-3G10), CD62L-BV650 (clone DREG-56). Cells were then washed twice with MACS buffer, and intracellular staining was performed with BD Transcription Factor Buffer Set according to the manufacturer's specification. The following antibodies were used to stain for intracellular proteins: PLZF-PE-CF594 (clone R17-809), Eomes-BUV737 (clone X4-83), T-bet-BV605 (clone 4B10), GZMK-eFluor660 (clone G3H69), GZMB-AF700 (clone GB11). Phenotypic analyses were performed on the Cytek Aurora flow cytometry system using SpectroFlo software (v3.0). Data were analyzed using FlowJo software (v10.7.1).

Flow cytometry -— CD1d, SLAMF1, SLAMF6

For murine experiments, thymocytes were resuspended in PBS, 5% FBS, 4mM EDTA and stained for 30 min at 4°C with: Fc blocker anti-CD16/32 (clone 93), CD4-AF488 (clone GK1.5), CD8α-APC (clone 53–6.7), CD1d-PE (clone 1B1). For murine thymus samples which were depleted of immune cells, the single cell suspension was resuspended in HBSS, 4% HI-FBS, 20mM HEPES, 10U/mL DNase I, 2.5mM EDTA, and stained for 30 min at 4°C with: Fc blocker anti-CD16/32 (clone 93), EpCAM-BV421 (clone G8.8), CD45-BV605 (clone 30-F11), UEA1-FITC, Ly-51-AF647 (clone 6C3), and CD1d-PE (clone 1B1). For flow cytometry experiments on human samples, thymocytes were resuspended in PBS, 2% FBS, and stained for 30 min at 4°C with: TruStain FcX, CD45-BV421 (clone HI30), CD4-AF488 (clone OKT4), CD8α-APC (clone RPA-T8), CD1d-PE (clone 51.1). For human samples which were depleted of immune cells and erythrocytes, cells were resuspended in PBS, 2% FBS, and stained for 30 min at 4°C with: TruStain FcX, CD45-AF647 (clone QA17A19), EPCAM-BV421 (clone 9C4), CDR2-AF488 (purified CDR2 antibody kindly provided by Dr. Sheena Pinto, conjugated with the AF488 antibody labeling kit from ThermoFisher Scientific), HLADR-BV711 (clone L243), CD1d-PE (clone 51.1). In all experiments, to measure viability cells were stained with the live/dead Fixable Near-IR dead cell stain kit, simultaneously with cell surface markers. Flow cytometry was performed on a BD LSR Fortessa Cell Analyzer (BD Biosciences).

Single-cell RNA sequencing

Prior to cDNA library preparation for the whole transcriptome (WTA) and VDJ libraries, all cell subsets from the different donors were pooled, with up to 12 unique sample tags combined per library. Single cell WTA and VDJ sequencing libraries were prepared using the BD Rhapsody Single-Cell Analysis System (BD Biosciences) according to the manufacturer's specifications. Libraries were quantified and pooled according to equivalent molar concentrations and sequenced on the NovaSeq sequencing platform at the University of Colorado Genomics Core with the following read lengths: read 1–150 cycles; read 2–150 cycles; and i7 index - 8 cycles.

Single-cell RNA-seq data analysis

The quality of sequencing reads was evaluated using FastQC and MultiQC. Sequencing reads (FASTQ) were mapped and sample tags were deconvoluted with The BD Rhapsody WTA Analysis Pipeline on the GRCh38 genome sequence. This pipeline produced a gene expression matrix for each sample, which records the number of UMIs for each gene associated with each cell barcode. Aggregated data were then imported into the R environment (version $\geq$4.0.3) and analyzed with Seurat (v4.3.0). Low-quality cells were filtered using the cutoffs nFeature_RNA $\geq$ 500 & nFeature_RNA <3000. Cells with a high mitochondrial content were removed using a batch-dependent threshold with the isOutlier function from the scater package (v1.26.1).[100] Genes expressed in less than 20 cells were ignored. This resulted in 78,607 cells with 17,204 genes for downstream analyses. The NormalizeData function of Seurat was performed using default parameters to remove the differences in sequencing depth across cells. Dimensionality reduction was performed prior to integration for visualization purposes (Figure S2A), by selecting 2000 highly variable genes for principal component analysis (PCA) and uniform manifold approximation and projection (UMAP). To integrate the data and remove batch-effects from the PCA subspaces based on the correct cell alignment, we used Harmony[101] following PCA to project cells into a shared embedding in which cells group by cell type rather than dataset-specific conditions. We then applied the RunUMAP function on 20 dimensions of the harmony embedding to obtain bidimensional coordinates for each cell. We determined the k-nearest neighbors of each cell using the FindNeighbors function and used this knn graph to cluster cells using the Louvain algorithm from FindClusters based on the same harmony dimensions as the RunUMAP function (20 dimensions, resolution 1.2). For analyses performed on individual lineages ($CD4^+$ T, $CD8^+$ T, iNKT, MAIT or γδ T cells) in Figures 2 and 4, the dataset was split up based on cell hashing tags. Each lineage from each tissue was re-analyzed individually using the same steps to obtain UMAPs and clusters in Figures 2 and 4. Plots displaying cells on UMAPs were generated using the SCpubR package (v2.0.2).[102]

LISI metric and analysis of cluster stability

The local inverse Simpson's index (LISI) was used to assess the degree of mixing during batch correction and dataset integration in scRNAseq analysis.[101] This approach helps evaluate the effectiveness of data integration methods by quantifying how well datasets are merged without introducing artificial batch effects. To assess the integration process, we employed the "integration LISI" (iLISI) score. iLISI measures the effective number of datasets within a neighborhood and provides an indication of how effectively the individual datasets were harmoniously integrated into a unified whole during the process. In addition, we used the "cell-type LISI" (cLISI) score to evaluate the accuracy of cell-type assignments in the integrated dataset. cLISI is a modified version of the LISI score, but instead of assessing dataset labels, it focuses on the accuracy of cell type assignments within the integrated data. As the specific identities of individual cells were not known beforehand, we assigned mock cell identities based on anticipated gene expression patterns. These mock identities were determined using prior knowledge of gene expression markers associated with distinct cell types. For instance, we identified DN thymocytes as cells expressing *PTCRA* > 1; B cells as cells expressing *CD19* > 1 and *IGKC* > 1; T_{regs} as cells expressing *FOXP3* > 1; MAIT cells as cells expressing *SLC4A10* > 1 and *FOXP3* < 1; $CD4^+$ T cells as cells expressing *CD4* > 1, *CD8A* < 1, *SLC4A10* < 1, *FOXP3* < 1, and *CCR7* > 1; DP thymocytes as cells expressing *RAG1* > 1 and *CD1C* > 1; and CD8αα thymocytes as cells expressing *CD8A* > 1 and *GNG4* > 1. These mock identities were used as initial cell type assignments and served as the basis for assessing the success of integration, as indicated by increased iLISI scores and the maintenance of a cLISI score of 1 (Figure S2B). Only cells with assigned mock identities were included in the cLISI analysis. To evaluate the stability of clusters, we conducted a bootstrapping procedure in which cells from each predefined cluster were repeatedly sampled and then subjected

to re-clustering. Cluster stability was assessed by examining co-assignment probabilities (CP), where higher CP values indicated greater cluster stability (Figure S2C). In essence, a high CP suggests that the cells within a cluster consistently grouped together across multiple iterations, reinforcing the reliability and robustness of that cluster's identity.

TCR analysis

V(D)J single cell sequencing data were mapped and quantified using the BD Rhapsody WTA Analysis Pipeline and the GRCh38 genome sequence. To connect the VDJ data with transcripts data for each cell, we established links based on cell indexes extracted from the consensus annotation files (VDJ_percell.csv) and MolsPerCell.csv files from each demultiplexed sample. Only TCR paired sequences were retained for subsequent analyses. TCR data from each VDJ-sequenced sample were combined together and added to the metadata of the Seurat object. Clonotypes were defined based on unique TCR VJ usage and complementary-determining region (CDR3) motifs. Basic TCR statistics, such as the distribution of length and counts were computed using the tidyverse package (v1.3.2). The assessment of clonotype diversity was conducted using the mean value of the Shannon index, computed through the diversity function of the vegan R package (v2.6–4) after 100 iterations. Prior to the diversity calculation, the data was subjected to rarefaction to match the lowest sequence count found within the studied groups. Chord diagrams were generated using the circlize package (v0.4.15)[103] and CDR3 motif logos using the ggseqlogo package (v0.1).[104] The stacked letters' cumulative height at each position signifies the degree of sequence conservation, portraying the relative abundance of amino acids, which is further depicted by the varying heights of individual letters within the stack.

Identification of differentially expressed genes between clusters

We identified cluster-enriched genes by using the FindAllMarkers function in Seurat with test.use = wilcox. This function identified differentially expressed genes for each cluster by comparing the gene expression for cells belonging to a cluster versus cells belonging to all other clusters. Only those genes that passed an adjusted *p* value (Benjamini-Hochberg) cutoff of 0.05, log fold change >0.4 and min.pct = 0.3 were included in Figure S3.

Characterizing the replicability of cell types defined by scRNAseq between studies and between species

We assessed the consistency of cell clusters in our integrated thymic data by comparing them with the human thymus atlas from the Park et al. dataset.[27] To do this, we focused exclusively on thymocytes, totaling 37,369 cells in our dataset. We also acquired the annotated AnnData object from the Park et al. dataset, which specifically contained T cells. To enable a meaningful comparison, we combined the two raw count matrices, concentrating on the top 2000 highly variable genes shared across both datasets. This resulted in a matrix containing 3,106 genes and 114,363 cells. To evaluate the consistency of cell types between these datasets, we employed the pyMN package to perform unsupervised MetaNeighbor analysis.[26] MetaNeighbor assesses the similarity of cell types by constructing a network of cells based on the correlation of their gene expression profiles. It then predicts cell type labels, hiding them from one dataset while using the other. The result is expressed as a mean area under the receiver operator characteristic (AUROC) score, which measures the probability of correctly identifying a cell's type based on its gene expression profile. We used the ggplot2 package to visualize the AUROC scores obtained from pyMN, comparing our integrated clusters with the thymocyte clusters defined in the Park et al. dataset. For assessing gene expression similarity between thymic lineages in Figure 2A, we considered donors as distinct datasets (study_id parameter); and cell lineages (based on cell hashing) as the cell groups of interest to compare (cell_type parameter), more particularly splitting thymocytes in each lineage into non-effector (clusters 0–11) versus effector states (clusters 12–17). MetaNeighbor was run on the top 2000 highly variable genes chosen on our integrated dataset. For assessing the replicability of cell clusters across species in Figure 6, we utilized the reference scRNAseq murine T_{inn} dataset (see below) and our human thymic iNKT, MAIT, and γδT individual Seurat objects from Figure 2. To ensure an appropriate comparison, we obtained orthologous genes between mouse and human with the biomaRt package.[105,106] We filtered the murine count matrix to retain only genes with known 1:1 orthologs in humans. Then, we performed unsupervised MetaNeighbor analysis with pyMN on the combined set of highly variable genes from both human and mouse datasets. Finally, we used ggplot2 to create visualizations of the AUROC scores returned by pyMN, including clusters that contained at least 1% of the cells in each species to ensure greater confidence in assessing the replicability of clusters across species.

Identification of gene expression programs

The count matrix was used for conducting consensus non-negative matrix factorization (cNMF).[28] This process enabled us to infer both identity and activity programs, along with their respective contributions in each cell. The usage of each program for each cell was added to the metadata of the Seurat object and displayed as a feature plot (Figure 1K). To determine the genes associated with each program, we plotted the gene ranks (ranging from most associated to least associated) against the gene_spectra_score output from the cNMF analysis. The plotted gene ranks were fitted to a sigmoid curve and the slope at the first elbow point was calculated as the minimum threshold for genes to be retained in a given GEP. The same slope was applied to every GEP to prevent bias in ranked gene selection, as the gene rankings between GEPs are not comparable and are relative to each GEP (as depicted in Figure S17). Cells from blood samples were assigned to the GEP with the highest usage (as provided by cNMF), to display an alluvial plot with ggalluvial in Figure 4D (v0.12.5).[107]

Scoring of gene signatures

Gene signatures were scored on our Seurat object, or on other dataset's Seurat or AnnData objects using either the function AddModuleScore in Seurat, or scanpy.tl.score_genes in scanpy. In both cases, the score is computed as the average expression of all genes contained in the gene list, and subtracting the average expression of 100 control genes (randomly chosen to match the expression bins of the gene list). Gene signatures used throughout this manuscript and their source can be found in Table S2.

Gene regulatory network inference

To deduce gene regulatory networks, we employed pySCENIC from a pre-built singularity container, aertslab/pyscenic:0.12.1, a tool utilizing *cis*-regulatory motif analysis to identify potential transcription factors (TFs) that might govern a cluster of co-expressed genes within individual cells.[47] pySCENIC was run using the –mask-dropouts flag and a normalized enrichment score threshold of 2 to help mitigate the effects of the varying degrees of sparsity across the datasets we generated. The initial step involved generating modules composed of transcription factors and co-expressed genes using GRNboost2.[108] These modules were pruned to remove indirect targets that lacked significant enrichment for the corresponding TF motif within ±10 kb from the transcription starting site of the putative target (cisTarget). This process yielded a collection of transcription factor regulons. Considering the inherent stochasticity in gene regulatory network inference using GRNBoost2, each run of pySCENIC may yield different quantities of regulons, along with distinct target genes associated with each TF. To mitigate this variability, we performed 100 pySCENIC runs and retained regulons present in 100% of the runs. We also removed regulons that did not have at least 5 target genes defining the regulon activity. Due to the high degree of noise in target genes, we retained target genes that appeared within a regulon in at least 95% of the runs. Furthermore, each target gene also had to overlap with the union of all possible retained ranked gene expression targets across all GEPs generated from cNMF. To identify regulons that were specific to the underlying biology of our cell types and GEPs, we calculated the AUC scores using the R package AUCell, located in the pySCENIC container, for each regulon based on the pruned target gene list. A regulon was deemed specific to a defined cell population if at least 20% of the cells within the annotated population scored in the 90th percentile of the overall AUC score for all cells.

Comparison of gene expression programs with gene signatures from the literature

To compare the genes characterizing each GEP with known peripheral blood T cell states defined in the literature (Figure S10), we obtained gene signatures identified from (1) differential expression (DE) analysis from bulk RNAseq between sorted naive, T_{cm}, T_{em} $CD4^+$ and $CD8^+$ T cell populations by Rose et al.[38]; (2) DE genes between cell clusters defined from scRNAseq of naive and memory $CD4^+$ T cells isolated from PBMCs by Cano-Gamez et al.[37]; (3) DE genes between cell clusters defined from scRNAseq of blood immune cells by Terekhova et al.[40] (4) DE genes between cell clusters defined from scRNAseq of T cells across nine human tissues by Poon et al.[39] In the Rose dataset, we kept genes that defined their Figures 2E and 2H (adjusted *p*-value $\leq$0.05). In the Cano-Gamez and Poon datasets, we kept DE genes with a minimum log fold-change of 0.25 (adjusted *p*-value threshold $\leq$0.05 or 0.01, respectively). In the Terekhova dataset, we used the top 100 differentially expressed genes shared in their Table S5. We computed a weighted Jaccard Index (JI) between the gene lists derived from our GEPs and those from the Rose, Cano-Gamez, Terekhova and Poon datasets (see quantification and statistical analysis). For the co-expression analysis of GEPs and gene lists from other datasets, we scored the gene lists on the entire integrated dataset. This was done using functions like Seurat's AddModuleScore with the blend = TRUE parameter. Additionally, GEP4, GEP5, and GEP6 were scored on the Poon et al. dataset using scanpy's tl.score_genes function, and their scores in specific cell clusters of interest were displayed in Figure S10B.

Pseudo-bulk differential expression analysis

To investigate for differentially expressed genes between αβ thymocytes lineages in Figure 2, we grouped cells by donor and lineage, restricting our analysis to only donors 2–4 where all αβ lineages were sorted, and also restricting ourselves to thymocytes found in clusters 3, 9, 10 and 11 in the integrated dataset (where $CD4^+$/iNKT and $CD8^+$/MAIT cells showed high gene expression similarity). We then used DESeq2 (v1.40.2)[109] to perform pseudo-bulk DE analysis between lineages using a Wald test. We restricted our analysis to genes which were significantly upregulated ($p_{adj} < 0.01$) in both $CD4^+$ and iNKT cells compared to $CD8^+$ and MAIT cells, and likewise for other comparisons shown in Figure 2. To investigate for cell lineage-specific gene signatures in PBMCs in Figure 4, we grouped cells by batch, cluster and lineage, restricting our analysis to only batches E, F and I where at least 3 or more cell lineages were sorted and sequenced within the same batch. We then used DESeq2 (v1.34.0)[109] to perform pseudo-bulk DE analysis with a likelihood-ratio test (LRT), where the full model included batch + cluster + lineage, and the reduced model included batch + cluster, in order to detect genes whose expression can be explained by lineage, and not by batch or cell state (i.e., cluster). We used the LRT test by computing pairwise comparisons, contrasting all lineages against each other (CD4vsCD8, CD4vsiNKT, etc.), for each comparison keeping DE genes with an adjusted *p*-value of 0.01. Then, to extract lineage-specific genes, for each lineage we kept genes that were commonly upregulated in at least 3 or more contrasts. We normalized the raw counts with the rlog function from DESeq2 and batch-corrected them with removeBatchEffect from the limma package (v3.56.2),[110] before displaying the final list of DE genes on a heatmap with the pheatmap package (v1.0.12).

Creation of a reference scRNAseq mouse T_{inn} dataset

ScRNAseq data from mouse thymic iNKT, MAIT and γδ T cells[51–59] were downloaded from Gene Expression Omnibus or the European Bioinformatics Institute (see key resources table). Data were analyzed using the Seurat package. Analyzed cells were selected to express between 800 and 4200 genes per cell, with less than 5% of mitochondrial reads. Datasets were merged and integrated using the FastMNN algorithm,[111] using 5000 variable features, k = 20 and auto.merge = TRUE. Cell clustering was carried out with a resolution parameter set at 0.5, and potential doublets were detected using scDblFinder[112] and subsequently eliminated. To discern differential gene expression between clusters, the FindAllMarkers function was employed, utilizing the MAST algorithm. The analysis considered latent features, specifically the number of genes per cell, and the sample identity, with a log2 fold change threshold of 0.3.

QUANTIFICATION AND STATISTICAL ANALYSIS

Pseudo-bulk differential expression analysis in thymic samples

Differentially expressed genes in Figures 2B and 2C between αβ thymocyte lineages were identified using a Wald test from the DESeq2 package (v1.40.2),[109] with a $p_{adj} < 0.01$ threshold. This analysis was restricted only to thymocytes from three sequencing batches (B, C, D; see Table S1) where all αβ lineages were sorted; and to thymocytes in clusters 3, 9, 10 and 11 where naive-like $CD4^+$/iNKT and $CD8^+$/MAIT had shown transcriptional similarity (based on Figures 1G, 1I, and 2A).

Pseudo-bulk differential expression analysis in PBMC samples

Differential expression analysis in Figure 4 was performed with an LRT analysis, to take into account the heterogeneity of batches and cell states among peripheral blood T cells (see method details). This analysis was restricted only to PBMCs from three sequencing batches (E, F, I; see Table S1), where at least three distinct T cell lineages were sorted and sequenced in the same batch. Only DE genes with $p_{adj} < 0.01$ were kept.

Comparison of GEPs with gene signatures from the literature

In Figure S10, we computed the Jaccard Index (JI) between the gene lists derived from our GEPs and those from the Rose, Cano-Gamez, Terekhova and Poon datasets. Since the gene lists varied in length, we weighted the JI to make it comparable across pairwise comparisons. This was achieved by dividing the JI by the maximal theoretical JI for each pairwise comparison, which is the ratio of the length of the smaller list to the length of the larger list. This "weighted Jaccard Index" is shown on the x axis of Figure S10A. To assess the significance of the observed JI, we performed a permutation analysis. We generated 1000 random gene lists A′ and B′, matching in length and expression pattern to the original lists A and B. We computed the weighted JI between these random lists and defined an empirical *p*-value by counting how many of these weighted JIs were greater than the observed weighted JI divided by the number of permutations. To account for multiple comparisons, we applied a Bonferroni correction to the empirical *p*-values. Adjusted *p*-values below 0.01 are shown as text in the figure.

Cell Reports, Volume *43*

Supplemental information

Unraveling the phenotypic states of human innate-like T cells: Comparative insights with conventional T cells and mouse models

Liyen Loh, Salomé Carcy, Harsha S. Krovi, Joanne Domenico, Andrea Spengler, Yong Lin, Joshua Torres, Rishvanth K. Prabakar, William Palmer, Paul J. Norman, Matthew Stone, Tonya Brunetti, Hannah V. Meyer, and Laurent Gapin

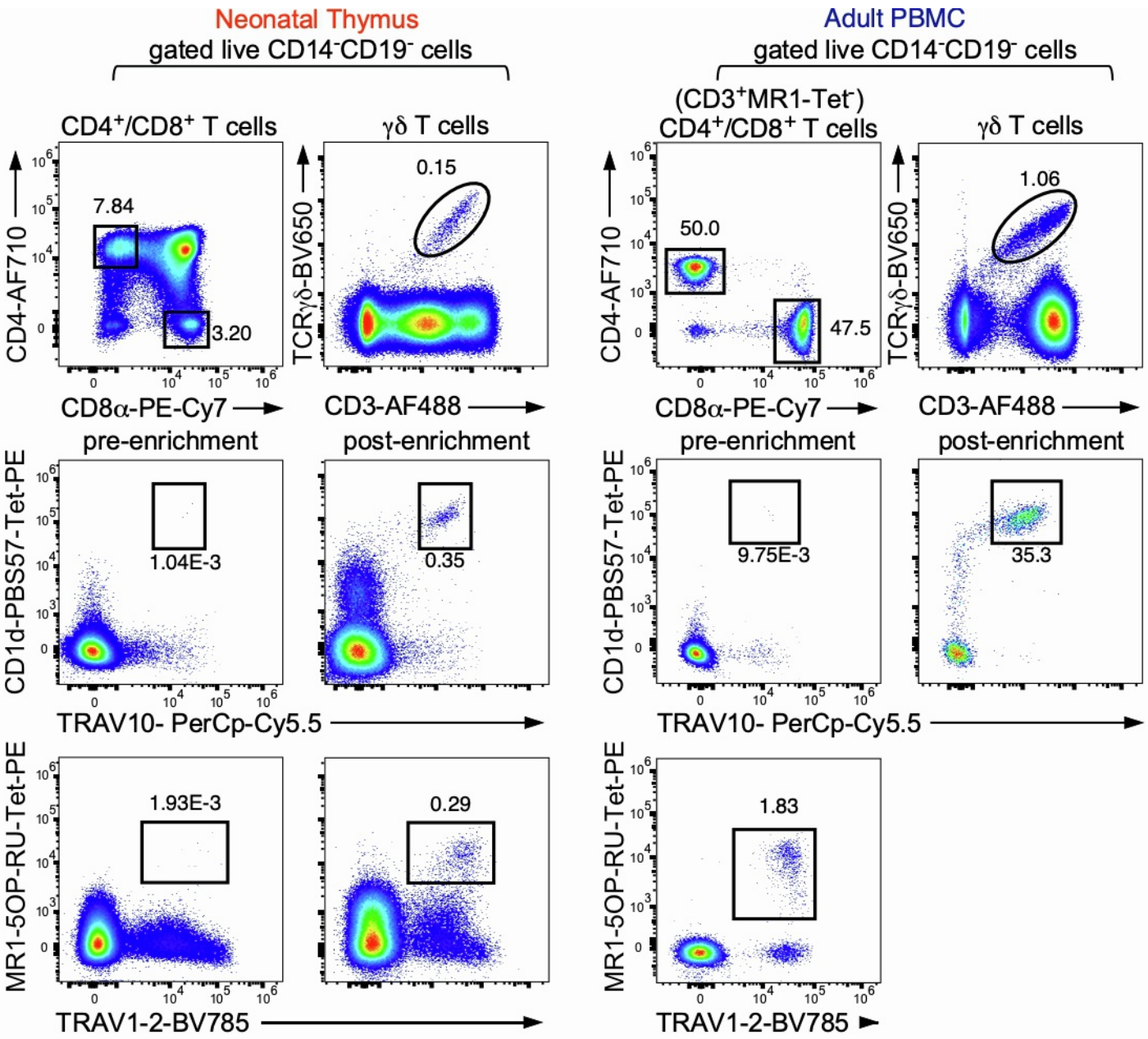

Supplementary Figure 1: Cell sorting strategy for single-cell sequencing. Non-myeloid ($CD14^-$), non-B-cell ($CD19^-$), live cells (viability dye efluor780) from both thymus and blood were sorted into CD4, CD8 and γδ T cells based on $CD4^+CD8^-$, $CD8^+CD4^-$ and $CD3^+TCR\gamma\delta^+$ marker expression, respectively. iNKT and MAIT cells were pre-enriched via CD1d-PBS57 and MR1-5OPRU magnetic beads and sorted based on binding to tetramer and TRAV10 or TRAV1-2 antibodies respectively.

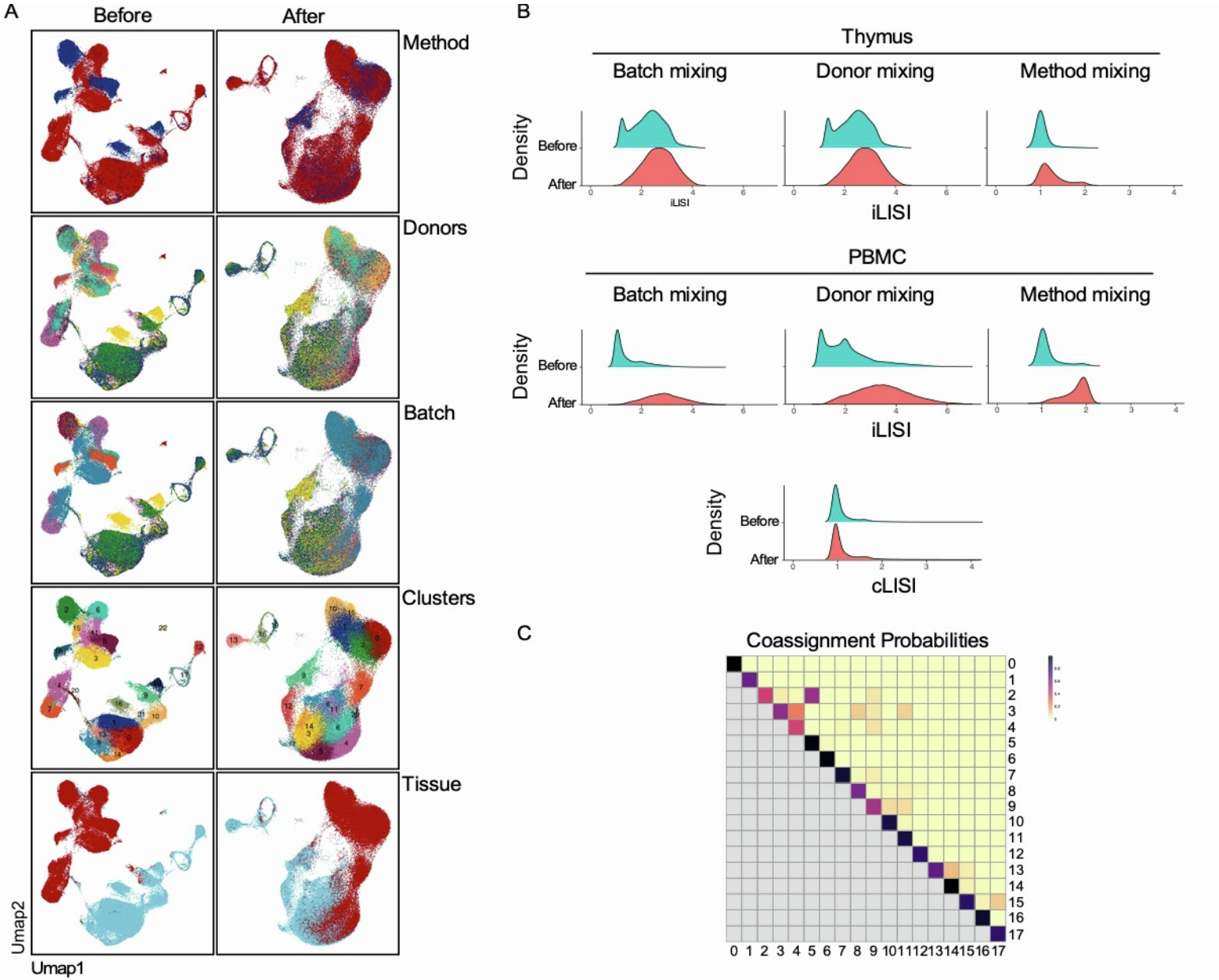

Supplementary Figure 2: Batch integration and quality control. A. UMAP projection before and after integration with Harmony, colored by method (RNAseq, RNAseq+VDJseq), donor (1-13), batch (A-I), clusters (1-17) and tissue (thymus and blood). B. Degree of mixing during batch correction and dataset integration measured as the local inverse Simpson's index (LISI). The top and middle panels show the integration LISI (iLISI), which measures the effective number of datasets within a neighborhood, for thymic and PBMC-derived cells, respectively. Mixing was assessed on batch, donor and method used (as in depicted in A); the lower panel depicts the cell-type LISI (cLISI), to evaluate the accuracy of cell-type assignment. Blue curves indicate LISI before integration, red after integration. C. Cell co-assignment probabilities within (diagonal) and across clusters (off diagonal) assessed by cell bootstrapping and re-cluster. High co-assignment probabilities indicate cluster stability.

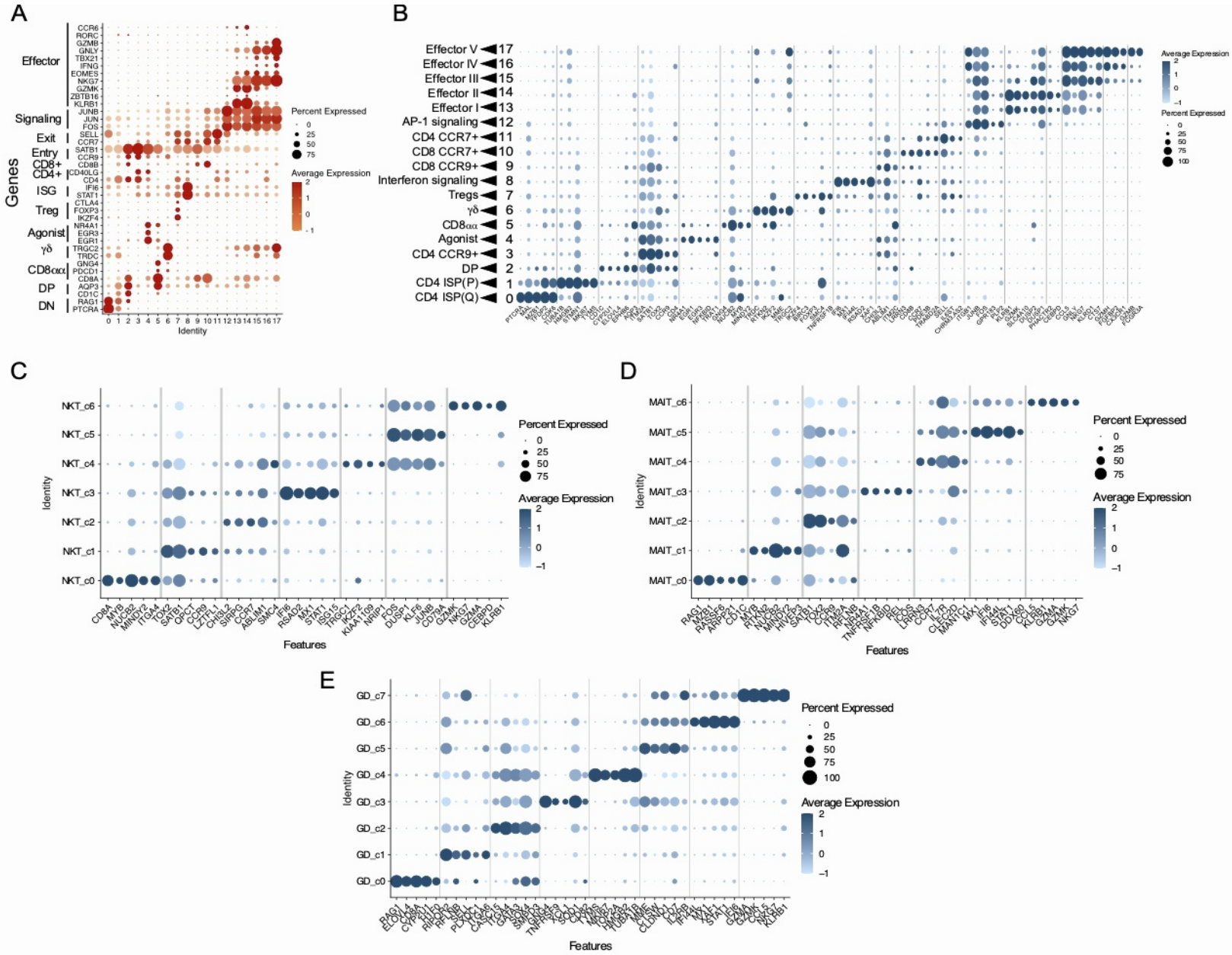

Supplementary Figure 3. Marker gene expression across cell clusters. A. Reference signature gene expression for clusters in Fig 1C and B. the top five genes that characterize these clusters in this dataset. Top five marker genes for C. iNKT, D. MAIT and E. γδ T cells corresponding to the clusters in Fig 2D.

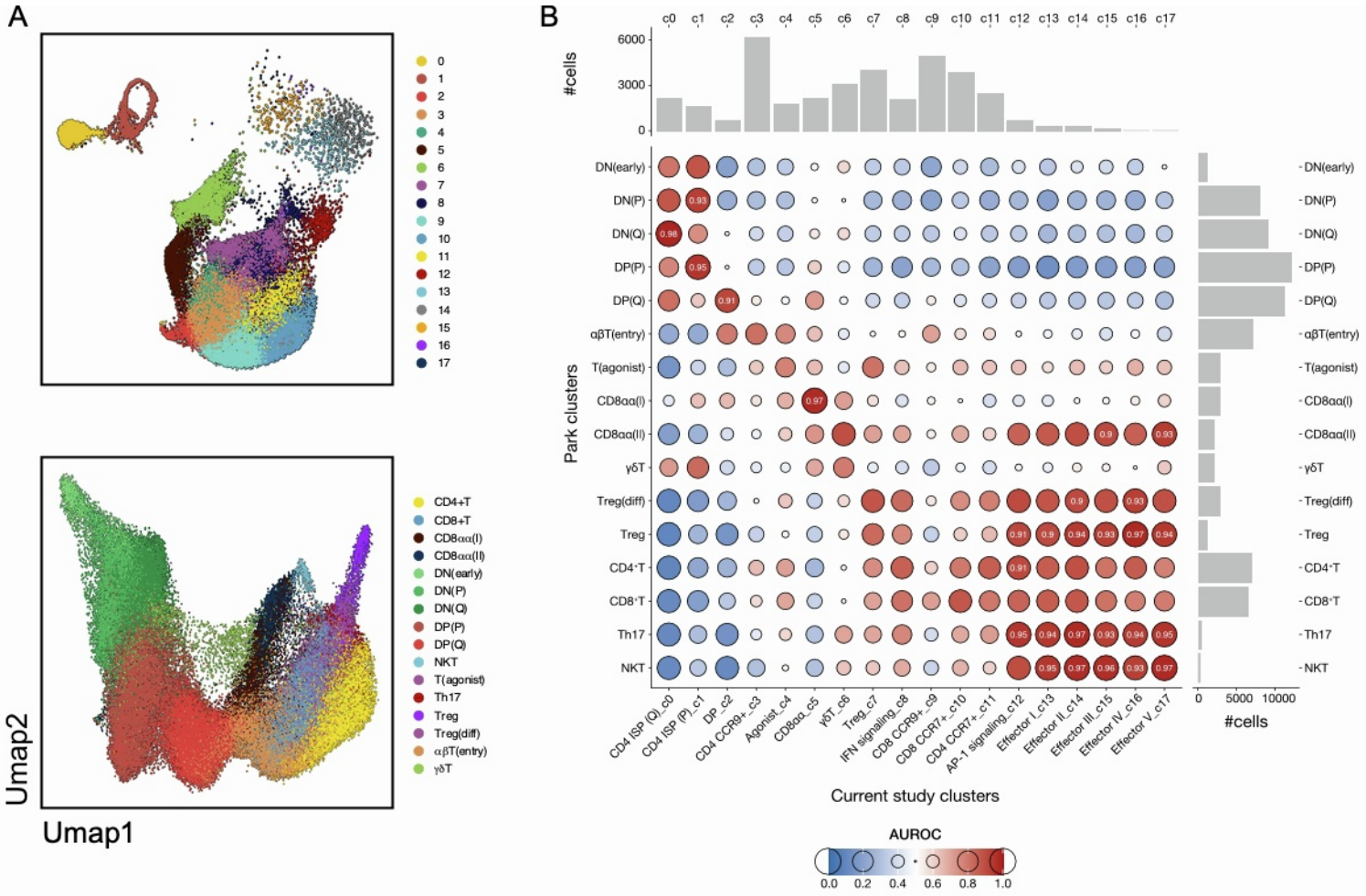

Supplementary Figure 4. Reproducibility of thymocyte data with human thymus atlas. A. UMAP representation of our integrated thymocyte data (top) and the Park *et al.* thymocyte data (bottom). Cells are colored by cluster.

B. Bubbleplot showing the MetaNeighbor AUROC score for pairwise similarities of our thymocyte clusters with the Park *et al.*[1] annotated thymocyte clusters. AUROC scores above 0.9 are written in white text.
Marginal bar plots represent the number of cells present in each cluster.

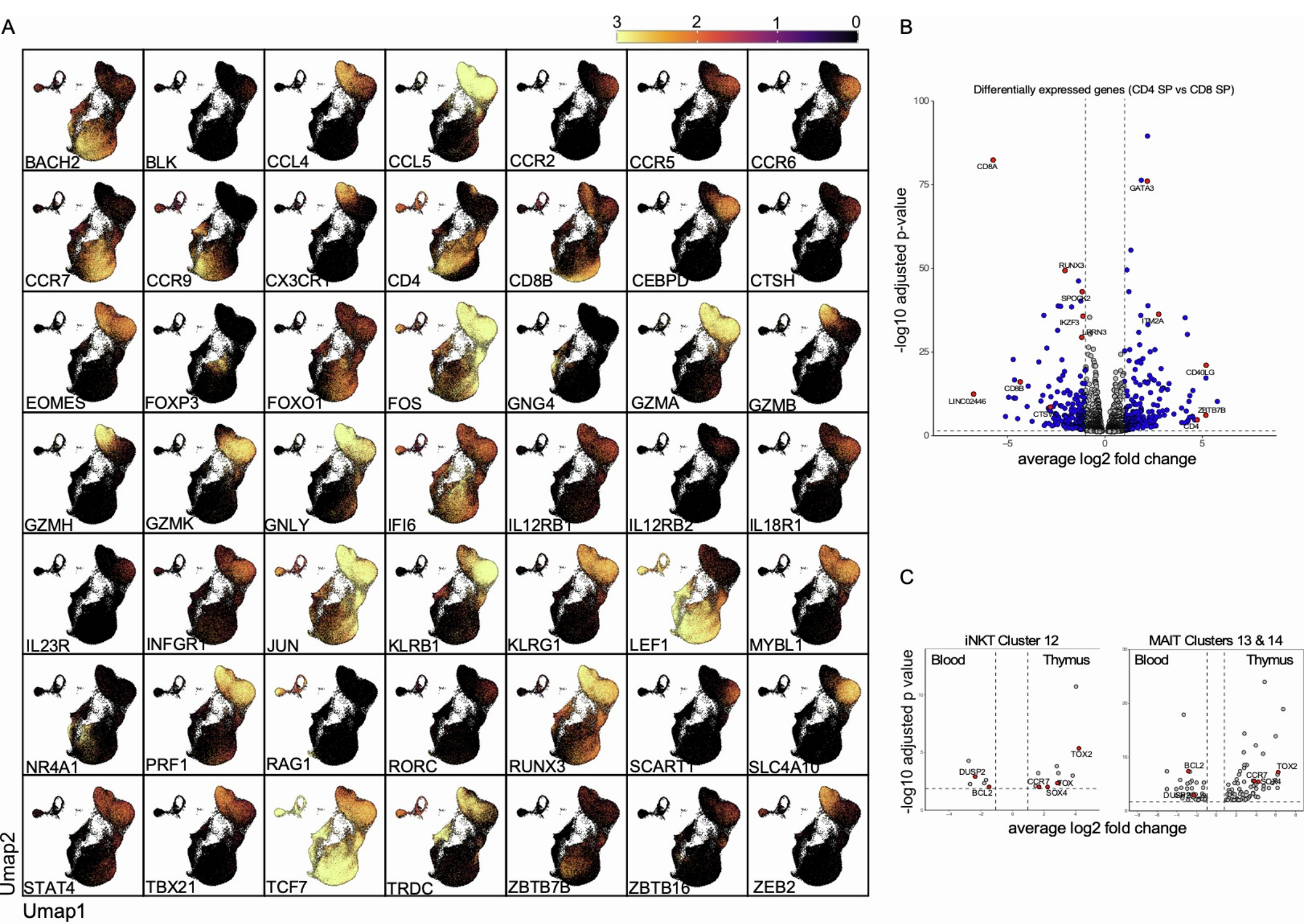

Supplementary Figure 5: Characteristics of gene expression on integrated dataset. A. Gene expression projection of signature genes.
B. Genes differentially expressed between thymic CD4 and CD8 SP T cells corresponding to clusters c3/c11 and c9/c10 in Fig 1C, respectively.
C. Genes differentially expressed between thymic and peripheral blood iNKT cells (left) and MAIT cells (right) in indicated clusters.

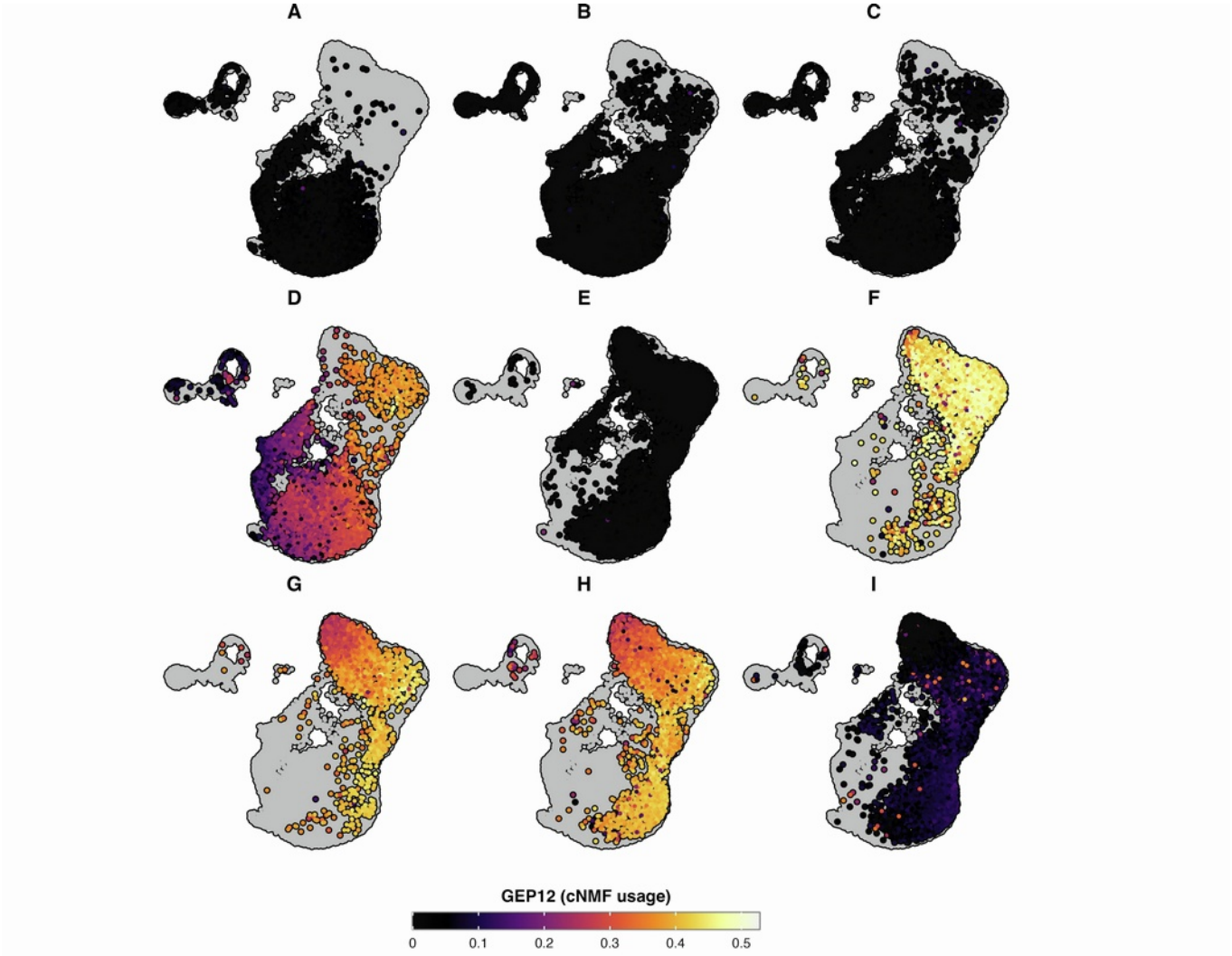

Supplementary Figure 6: Projection of GEP12 onto integrated T_{inn} and T_{conv} object.

Each panel shows cells from a given sequencing batch, color-coded by the cNMF usage of GEP12. There is a clear separation of batches A-C, E, I and D, F-H, which align with the sequencing method used, RNAseq only or RNAseq+VDJseq, respectively (see Sup Table 1).

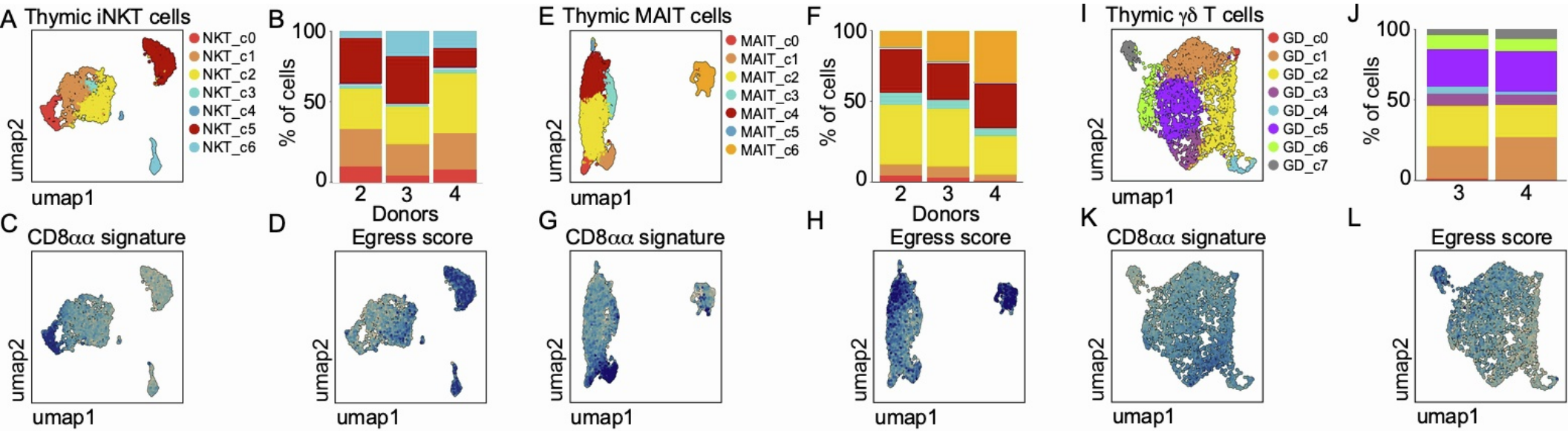

Supplementary Figure 7: Separate analysis of human innate T cell development. Clustering of hashtag-separated thymic iNKT (A), MAIT (E) and γδ T cells (I) and the respective proportion of cells per cluster and donor (B, F, J), the projection of the CD8αα signature (C, G, K) and egress score (D, H, L).

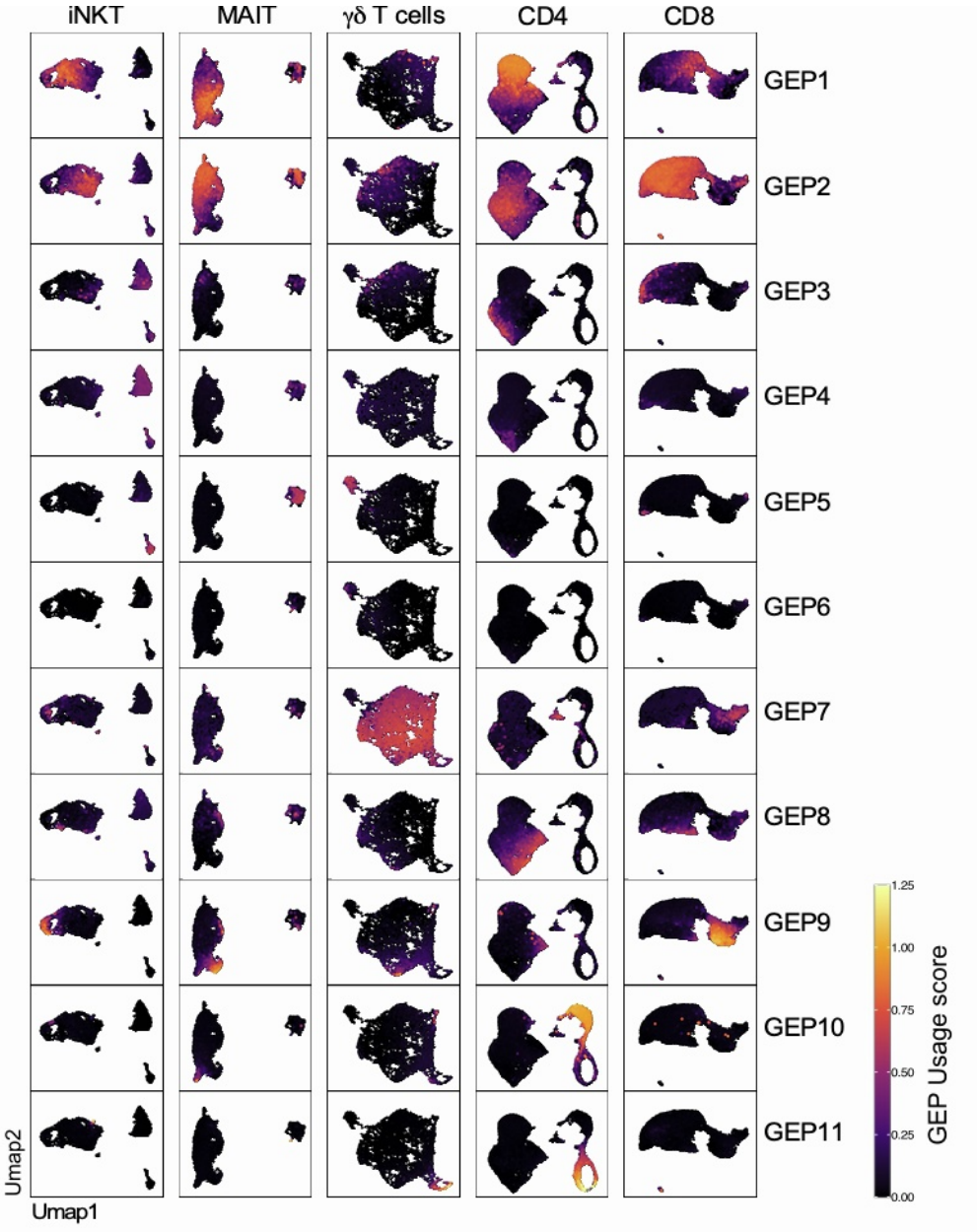

Supplementary Figure 8: Gene expression programs (GEP) in thymic T cell types. Cells are color-coded based on their respective GEP usage (rows) and cell types (columns). GEP usage derived from cNMF usage file.

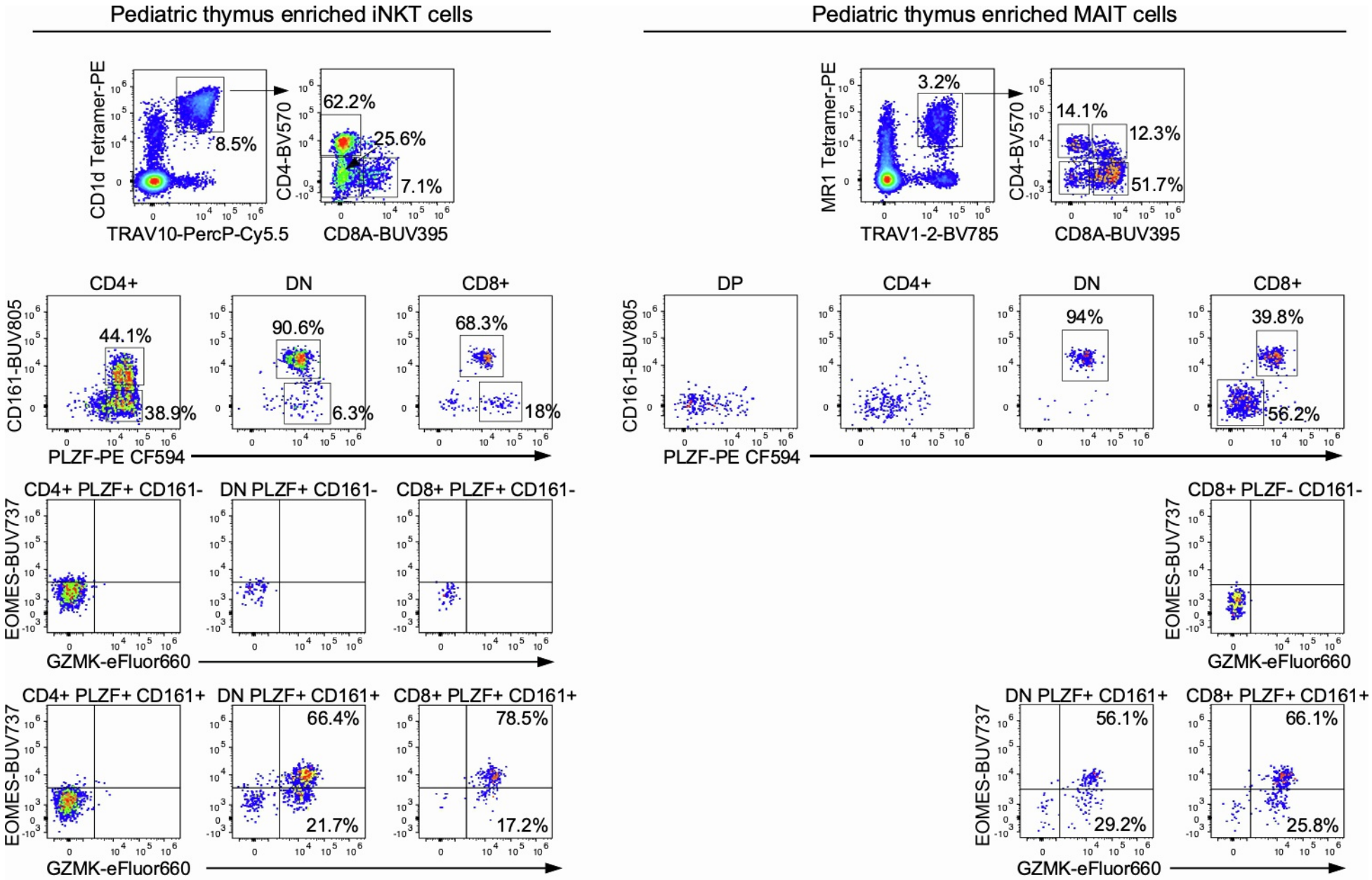

Supplementary Figure 9: Effector phenotyping of thymic iNKT and MAIT cells by flow cytometry. Thymic iNKT (TRAV10^{+} CD1d-PBS57^{+}) and MAIT (TRAV1-2^{+} MR1-5OPRU^{+}) cells from postnatal thymus were analyzed by flow cytometry for the expression of co-receptors CD4 and CD8; transcription factor PLZF; and effector markers CD161, EOMES, GZMK. iNKT and MAIT cells were pre-enriched via CD1d-PBS57 and MR1-5OPRU magnetic beads.

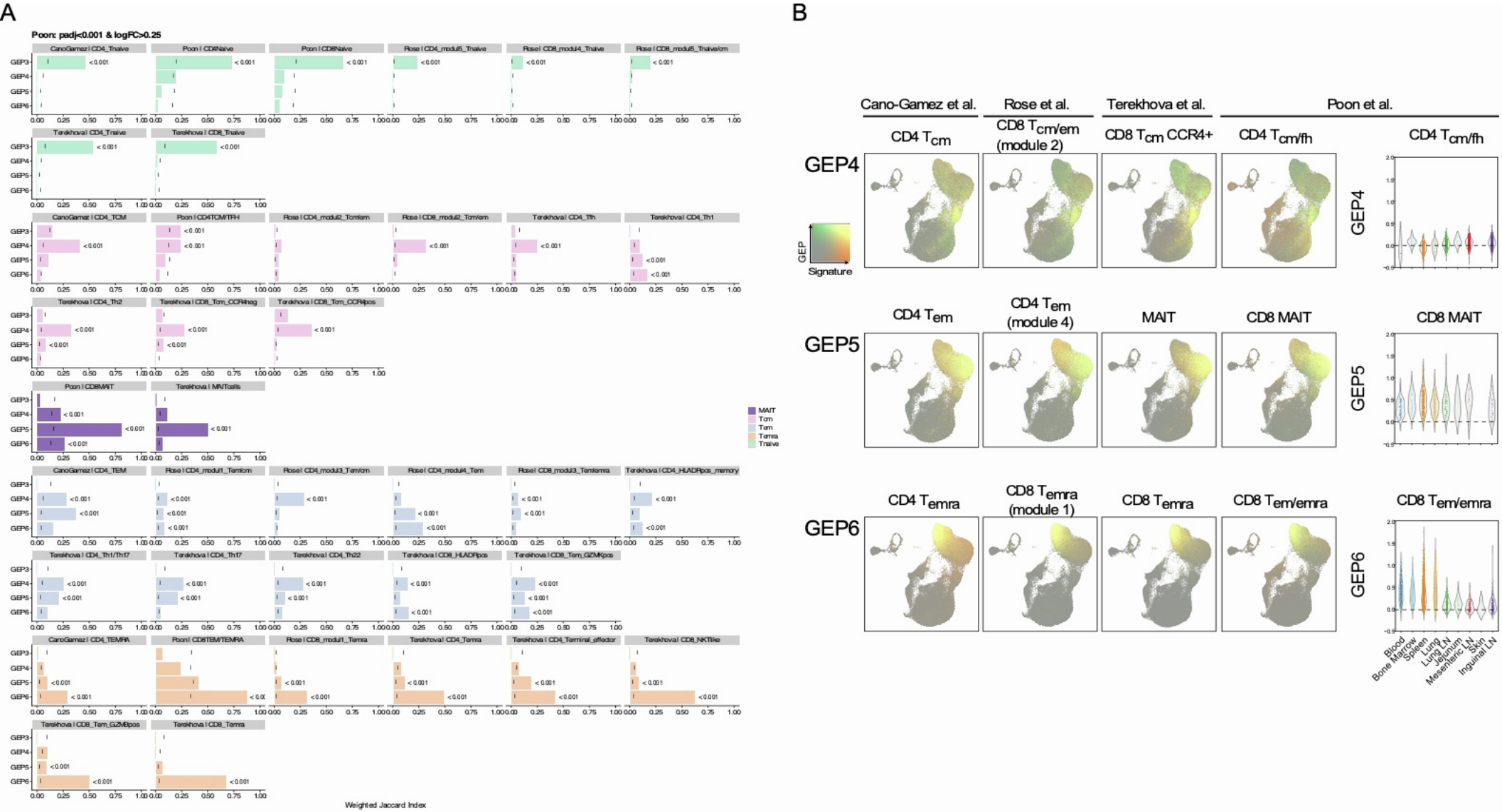

Supplementary Figure 10: Effector gene expression programs (GEPs) are consistent across datasets and human tissues. A. Proportion of genes in each peripheral GEP (3-6) corresponding to genes in public signature gene lists (Poon *et al.*[39], Rose et al.[38], Cano-Gamez *et al.*[37], Terekhova *et al.*[40]) measured by weighted Jaccard Index. For each GEP, the top gene lists with the highest overlap are shown. Tick marks represent the overlap expected from an empirical null distribution (see methods). B. Co-expression of effector GEPs (GEP4-6) and signature gene lists represented on integrated UMAP. For each GEP the co-expression with the gene list corresponding to the highest weighted Jaccard Index (from A) are shown. For the Poon dataset, violin plots on the right represent the effector GEPs scored in cells from the CD4 $T_{cm/fh}$, CD8 MAIT, or CD8 $T_{em/emra}$ clusters, across tissues; the horizontal dashed line is the median score across all clusters and all tissues from the Poon dataset.

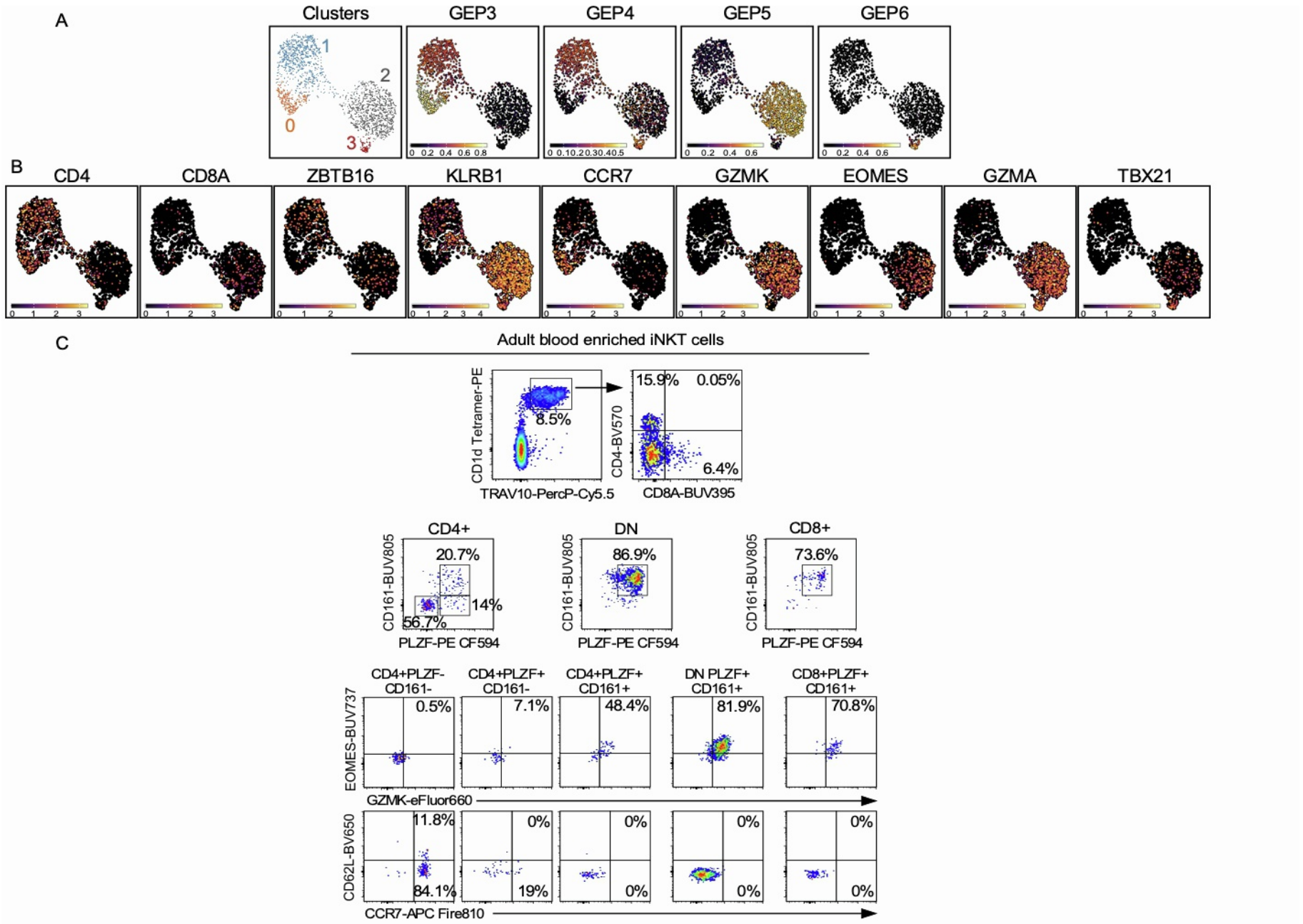

Supplementary Figure 11: Naïve and effector gene and protein expression of adult peripheral blood iNKT cells. A. Cluster assignment (as in Fig. 4A) and projection of naive-like (GEP3) and effector (GEP4-6) on adult peripheral blood iNKT cells (identified by cell hashtag). B. Gene expression projection of co-receptors (*CD4*, *CD8*), transcription factors *ZBTB16* (encoding PLZF) and *TBX21* (encoding TBET), naïve T cell marker CCR7 and effector markers *KLRB1* (encoding CD161), *EOMES*, and granzymes *GZMA*, *GZMK*;

C: Flow cytometry of adult peripheral blood iNKT cells (TRAV10^{+} CD1d-PBS57^{+}) for a characteristic subset of markers in B.

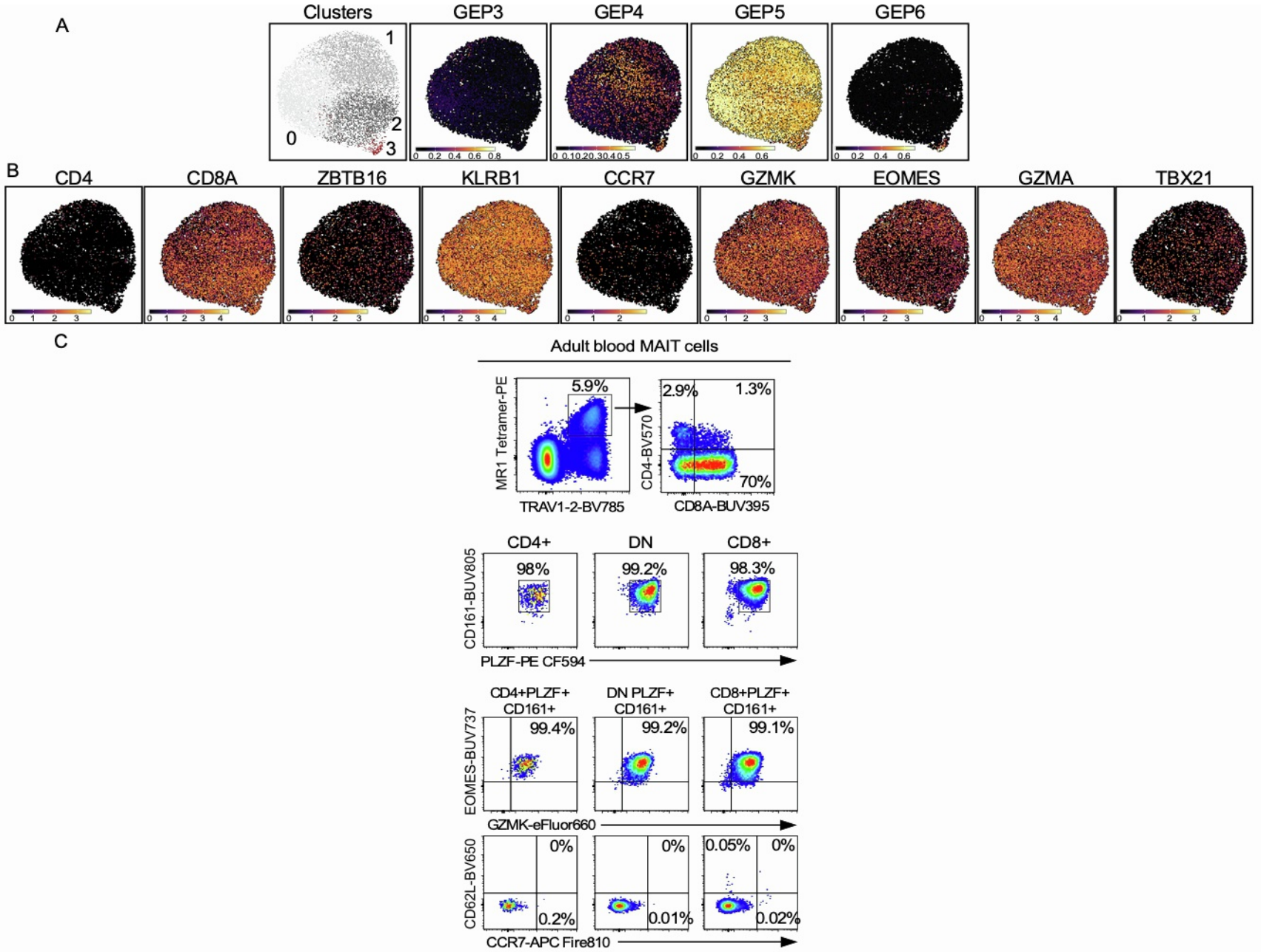

Supplementary Figure 12: Naïve and effector gene and protein expression of adult peripheral blood MAIT cells.
A. Cluster assignment (as in Fig. 4A) and projection of naive-like (GEP3) and effector (GEP4-6) on adult peripheral blood MAIT cells (identified by cell hashtag). B. Gene expression projection of co-receptors (*CD4*, *CD8*), transcription factors *ZBTB16* (encoding PLZF) and *TBX21* (encoding TBET), naïve T cell marker *CCR7* and effector markers *KLRB1* (encoding CD161), *EOMES*, and granzymes *GZMA*, *GZMK*; C: Flow cytometry of adult peripheral blood MAIT cells (TRAV1-2^{+} MR1-5OPRU^{+}) for a characteristic subset of markers in B.

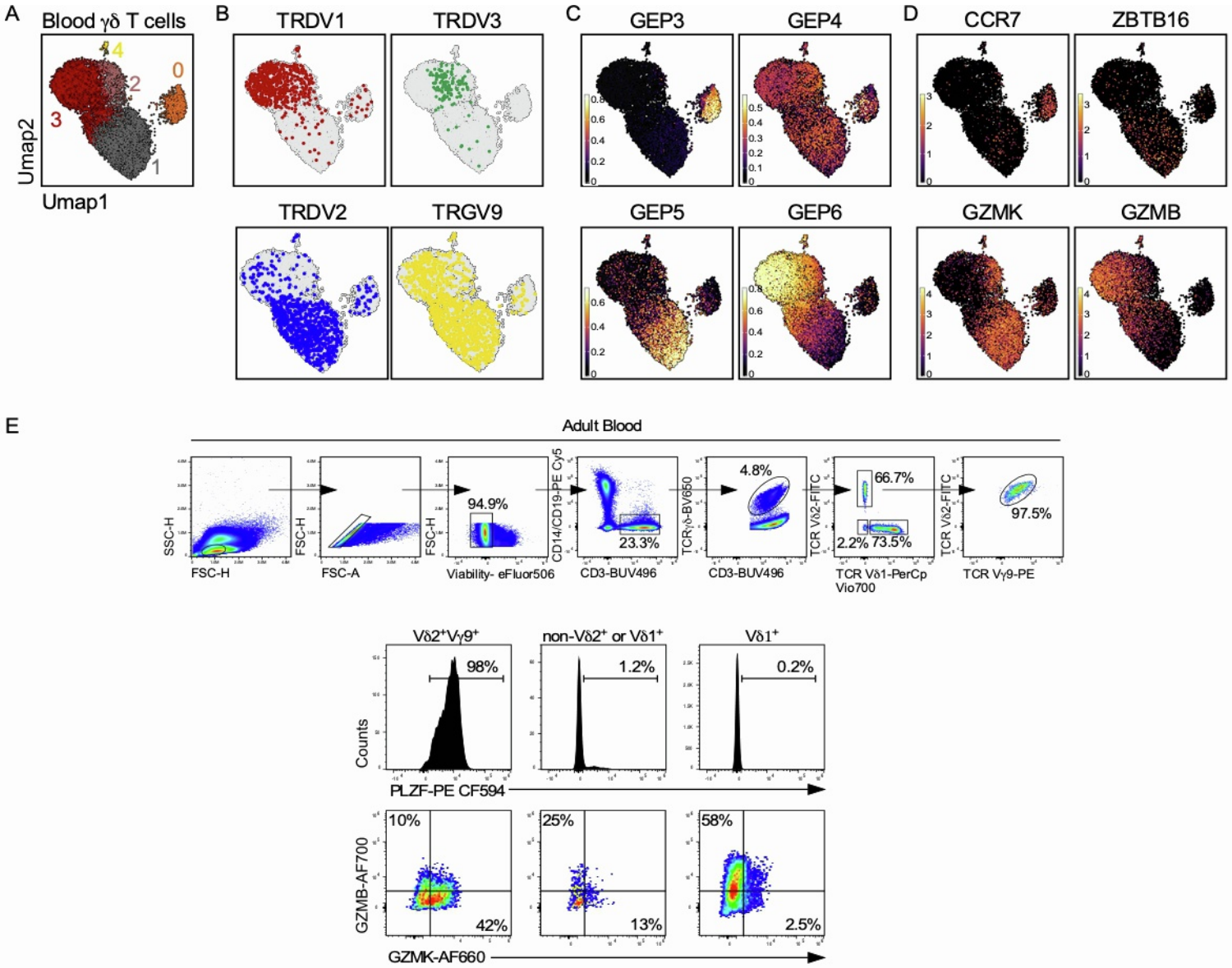

Supplementary Figure 13: Gene and protein expression of adult peripheral blood γδ T cells. A. Cluster assignment (as in Fig. 4A). B. γ and δ variable segment usage (D-V1-3, G-V9), and C. projection of naive-like (GEP3) and effector (GEP4-6) on adult peripheral blood γδ T cells (identified by cell hashtag). D. Gene expression projection of transcription factors *ZBTB16* (encoding PLZF), naïve T cell marker *CCR7* and granzymes *GZMB*, *GZMK*; E: Flow cytometry of adult peripheral blood γδ T cells. γδ T cells were separated by γ and δ chain usage, either as $Vδ2^+Vγ9^+$, $Vδ1^+$, or non-$Vδ1^+$ non-$Vδ2^+$ cells and analyzed for their expression of the granzymes in D.

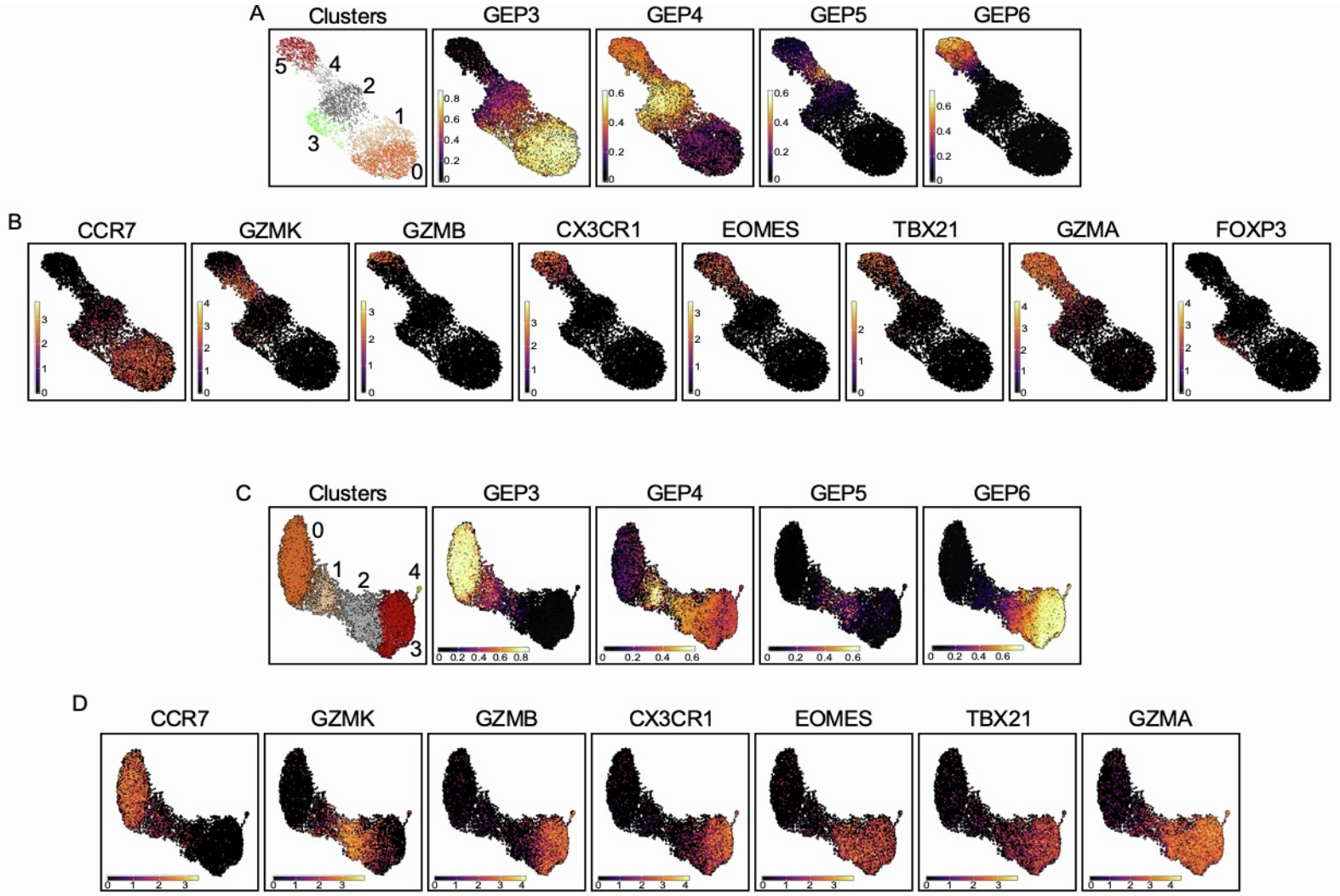

Supplementary Figure 14. Characteristic gene and protein expression of adult peripheral CD4 and CD8 T cells. A./C. Cluster assignment (as in Fig. 4A) and projection of naive-like (GEP3) and effector (GEP4-6) on adult peripheral blood CD4 and CD8 T cells (identified by cell hashtag), respectively. B./D. Gene expression projection of transcription factors *TBX21* (encoding TBET), *FOXP3*, naïve T cell marker *CCR7* and effector marker *EOMES*, chemokine receptor *CX3CR1* and granzymes *GZMA*, *GZMB*, *GZMK*.

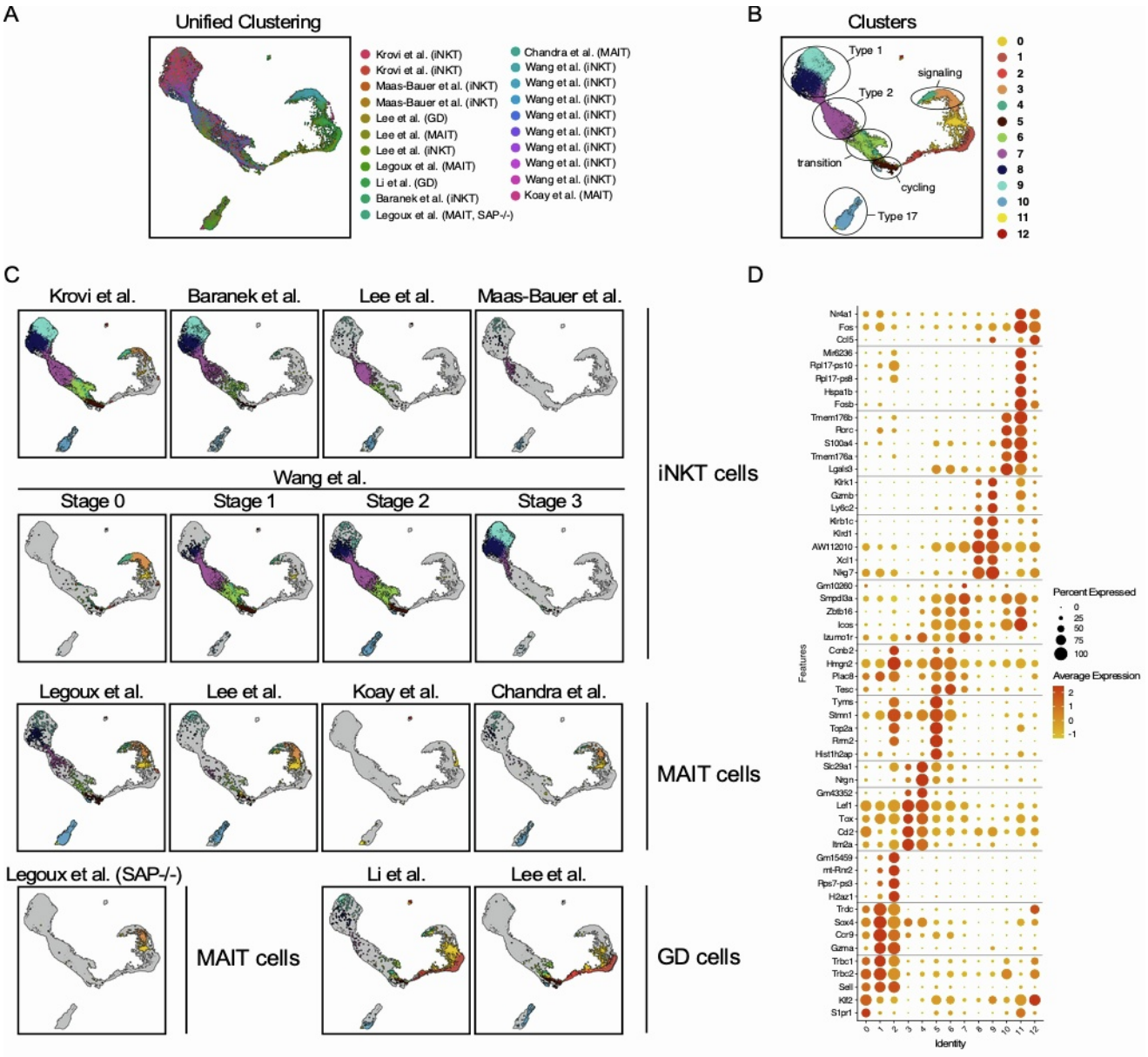

Supplementary Figure 15. Reference mouse T_{inn} dataset. A. Integration of single-cell RNAseq data from flow-sorted mouse iNKT, MAIT, or γδ T cells combined from nine independent studies (Refs 52-58) and B. their annotation into 13 clusters, C. spanning across studies and cell lineages. D. Bubble plot of key genes characterizing the 13 clusters.

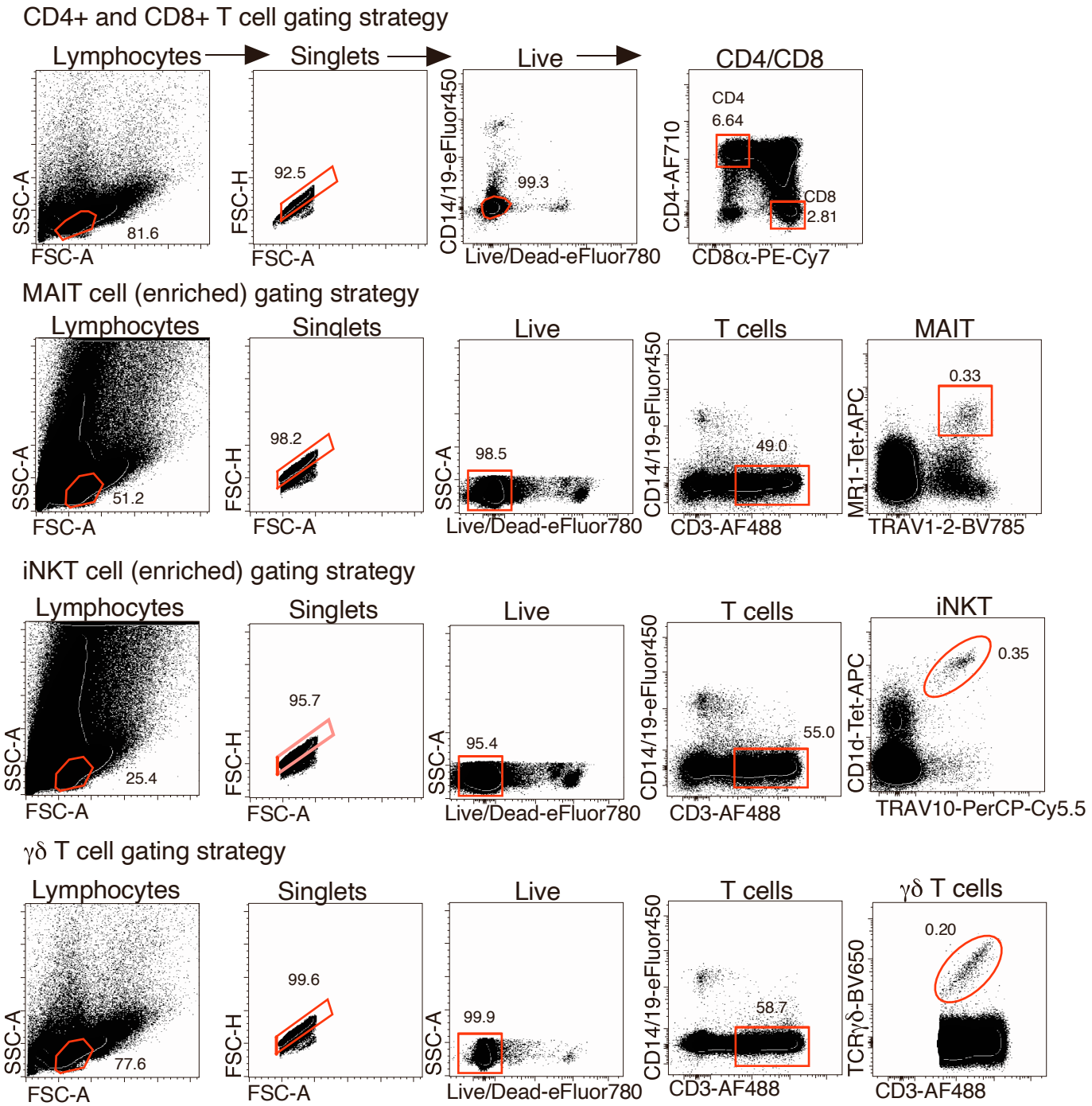

Supplementary Figure 16. Gating strategies implemented to identify the various T cell populations for analyses and sorting. The target (red gate) cell population in each panel is indicated above each panel. iNKT and thymic MAIT cells were pre-enriched by CD1d-PBS57 and MR1-5OPRU tetramers and magnetic beads, respectively.

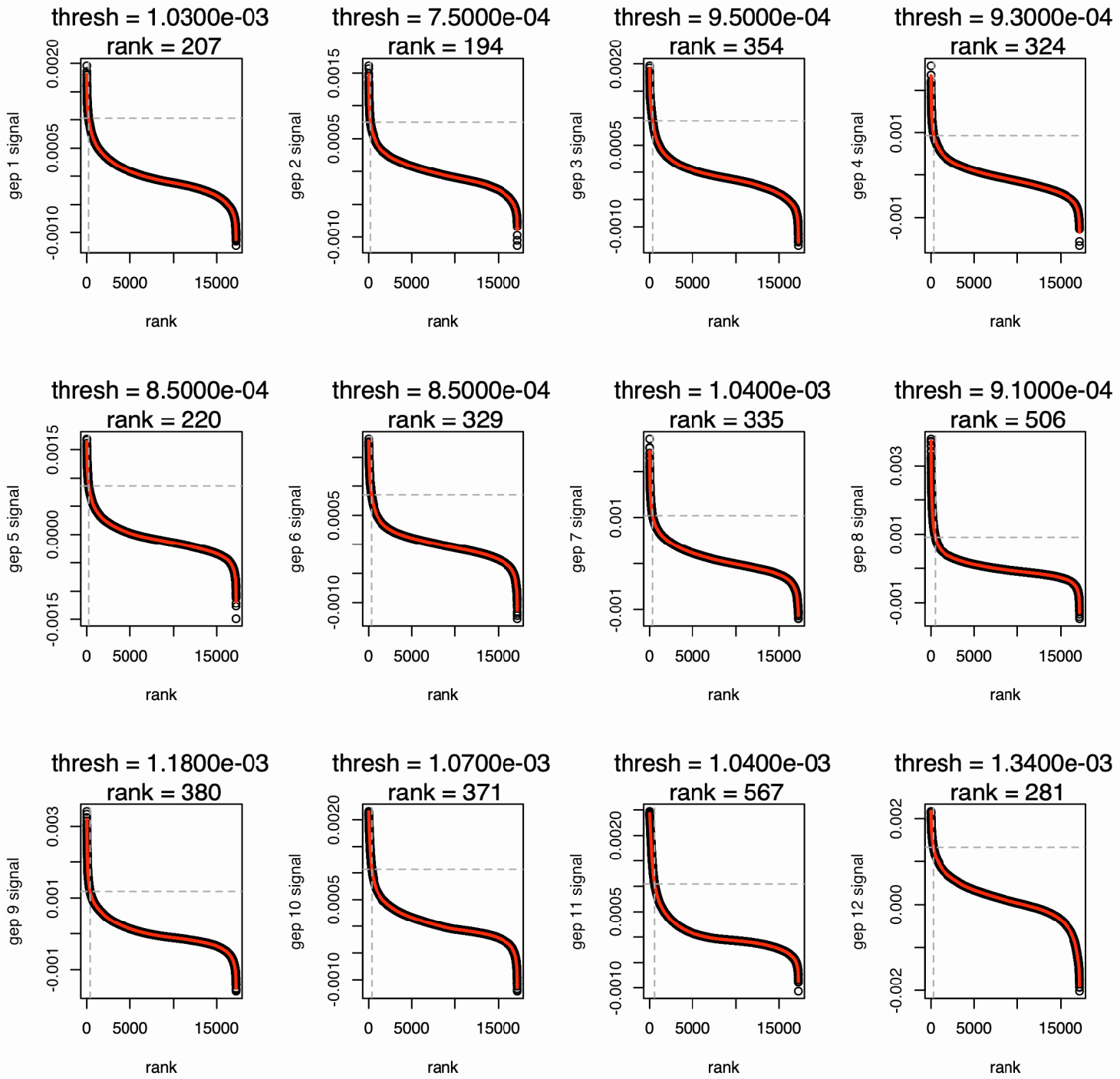

Supplementary Figure 17. Determining genes associated with cNMF derived Gene Expression Programs (GEPs). Gene ranks (sorted most to least associated, x-axis) are displayed against their gene_spectra_score output from the cNMF analysis (y-axis) as black dots. The slope at the first elbow point in the fitted sigmoid curve (red line) was calculated as the minimum threshold for genes to be retained in the given GEP. The same slope (grey dashed line) was applied to every GEP to prevent bias in ranked gene selection, as the gene ranking between GEPs are not comparable and relative to each GEP.